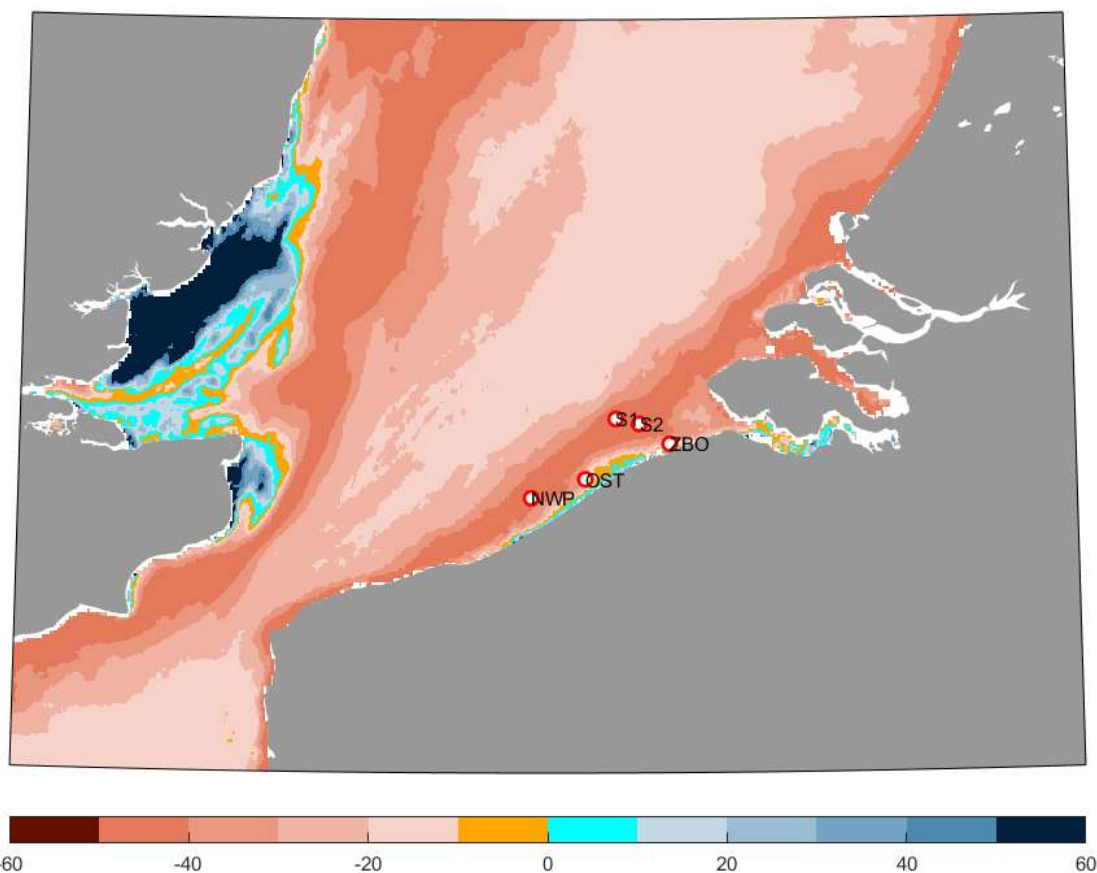**MOnitoring en MOdellering van het cohesieve sedimenttransport en evaluatie van de effecten op het mariene ecosysteem ten gevolge van bagger- en stortoperatie (MOMO)**

Activiteitsrapport (1 januari - 30 juni 2023)

Michael Fettweis, Xavier Desmit

MOMO/10/MF/202310/NL/AR/3

Inhoudstafel

1. Inleiding

1.1. Voorwerp van deze opdracht

Het MOMO-project (monitoring en modellering van het cohesieve sedimenttransport en de evaluatie van de effecten op het mariene ecosysteem ten gevolge van bagger- en stortoperatie) maakt deel uit van de algemene en permanente verplichtingen van monitoring en evaluatie van de effecten van alle menselijke activiteiten op het mariene ecosysteem waaraan België gebonden is overeenkomstig het verdrag inzake de bescherming van het mariene milieu van de noordoostelijke Atlantische Oceaan (1992, OSPAR-Verdrag). De OSPAR Commissie heeft de objectieven van haar Joint Assessment and Monitoring Programme (JAMP) gedefinieerd tot 2021 met de publicatie van een holistisch "quality status report" van de Noordzee en waarvoor de federale overheid en de gewesten technische en wetenschappelijke bijdragen moeten afleveren ten laste van hun eigen middelen.

De menselijke activiteit die hier in het bijzonder wordt beoogd, is het storten in zee van baggerspecie waarvoor OSPAR een uitzondering heeft gemaakt op de algemene regel "alle stortingen in zee zijn verboden" (zie OSPAR-Verdrag, Bijlage II over de voorkoming en uitschakeling van verontreiniging door storting of verbranding). Het algemene doel van de opdracht is het bestuderen van de cohesieve sedimenten op het Belgisch Continentaal Plat (BCP) en dit met behulp van zowel numerieke modellen als het uitvoeren van metingen. De combinatie van monitoring en modellering zal gegevens kunnen aanleveren over de transportprocessen van deze fijne fractie en is daarom fundamenteel bij het beantwoorden van vragen over de samenstelling, de oorsprong en het verblijf ervan op het BCP, de veranderingen in de karakteristieken van dit sediment ten gevolge van de bagger- en stortoperaties, de effecten van de natuurlijke variabiliteit, de impact op het mariene ecosysteem in het bijzonder door de wijziging van habitats, de schatting van de netto input van gevaarlijke stoffen op het mariene milieu en de mogelijkheden om deze laatste twee te beperken.

Een samenvatting van de resultaten uit de vergunningsperioden 2017-2021 kan gevonden worden in het "Vooruitgangsrapport (juni 2019) over de effecten op het mariene milieu van baggerspeciestortingen" (Lauwaert et al. 2019) en het Syntheserapport over de effecten op het mariene milieu van baggerspeciestortingen" (Lauwaert et al., 2021) die gepubliceerd werden conform art. 10 van het K.B. van 12 maart 2000 ter definiëring van de procedure voor machtiging van het storten in de Noordzee van bepaalde stoffen en materialen.

1.2. Algemene doelstellingen

Het onderzoek uitgevoerd in het MOMO project kadert in de algemene doelstellingen om de baggerwerken op het BCP en in de kusthavens te verminderen, om de effecten van het storten van baggerspecie te kwantificeren en om een gedetailleerd inzicht te verwerven van de fysische processen die plaatsvinden in het mariene kader waarbinnen deze baggerwerken worden uitgevoerd. Dit impliceert enerzijds beleidsondersteunend onderzoek naar de vermindering van de sedimentatie op de baggerplaatsen en het evalueren van alternatieve stortmethoden. Anderzijds is vernieuwend onderzoek noodzakelijk om beter de effecten van het storten van baggerspecie in te schatten. Dit onderzoek is specifiek gericht op het dynamische gedrag van slib in de waterkolom en op de bodem en de interacties tussen fysische en biologische processen en zal uitgevoerd worden met behulp van modellen, in situ metingen en remote sensing data.

De specifieke acties die binnen dit onderzoek uitgevoerd worden om de algemene doel-stellingen in te vullen zijn:

1. Streven naar een efficiënter stortbeleid door een optimalisatie van de stortlocaties.

2. Continue monitoring van het fysisch en biogeochemisch milieu waarbinnen de baggerwerken worden uitgevoerd (Taak 1) en aanpassing van de monitoring aan de nog op te stellen targets voor het bereiken van de goede milieutoestand (GES), zoals gedefinieerd zal worden binnen MSFD;

3. Uitbouw en optimalisatie van het numerieke modelinstrumentarium, ter ondersteuning van het onderzoek (Taak 2.1).

1.3. Algemeen Onderzoek 2012-2026

Het onderzoek heeft als doel om de effecten van baggerspeciestortingen op het mariene ecosysteem (fysische en biogeochemische aspecten) te onderzoeken. Hiervoor worden in situ metingen verzameld, gebruik gemaakt van remote sensing data en worden numerieke modellen ingezet. Voor de vergunningsperiode 2022-2026 worden volgende taken voorzien:

1) In situ en remote sensing metingen en data-analyse

De monitoring van effecten van baggerspeciestortingen gebeurt met behulp van een vast meetstation in de nabijheid van MOW1, en met meetcampagnes met de RV Belgica (een 10-tal meetcampagnes voor het verzamelen van traject informatie, profielen en de calibratie van sensoren; en een 10-tal campagnes voor het onderhoud van het meetstation te MOW1). De geplande monitoring is gericht op het begrijpen van processen, zodoende dat de waargenomen variabiliteit en de effecten van baggerspeciestortingen in een correct kader geplaatst kunnen worden. Een belangrijk deel is daarom gericht op zowel het uitvoeren van de in situ metingen, het garanderen van kwalitatief hoogwaardige data en het archiveren, rapporteren en interpreteren ervan. Remote sensing data afkomstig van onder andere satellieten worden gebruikt om een ruimtelijk beeld te bekomen.

2) Uitbouw en optimalisatie van het modelinstrumentarium

Het tijdens de voorbije jaren verbeterde en aangepaste slibtransportmodel zal verder worden ontwikkeld. Dit zal parallel gebeuren met de nieuwe inzichten die voorvloeien uit de metingen en de procesgerichte interpretatie van de metingen.

3) Ondersteunend wetenschappelijke onderzoek

Monitoring gebaseerd op wetenschappelijke kennis is essentieel om de effecten van menselijke activiteiten (hier het storten van baggerspecie) te kunnen inschatten en beheren. Om te kunnen voldoen aan de door OSPAR opgelegde verplichtingen van monitoring en evaluatie van de effecten van menselijke activiteiten is het ontwikkelen van nieuwe monitorings- en modelleractiviteiten nodig. Dit houdt in dat onderzoek dat de actuele stand van de wetenschappelijke kennis weerspiegelt wordt uitgevoerd en dat de hieruit voortvloeiende nieuwe ontwikkelingen geïntegreerd zullen worden in zowel de verbetering van het modelinstrumentarium als voor het beter begrijpen van het kustnabije ecosysteem.

1.4. Onderzoek Januari 2022 – December 2024

Voor de periode 2019-2021 werd rekening gehouden werd met de aanbevelingen voor de minister ter ondersteuning van de ontwikkeling van een versterkt milieubeleid zoals geformuleerd in het "Syntheserapport over de effecten op het mariene milieu van baggerspeciestortingen (2021)" dat uitgevoerd werd conform art. 10 van het K.B. van 12 maart 2000 ter definiëring van de procedure voor machtiging van het storten in de Noordzee van bepaalde stoffen en materialen.

Taak 1: In situ en remote sensing metingen en data-analyse

Taak 1.1 Langdurige metingen te MOW1 en W05

Sinds eind 2009 worden er continue metingen uitgevoerd te MOW1 met behulp van een meetframe (tripode). Met dit frame worden stromingen, slibconcentratie, korrelgrootte-verdeling van het suspensiemateriaal, saliniteit, temperatuur, waterdiepte en zeebodem altimetrie gemeten. Om een continue tijdreeks te hebben, wordt gebruik gemaakt van 2 tripodes. Na ongeveer 1 maand wordt de verankerde tripode voor onderhoud aan wal gebracht en wordt de tweede op de meetlocatie verankerd. Op de meetdata wordt een kwaliteitsanalyse uitgevoerd, zodat de goede data onderscheiden kunnen worden van slechte of niet betrouwbare data.

Veranderingen in kustnabije ecosystemen zijn dikwijls gecorreleerd met veranderingen van de helderheid van het water of de concentratie aan particulair suspensiemateriaal (SPM) en dus ook met het gehalte aan particulair organisch materiaal. De zone waar de invloed van het minerale en kustnabij suspensiemateriaal overgaat in een zone met dominantie van organisch suspensiemateriaal van mariene origine is van bijzonder belang. De monitoring wordt uitgebreid met de verankering van een meetboei in locatie W05 (51°N 24.96', 2°E 48.7'). W05 is één van de drie monitoringspunten waar waterstalen en sensormetingen maandelijks worden uitgevoerd.

Taak 1.2 Calibratie van sensoren tijdens in situ metingen

Tijdens meetcampagnes met de R/V Belgica zullen een voldoende aantal 13-uursmetingen uitgevoerd worden met als hoofddoel het kalibreren van optische of akoestische sensoren en het verzamelen van verticale profielen. De metingen zullen plaatsvinden in het kustgebied van het BCP (MOW1, W05). De optische metingen (Optical Backscatter Sensor) zullen gekalibreerd worden met de opgemeten hoeveelheid materie in suspensie (gravimetrische bepalingen na filtratie) om te komen tot massa concentraties

Taak 1.2 Bio-geo-chemische monitoring van het SPM (BGCMonit)

SPM bestaat uit minerale deeltjes van fysicochemische (b.v. kleimineralen, kwarts, veldspaat) en biogene oorsprong (b.v. calciet, aragoniet, opaal), levend (bacteriën, fyto- en zoöplankton) en niet-levend organisch materiaal (b.v. fecale pellets, detritus, exopolymeren), en partikels van menselijke oorsprong (microplastiek). Het SPM kan door hydrofobe organische polluenten of metalen gecontamineerd zijn. De samenstelling en concentratie van het SPM inclusief de hydrofobe polluenten verandert in functie van de tijd en de locatie. Deze variaties worden beïnvloed door de interacties tussen de fysische processen (getij, meteo, klimaat), biologische cycli (algenbloei), chemische processen (koolstofcyclus) en menselijke activiteiten (aanvoer van nutriënten, bagger- en stortactiviteiten, offshore constructies). De samenstelling van het particulair en opgelost suspensiemateriaal zal bepaald worden tijdens meetcampagnes met de RV Belgica tijdens een 10-tal campagnes per jaar. Naast de totale hoeveelheid aan SPM worden ook de concentraties aan verschillende organische bestanddelen (POC, PON, TEP, chlorofyl en phaeofytine) bepaald. De opgeloste stoffen zijn inorganische nutriënten, DOC, DIC en alkaliniteit. Stalen van suspensiemateriaal zullen genomen worden met de centrifuge om de samenstelling ervan te bepalen.

Taak 1.4: Archivering en verwerking van de data

De meetdata worden gearchiveerd en er wordt een kwaliteitsanalyse uitgevoerd, zodat de goede data onderscheiden kunnen worden van slechte of niet betrouwbare data. Slechte data kunnen bv optreden doordat het instrument slecht heeft gewerkt en verkeerd werd ingesteld. Niet betrouwbare data zijn typisch geassocieerd met bv biofouling. De data en metadata worden gearchiveerd. De metingen worden verwerkt en geïnterpreteerd. En

zullen dienen als basis voor het verder gebruik bij wetenschappelijke vraagstellingen.

Taak 2: Uitbouw en optimalisatie van het modelinstrumentarium

Taak 2.1: Opstellen van een slibtransportmodel voor het BCP met Coherens V2

Een slibtransportmodel zal worden geïmplementeerd met de software Coherens V2. De software laat toe om rekening te houden met gemengde sedimenten en dus met de interactie tussen zand en slib en laat morfologische berekeningen toe door een verbeterde implementatie van het schema voor het massabehoud en gebruik van lagen met gemengde sedimenten. Verdere aanpassingen en verbeteringen aan het model zullen worden uitgevoerd, meer bepaald:

- Kritische bodemschuifspanning voor erosie van gemengde sedimenten,
- Formulering voor de bodemschuifspanning,
- Koppeling van het model met het TILES voxel model voor een betere voorstelling van de bodemkarakteristieken.

Taak 2.2: Validatie van het slibtransportmodel voor het jaar 2013 (stortproef)

Een eerste toepassing van het model kan het jaar 2013 zijn, waarin de terreinproef voor alternatieve stortplaats alsook een intensieve monitoring plaatsvond. Deze laatste zal gebruikt worden voor de validatie van het model. Verder zal het model vergeleken worden met andere modellen van het BCP.

Taak 2.3: Optimalisatie baggerwerken

Een operationeel stortmodel zal worden opgezet in overleg met aMT. Dit model zal geïntegreerd worden in de binnen BMM-OD Natuur beschikbare operationele modellen. Het model zal gebruikt worden om in functie van de voorspelde fysische (wind, stroming, golven, sedimenttransport, recirculatie), economische (afstand, grootte baggerschip) en ecologische aspecten op korte termijn een keuze te kunnen maken tussen de beschikbare stortlocaties. Een eerste test hiervoor werd uitgevoerd in Van den Eynde en Fettweis (2011) waarin werd aangetoond dat door een optimale positie te kiezen voor het storten van baggerspecie in functie van de meteorologische omstandigheden, een vermindering van de aanslibbing van de vaargeulen en haven van Zeebrugge kan worden verwacht.

Het model zal worden gebruikt voor de optimalisatie van de baggerwerken. Verschillende simulaties kunnen worden uitgeoefend waarbij de invloed van de verschillende mogelijke stortplaatsen kunnen worden geëvalueerd.

Taak 2.4: Flocculatiemodel

De inzichten die voortvloeien uit de in situ data (Taken 1.4, 3.1 en 3.2) zullen worden geïntegreerd in een numeriek model dat het verband tussen SPM, TEP en flocculatie langsheen temporele (getij, seizoenen) en geografische (waterkolom, onshore-offshore) schalen combineert. Het model zal worden opgezet als 1D verticaal en zal gekoppeld worden met het 2 klassen populatie model van Lee et al. (2011). Hierdoor zal de verticale verdeling van de minerale en de organische fractie van het SPM en hun interactie kunnen worden voorspeld.

Taak 3: Ondersteunend wetenschappelijk onderzoek

Monitoring gebaseerd op wetenschappelijke kennis is essentieel om de effecten van menselijke activiteiten (hier het storten van baggerspecie) te kunnen inschatten en beheren. Om te kunnen voldoen aan de door OSPAR opgelegde verplichtingen van monitoring en evaluatie van de effecten van menselijke activiteiten is een verdere implementatie van huidige en het ontwikkelen van nieuwe monitoringsactiviteiten nodig. Meer specifiek gericht op de activiteit 'storten van baggerspecie' worden hier – wat het fysische milieu betreft - turbiditeit, samenstelling van de zeebodem, bathymetrie en

hydrografische condities beoogt. Deze taak speelt hierop in door de ontwikkeling en de implementatie van nieuwe tools die de actuele stand van de wetenschappelijke kennis weerspiegelen teneinde de mathematische modellen te optimaliseren en verfijnen.

Taak 3.1: SPM samenstelling - minerale fractie

Door de aanwezigheid van gemengde sedimenten in de zeebodem (zand en slib) zal tijdens sterke stroming en of hoge golven ook een gemengde minerale fractie in suspensie komen. Dit heeft twee consequenties voor monitoring. Ten eerste reageren akoestische en optische sensoren verschillend op zand en slib, zodat de verzamelde tijdreeksen een grotere onnauwkeurigheid hebben tijdens zo'n momenten (Fugate & Friedrichs, 2002; Baschek et al., 2017; Schwarz et al, 2017; Fettweis et al., 2019). Ten tweede bevatten zandkorrels geen mineraal-gebonden organisch materiaal en stalen genomen tijdens dit soort momenten kunnen dus de onzekerheid van het SPM-POM model vergroten. Indien er geen rekening gehouden wordt hiermee zal de SPM concentratie onder- of overschat worden alsook de afgeleid organische fracties. Doel is om de zand en slibfractie te identificeren door gebruik te maken van innovatieve meettechnieken (Pearsons et al., 2021) die optische en akoestische sensoren combineren. Het ultieme doel is om te komen tot tijdreeksen van zand- en slibconcentratie te MOW1.

Uit visuele inspecties van de bodemsamenstelling te MOW1 tijdens de laatste jaren blijkt dat het sediment zandiger is geworden. De hypothese is, dat dit verband houdt met erosie van de vooroever na de strandopspuitingen die de voorbije jaren werden uitgevoerd. Aan de hand van de boven aangehaalde methode zal nagegaan worden of er een trend naar zandaanrijking kan vastgesteld worden in de omgeving van MOW1.

Taak 3.2: SPM samenstelling - organische fractie

Het semi-empirisch POM-SPM model (Fettweis et al., 2022) zal verfijnd worden met de nieuwe data verzameld in taak 1.3. Hierdoor zal de inschatting van de minerale en de vers en mineraal-gebonden organische fractie nauwkeuriger kunnen worden gedaan.

Op basis van dit POM-SPM model kan de samenstelling van het suspensiemateriaal (minerale fractie, vers en mineraal gebonden POC, PON en TEP) worden berekend voor de tijdreeksen te MOW (vanaf 2005) en voor de satellietdata (vanaf 1997). Dit zal toelaten om de geografische en temporele variabiliteit van de transitiezone tussen het kustgebonden turbiditeitsmaximum en de offshore wateren te kwantificeren. De dynamica van het suspensiemateriaal in beide gebieden is verschillend, wat consequenties heeft naar de modellering ervan. Verder kan uit de lange tijdsreeksen gekeken worden of het gebruik van de stortplaatsen, meer bepaald S1, geleid heeft tot een zeewaartse uitbreiding van het turbiditeitsmaximum.

Taak 3.3: Trends in SPM concentratie

Om significante statistische trends te kunnen documenteren in SPM concentratie over de laatste decades, zijn metingen nodig die een lange tijdspanne omvatten en een groot gebied omvatten. Deze data zijn helaas niet beschikbaar. Wat er wel beschikbaar is zijn de tripode metingen te MOW1 (vanaf 2005) en op andere locaties, de puntmetingen verzameld met onderzoeksschepen in het Belgisch Deel van de Noordzee sinds ongeveer 1970 (cf. Belspo 4DEMON project) en satellietbeelden (vanaf 1997). De tripode data geven de temporele variabiliteit weer, maar zijn heel beperkt wat ruimtelijke spreiding betreft. De 4DEMON en satellietbeelden zijn beschikbaar over een lange periode en over een groot gebied, maar kunnen de temporele schaal niet oplossen. Om deze heterogene datasets samen te kunnen gebruiken, zal gekeken worden naar de statistische verschillen tussen de datasets en naar een manier om deze te combineren. Doel is om mogelijke trends in de SPM concentratie te identificeren en deze te linken aan natuurlijke veranderingen of aan menselijke activiteiten.

De trendanalyse van de historische data zal de basis vormen om de verandering van de SPM concentratie in de nabijheid van de nieuwe stortplaats ZBW te kwantificeren.

Taak 4: Rapportage en outreach

Om de zes maanden zal er een activiteitenrapport worden opgesteld dat de onderzoeksresultaten beschrijft. Jaarlijks wordt er een 'factual data' rapport opgesteld van de verzamelde meetgegevens. De resultaten uit het onderzoek zullen tevens worden voorgesteld op workshops, conferenties en in de wetenschappelijke literatuur.

1.5. Gerapporteerde en uitgevoerde taken

Periode Januari 2022 - Juni 2022

Taak 1.1: De meetreeks te MOW1 werd verdergezet.

Taak 1.2: Calibratie van OBS sensoren werd uitgevoerd tijdens RV Begica campagnes 2022/01, 2022/03, 2022/06, 2022/09 en 2022/14.

Taak 3.1: De akoestische en optische sensoren werden gebruikt om veranderingen in sedimentsamenstelling te zien te MOW1. Eerste resultaten worden getoond in hoofdstuk 2.

Taak 3.2: Intensieve bio-geochemische monitoring werd uitgevoerd te MOW1, W05 en W08 tijdens RV Belgica campagnes 2022/01, 2022/03, 2022/07, 2022/11, 2022/14). Eerste resultaten worden besproken in hoofdstuk 3.

Periode Juli 2022 - December 2022

Taak 1.1: De meetreeks te MOW1 werd verdergezet.

Taak 1.2: Calibratie van OBS sensoren werd uitgevoerd tijdens RV Begica campagnes 2022/17, 2022/19, 2022/21, 2022/24, 2022/28 en 2022/32.

Taak 2.4: De interactie van phytoplankton en SPM resulteert in de vorming van grotere vlokken met hogere valsnelheden. In een labo experiment werd de flocculatie bestudeerd tussen klei en phytoplankton deeltjes. Een twee-klassen flocculatiemodel werd opgesteld om de experimentele data kwantitatief te analyseren, zie paper in appendix 1.

Taak 3.2: Intensieve bio-geochemische monitoring werd uitgevoerd te MOW1, W05 en W08 tijdens RV Belgica campagnes 2022/17, 2022/19, 2022/21, 2022/24, 2022/28 en 2022/32). Eerste resultaten worden besproken in hoofdstuk 3.

Taak 3.3: De informatieverlies van niet continue tijdreeksen werd bepaald. Dit zal de basis vormen voor de trendanalyse in SPM concentratie over een langere periode, zie hoofdstuk 2.

Periode Januari 2023 - Juni 2023

Taak 1.1: De meetreeks te MOW1 werd verdergezet.

Taak 1.2: Calibratie van OBS sensoren werd uitgevoerd tijdens RV Begica campagnes 2023/01, 2023/04, 2023/06, 2023/08 en 2023/10.

Taak 2.1: Een slibtransportmodel van het BCP gebaseerd op Coherens V2 werd opgesteld, zie hoofdstuk 3.

Taak 2.4: Een 2D horizontaal flocculatiemodel werd gevalideerd voor het BCP (zie appendix 3). De resultaten tonen het nut van een flocculatiemodel voor grootschalig SPM transport modellering. Tegelijkertijd onderstrepen ze tekortkomingen die het gevolg zijn van de transitie tussen kust en offshore en die zich uiten in verschillende SPM dynamica (zie ook hoofdstuk 2). Dit dient opgenomen te worden in toekomstige modelleringen.

Taak 3: De resultaten beschreven in hoofdstuk 2 hebben mogelijks consequenties voor het storten van baggerspecie. Zij tonen immers aan dat er een duidelijk verschil tussen een kustnabije zone die gedomineerd wordt door minerale deeltjes en een offshore zone die vooral uit organische deeltjes bestaat. Er is geen (of weinig) uitwisseling tussen deze twee zones.

Taak 3.1: Analysen werden uitgevoerd gebaseerd op akoestische en optische sensoren van de tripode te MOW1 om de slib en zand fractie van het SPM te bepalen.

Taak 3.2: De bio-geochemische monitoring werd verdergezet te MOW1, W05 en W08

tijdens RV Belgica campagnes 2023/01, 2023/04, 2023/06, 2023/08 en 2023/10.

Deze data werden gebruikt om de transitie tussen kust en offshore gebaseerd op SPM dynamica en samenstelling te definiëren, zie hoofdstuk 2.

Presentaties van de bio-geochemische data werden gegeven op de ASLO conferentie, zie appendix 1.

Taak 3.3:   De studie over informatieverlies van niet continue tijdreeksen werd gepubliceerd, zie appendix 2.

1.6. Publicaties

Hieronder wordt een overzicht gegeven van publicaties met directe betrokkenheid van het KBIN waar resultaten en data uit het MOMO project in werden gebruikt.

Activiteits-, Meet- en Syntheserapporten

Fettweis M, Desmit X. 2023 MOMO activiteitsrapport (1 januari - 30 juni 2023). BMM-rapport MOMO/10/MF/202310/NL/AR/3, 29pp + app.

Fettweis M, Desmit X. 2023 MOMO activiteitsrapport (1 juli – 31 december 2022). BMM-rapport MOMO/10/MF/202303/NL/AR/2, 27pp + app.

Fettweis M, Baeye M, Desmit X. 2022 MOMO activiteitsrapport (1 januari – 30 juni 2022). BMM-rapport MOMO/10/MF/202210/NL/AR/1, 21pp + app.

Conferenties/Workshops

Kallend A, Dujardin J, De Rijcke M, Fettweis M, Sabbe K, Vyverman W, Desmit X. 2023. Interactions between phytoplankton, marine gels and suspended particulate matter in a dynamic, shallow coastal system before and during the phytoplankton spring bloom. ASLO Aquatic Sciences Meeting, 4–9 June, Palma de Mallorca (Spain).

Schartau M, Fettweis M, Desmit X, Terseleer N, Riethmüller R. 2023. From brown to blue water: Unraveling spatio-temporal variations in organic matter composition of suspended particulate matter. ASLO Aquatic Sciences Meeting, 4–9 June, Palma de Mallorca (Spain).

Baeye M, Delhaye L, Fettweis M. 2022. Acoustic and optical turbidity response to altering particle size distribution during extreme events. EuroSea/OceanPredict workshop, 29 June – 1 July, Exeter (UK).

Fettweis M, Desmit X, Terseleer N, Parmentier K, Van der Zande D, Schartau M, Lee BJ, Riethmüller R. 2022. The characteristics of the organic matter in biomineral flocs. Ocean Science Meeting, 24 February – 4 March, Honolulu (USA).

Peer reviewed artikels

Escobar S, Bi Q, Fettweis M, Monbaliu J, Wongsoredjo S, Toorman E. 2023. A 2DH flocculation model for coastal domains. Ocean Dynamics 73, 333-358. doi:10.1007/s10236-023-01554-y

Fettweis M, Riethmüller R, Van der Zande D, Desmit X. 2023. Water quality monitoring in coastal seas: How significant is the information loss of patchy time series? Science of the Total Environment 873, 162273. doi:10.1016/j.scitotenv.2023.162273.

Fettweis M, Schartau M, Desmit X, Lee BJ, Terseleer N, Van der Zande D, Parmentier K, Riethmüller R. 2022. Organic matter composition of biomineral flocs and its influence on suspended particulate matter dynamics along a nearshore to offshore transect. Journal of Geophysical Research Biogeosciences, 126, e2021JG006332. doi:10.1029/2021JG006332

Ho NQ, Fettweis M, Hur J, Desmit X, Kim JI, Jung DW, Lee SD, Lee S, Choi YY, Lee BJ. 2022. Flocculation kinetics and mechanisms of microalgae- and clay-containing suspension in different microalgae growth phases. Water Research 226, 119300. doi:10.1016/j.watres.2022.119300

Ho QN, Fettweis M, Spencer KL, Lee BJ. 2022. Flocculation with heterogeneous composition in water environments: A review. Water Research. 118147. doi:10.1016/j.watres.2022.118147

2. The transition zone between coastal and offshore waters unraveled by the suspended particle composition

The dynamic nature of shelf regions is responsible for variable patterns of suspended particulate matter (SPM) concentration. This variability is particularly pronounced within nearshore waters where fine-grained sediments are abundant. The SPM dynamics are controlled by a combination of physical and biological processes and particle characteristics (Eisma 1986; Moulton et al. 2023). Also, SPM in a turbulent flow field is further subject to flocculation, which by changing particle size and density will affect their settling velocity (e.g. Eisma 1986). These dynamics depend on the concentration and composition of the SPM, considering their mineral and particulate organic matter (POM) constituents (Dyer 1989; Maggi & Tang 2015; Maerz et al. 2016; Blattmann et al. 2019).

Despite the extensive variations in SPM concentration, a typical feature is the persistence of a horizontal, cross-shore gradient, with higher SPM concentrations in the shallow coastal waters and lower concentrations offshore. This cross-shore gradient in SPM concentration is associated with a higher particulate organic matter (POM) content of SPM offshore, in contrast to a lower content found inshore (e.g. Eisma & Kalf 1979; Jago et al. 1993). For the southern North Sea, with its tidal flats in the Wadden Sea, Postma (1984) stressed the importance of tidal asymmetries and particle trapping by density circulation and proposed the concept of a 'line of no return' located at some distance from the coast. This line would represent a boundary away from the coast beyond which any cross-transport of SPM towards the coast becomes improbable. As a consequence, POM produced nearshore tends to be sustained within the coastal area and POM produced beyond the line tends to remain offshore. In this perspective, only dissolved compounds (nutrients and dissolved organic matter) are advected across the line, which in turn may promote POM production further offshore.

From another perspective, the line of no return can be interpreted as the outer limit to a transition zone between coastal and offshore areas, characterized by a specific depth range (Morgan et al. 2018), where aggregated particles or flocs exhibit maxima in sinking velocity (Maerz et al. 2016). Likewise, such a transition zone can be associated with similar concentrations of fresh and mineral-associated POM (Schartau et al. 2019; Fettweis et al. 2022), and it may also reveal significant changes in phytoplankton order richness (Jung et al. 2017). The inner shelf, defined as the area where the surface and bottom turbulent boundary layers overlap (Moulton et al. 2023) could also be interpreted as a transition between coastal and offshore waters. One might thus assume that the distribution of SPM relies, at least partially, on different hydrodynamic conditions. The definition of Moulton et al. (2023), however, does not hold for some parts of the southern North Sea. For instance, the Belgian nearshore exhibits a cross-shore gradient in SPM concentration, salinity and bathymetry, while the water column is well mixed vertically throughout the year. On the other hand, the nearshore area of the German Bight and the Seine Bay exhibits mainly stratification due to freshwater input; this stratification, however, weakens towards the offshore as the river plume is getting diluted by sea water (Becker et al. 1992; Brenon & Le Hir 1999). The occurrence of salinity gradients in the nearshore results in tidal straining, which leads to a near-bottom residual current toward the coast (e.g. Simpson et al. 1990; Becherer et al. 2016; Du et al. 2022). This partially explains the persistent cross-shore gradients in SPM concentration found in many nearshore areas (Maerz et al. 2016). The above examples suggest that the cross-shore gradient in SPM concentration may occur independently of the existence of a separation between surface and bottom turbulent

layers as proposed by Moulton et al. (2023). It therefore stands to reason that there are specific sedimentological, physical and biogeochemical conditions and processes that can lead to a particular distribution in the concentration and composition of SPM, but which are hidden or overlooked in a pure analysis of hydrodynamics based on density profiles.

In this study, we aim at inferring information about the transition from nearshore to offshore waters by analysing spatio-temporal variations in the concentration and composition of SPM. We hypothesize that by disaggregating changes in the amount and composition of SPM over time and space, we can better distinguish between nearshore waters, where particles are controlled primarily by turbulence, resuspension, flocculation, and deposition, and offshore regions, where variations in SPM concentration and composition are significantly controlled by the production and decay of plankton and detritus in the water column. Our approach applies a semi-empirical model onto field data of SPM and POM concentration from the Belgian shelf to extract POM properties (such as fresh and mineral associated POM) along their cross-shore gradient (Fettweis et al. 2022). The model equations are then applied to remote sensing derived SPM concentration of the whole North Sea to derive the POM properties in a larger domain.

2.1. Study domain

The studied domain is the southern North Sea and the English Channel with a focus on the German Bight, the Thames and East Anglia plume, the Southern Bight and the Bay of Seine. The bathymetry in the domain and along four specific transects ('GE', 'UKNL', 'UKBE', 'FR') is shown in Figure 2.1. Bathymetry data is gridded on a 15 arc-second geographic latitude and longitude grid, that is, any grid cell size is ~450 m on the latitude axis and ~280 m on the longitude axis (source: GEBCO 2022 Grid; see Acknowledgments). Bathymetry along the transects was smoothed with a LOESS function (span=0.2) in MATLAB R2019a to facilitate further interpretation.
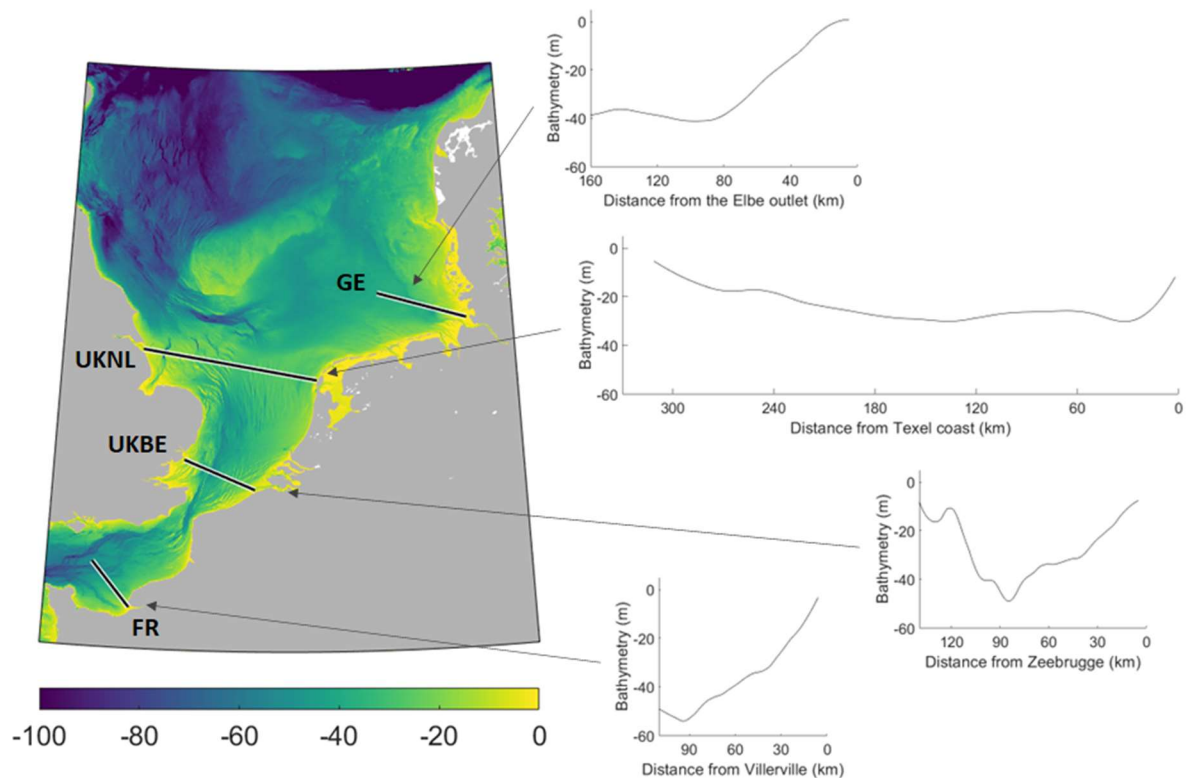

Figure 2.1 Bathymetry of the southern North Sea [m]. The black lines are showing the four transects used in this study. Side graphs on the right show the smoothed (LOESS) bathymetry along the transects.

11

The tides in the study area are principally semidiurnal and progress cyclonically around the North Sea, with the largest amplitudes along the coasts of the English Channel, eastern England, the Southern Bight and the German Bight (e.g. Otto et al. 1990; Huthnance 1991). In the central Southern Bight, the west of Denmark and the west of south Norway amphidromic points occur. The winds are variable and dominated by eastward moving depressions. The residual circulation along the North Sea coasts is cyclonic, along the English coast a southerly direction dominates up to the East Anglia coast where it turns offshore towards the northeast. Atlantic water enters the North Sea from the North and through the English Channel and the Dover Strait (Prandle et al. 1996). The freshwater inflow from the Seine, Scheldt, Rhine, Weser, Elbe and smaller rivers results in coastal water masses with salinities lower than 33 and in density currents up to typically 20-40 kms offshore along the southern North Sea (Prandle et al. 1997; Rijnsburger et al. 2016; Kopte et al. 2022). The SPM transport pattern in the North Sea follows the general residual current patterns and is restricted to a narrow band along the coast, except along the East Anglian coast, where the SPM is transported offshore towards the German Bight and the Norwegian trench, see Figure 2.2. The origin of the fine-grained sediments is from rivers, erosion of recent and geological layers (e.g. mud banks along the Belgian coast), coastal erosion (English Channel, east English coast) and human impacts, see e.g. Eisma (1981), Dyer & Moffat (1998), Gerritsen et al. (2001), Fettweis et al. (2009) and Adriaens et al. (2018). Satellite images show a clear difference between winter and summer SPM concentration, featuring a systematic decrease in summer across the continental shelf. This decrease is mainly caused by the interaction between mineral and organic particles (Engel et al., 2020; Fettweis et al., 2022). During the growing season, phytoplankton excrete exopolysaccharides that aggregate into sticky transparent exopolymeric particles (TEP) enhancing the floc size and the settling of the SPM. The argument to favor microbial activity as the main cause is the seasonal variations in floc size and settling velocity, with higher settling in summer than in winter. Resuspension caused by waves, wind climate, or storms have a weaker correlation with this observed seasonality (Fettweis & Baeye, 2015).
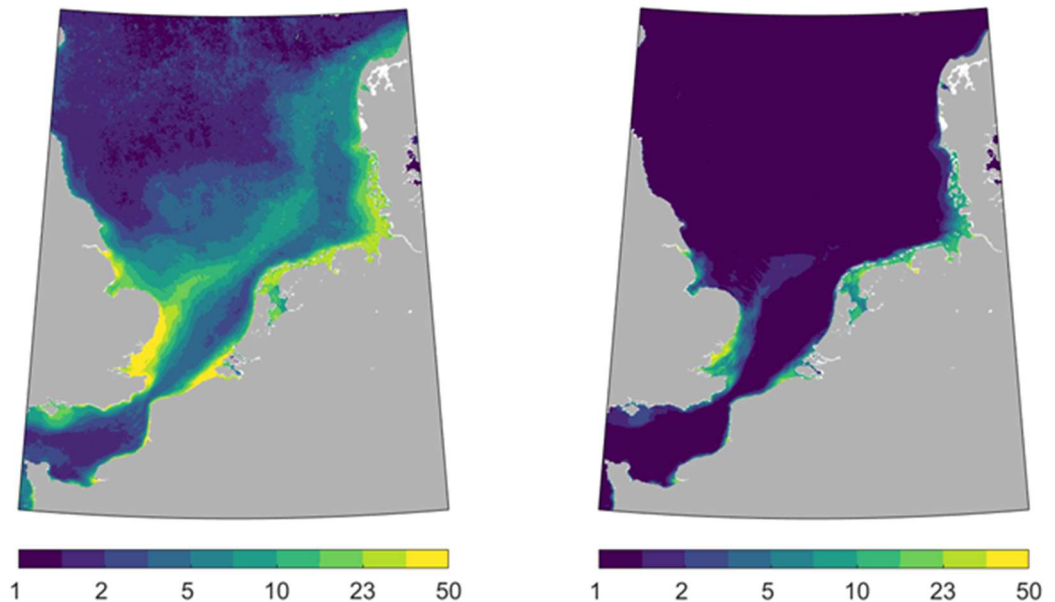

Figure 2.2: Multiyear mean (2017-2021) of winter (left, December – February) and summer (right, June – August) surface SPM concentration (mg/l) in the North Sea. OLCI product, resolution 1x1 km².

2.2. Methods

2.2.1. *Remote sensing data of SPM concentration*

The satellite-based SPM concentration was generated using the Nechad et al. (2009, 2010) algorithm applied to the standard Sentinel-3/OLCI remote sensing reflectance product (RRS) provided by the EUMETSAT water processor (PB 2.00, https://earth.esa.int/eogateway/documents/20142/1564943/Sentinel-3-OLCI-Marine-User-Handbook.pdf) after applying recommended quality flags (LAND, CLOUD, CLOUD_AMBIGUOUS, CLOUD_MARGIN, AC_FAIL). While a single band can be used for SPM estimation the optimal band depends on SPM concentration – if RRS is too low (e.g. for longer wavelengths in low SPM waters) then SPM estimation will be significantly affected by noise or errors in RRS – If RRS is too high (e.g. for shorter wavelengths in high SPM waters) then the saturation phenomenon means that RRS becomes insensitive to changes in SPM. This has led to the development of "switching single band algorithms" (Novoa et al. 2017) using the basic single band formulation of (Nechad et al. 2010) but with different wavelengths used at different SPM concentrations and typically a smooth weighting between two adjacent spectral bands to avoid image artifacts. The Novoa et al. (2017) approach is applied to the SPM products providing a multi-band SPM and TUR product using two bands (red: 665 nm and near-infrared: 865 nm). Daily images of surface SPM concentrations in the period 2017-2021 were extracted in the North Sea (lon [-4 10], lat [48 59]) with a spatial resolution of 1km x 1km. Daily images were then averaged to get monthly images over the same period, and data were extracted along the different transects of the study (Figure 2.2).

2.2.2. *In situ data of PON and SPM concentration*

The in situ data of SPM and PON concentration have been collected between October 2004 and August 2022 on the Belgian Continental Shelf (BCS). The data set consists of hourly, 1.5 hourly or 2 hourly water samples collected during 243 tidal cycles or half tidal cycles in 12 stations, 3 of them being more sampled: one located in the nearshore coastal turbidity maximum area (MOW1, water depth about 10m), one along the outer margin of the coastal turbidity maximum (W05; transition zone; water depth about 20m), and the third one in the offshore area under complete Channel water influence (W08, water depth about 25m). The amount of SPM-PON data pairs is equal to 2539 well distributed over each month, with slightly less data in summer and autumn than winter and spring.

At every sampling occasion, three subsamples for SPM concentration were taken and filtered on board using pre-combusted (405°C, 24 hours), rinsed, dried for 24h at 105°C and pre-weighted 47mm GF/C filters. After sampling the filters were rinsed with ultrapure water (resistivity 18.2 MΩ.cm normalized at 25°C) and immediately stored at -20°C, before being dried during 24 hours at 50°C and weighted to obtain the concentration. The uncertainty (expressed as the RMSE of the triplicates divided by the mean value) decreases with increasing concentration from 8.5% (SPM concentration < 5 mg/l) to 6.7% (<10 mg/), 3.5% (10–50 mg/l) and 2.1% (>100 mg/l) and represent the random error related to the lack of precision during filtrations. Especially in clearer water, systematic errors due to the offset by salt or other errors become much larger than the random errors (Neukermans et al. 2012). These are not included, and have been estimated based on Stavn et al. (2009) and Röttgers et al. (2014) as 1 mg/l. The samples for PON were filtered on board using 25mm GF/C filters (pretreated as above for SPM), stored immediately at -20°C, before being analyzed using a Thermo Finnigan Flash EA1112 elemental analyzer (for details see Ehrhardt & Koeve, 1999). The analytical uncertainty for PON is 18% augmented with the uncertainty of the SPM concentration due to filtration.

2.2.3. Model of PON content versus SPMC

Schartau et al. (2019) and Fettweis et al. (2022) have modelled the POM content of SPM (i.e., the ratio of POM and SPM concentrations) as a function of SPMC. The POM content of SPM shows high values at low SPMC and low values at high SPMC. This relationship is not only observed along the inshore-offshore transect in both the German Bight and on the Belgian continental shelf, but also vertically between the surface and the bottom of the water column during the tidal cycle (Fettweis et al. 2022). A semi-empirical model has been proposed by Schartau et al. (2019) based on the discrimination between mineral-associated POM (POM_m) and fresh POM (POM_f). The boundary condition of the model is that, when SPMC value tends to zero, the POM content of SPM tends to one. Therefore, under low SPMC when SPM is dominated by POM (typically offshore), the POM_m fraction becomes very low and the POM_f fraction dominates POM. On the contrary, when SPMC is high, the POM content of SPM decreases to low values. Under these conditions, while the SPM is dominated by mineral particles (typically onshore), the POM_m fraction dominates POM. The same goes for any component of POM (e.g., POC, PON, TEP).

Here we study the PON component of POM as its fresh fraction PON_f is a proxy for the living biomass, mainly phytoplankton, and the detritus. By fitting the model to the PON data (maximum likelihood estimate), we can extract the parameters of the model (K_{POM}, $f_{1,PON}$ and $f_{2,PON}$) to recalculate the PON concentration from SPM concentration (SPMC), and also the components PON_f and PON_m (eq. 2.1-2.3):

$$PON_{mod} = SPMC_{obs} \frac{K_{POM}(f_{2,PON} \times m_{POM} + f_{1,PON}) + f_{2,PON} \times m_{POM} \times SPMC_{obs}}{(K_{POM} + SPMC_{obs})(m_{POM} + 1)} \quad (2.1)$$

$$PON_f = f_{1,PON} \frac{K_{POM}}{\frac{K_{POM}}{SPMC_{obs}} + 1} \frac{1}{m_{POM} + 1} \quad (2.2)$$

$$PON_m = f_{2,PON} SPMC_{obs} \frac{m_{POM}}{m_{POM} + 1} \quad (2.3)$$

Where m_{POM} is a factor specifying the amount of suspended POM_m along with mineral particles. Variations of m_{POM} are assumed to depend on the sediment composition (Fleming & Delafontaine, 2000), and in this study we assume m_{POM} constant (0.13) across the studied area. K_{POM} is a saturation parameter controlling the net accumulation of POM_f in the water column. Its monthly variation, thus, reflects the seasonal variation of POM_f and is assumed to be a function of available nutrients (see Schartau et al. 2019). The parameter $f_{1,PON}$ expresses the ratio of fresh PON to fresh POM (PON_f:POM_f), and $f_{2,PON}$ is the ratio of mineral-associated PON to mineral-associated POM (PON_m:POM_m). Therefore, $f_{1,PON}$ and $f_{2,PON}$ are expected to vary seasonally (see Fettweis et al. 2022).

This semi-empirical statistical model is applied to the in situ PON and SPM concentration data of the BCS (Section 2.2.2) in order to derive its parameters on a monthly basis. Then, the model is applied pixel wise to the satellite surface SPM concentration (Section 2.2.1) from the southern North Sea, assuming the same model parameters for all areas, thereby providing information on the fresh and mineral attached PON concentration in addition to the original SPM concentrations.

2.3. Results

2.3.1. Modeled PON_f and PON_m

Like SPM itself, the PON content of SPM varies as a function of SPMC along the coastal-offshore gradient with higher values offshore (Figure 2.3; see also Fettweis et al. 2022). The PON content increases in the spring and summer while phytoplankton blooms and detritic particles accumulate in the bulk, until the fall and winter when heterotrophic processes dominate. The model was fitted onto the data, reproducing these coastal-offshore and seasonal trends, and providing monthly values for its parameters (Figure 2.3, Table 2.1). These parameters allow calculating a modelled PON concentration from the observed SPMC, and also the fractions PON_f and PON_m (eq. 2.2 and 2.3). The values of Table 2.1, generated by fitting the model on the available Belgian data, are applied to all transects in this study, assuming they are representative of more global North Sea dynamics.

Table 2.1: Monthly model parameters obtained from model fitting for POC and PON along the coastal-offshore gradient on the BCS.

Month	POC			PON		
	K_{POM}	$f_{1,POC}$	$f_{2,POC}$	K_{POM}	$f_{1,PON}$	$f_{2,PON}$
	mg l^{-1}	mg-C mg^{-1}	mg-C mg^{-1}	mg l^{-1}	mg-N mg^{-1}	mg-N mg^{-1}
Jan	1.990	0.069	0.260	2.0000	0.0095	0.0295
Feb	0.930	0.205	0.249	2.6600	0.0145	0.0295
Mar	2.180	0.156	0.262	2.6800	0.0210	0.0295
Apr	5.890	0.160	0.237	4.4700	0.0290	0.0295
May	6.240	0.147	0.264	8.0000	0.0195	0.0300
Jun	5.490	0.129	0.276	4.4600	0.0210	0.0390
Jul	3.050	0.156	0.269	3.7700	0.0260	0.0310
Aug	3.070	0.137	0.258	3.9000	0.0205	0.0300
Sep	0.950	0.320	0.253	1.9900	0.0290	0.0295
Oct	1.530	0.154	0.273	2.5500	0.0165	0.0295
Nov	1.110	0.115	0.279	2.1300	0.0095	0.0295
Dec	2.650	0.044	0.278	1.6300	0.0095	0.0295

2.3.1. Multiyear modeled PON_f and PON_m

Using our model, we estimated PON, PON_m and PON_f concentrations from SPMC and applied it pixelwise to the satellite images in the southern North Sea, which generates qualitative information in addition to the quantitative SPMC. We use PON_{diff}, the difference between PON_m and PON_f concentrations (PON_m - PON_f), to highlight the spatio-temporal variations of the PON dynamics and composition. It is shown for the months of January and April 2020 at Figure 2.4. PON_{diff} varies in time and space as both fractions PON_m and PON_f undergo biogeochemical transformations. In winter, PON_{diff} shows the highest values at the coast due to the dominance of PON_m while that concentration decreases fast toward the offshore, where values are typically closer to zero as both PON_m and PON_f are low and closer in concentration. A notable exception offshore is the turbid Thames River plume carrying SPM from East Anglia across the sea to the German Bight and the coast of Denmark, where PON_m dominates. In the spring, PON_{diff} shows its minimum values in a narrow area close to the coast. In that area, the freshly produced fraction of PON in spring is found in higher concentrations than the mineral-associated PON, which leads to negative values of PON_{diff}. While PON_f concentration in spring is a proxy for phytoplankton biomass, PON_m always reflects the mineral fraction of SPM.
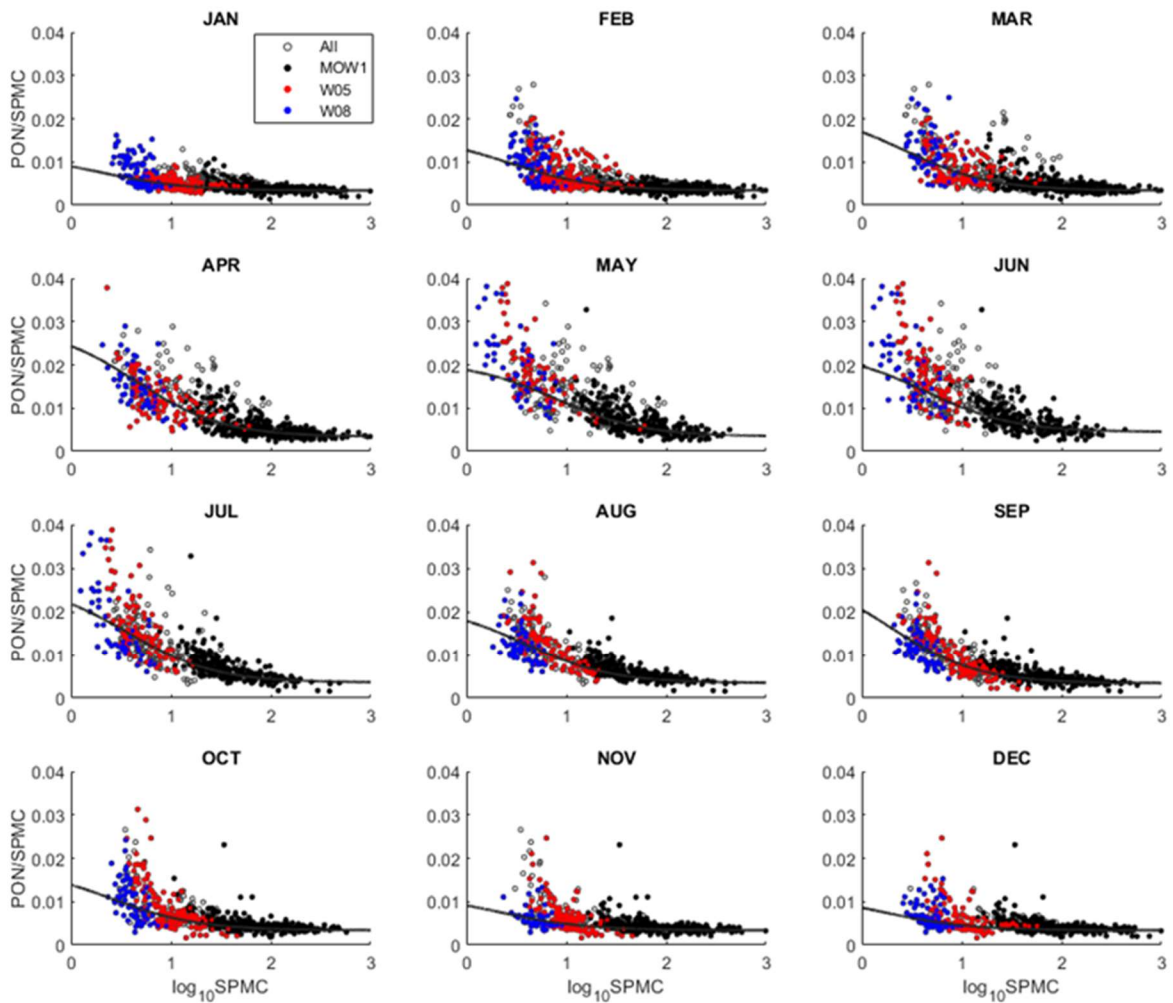
Figure 2.3: PON content of SPM as a function of SPMC, in situ monthly data sampled at twelve stations along the coastal-offshore gradient on the BCS. Three stations are relatively more sampled: MOW1, W05 and W08 (see legend for colors). The black line represents the model fitting (maximum likelihood estimation).

2.3.2. Variations of PON with distance from the coast

The monthly variations of PON have been calculated for the four selected transects (see Figure 2.1). All the coastal-offshore gradients of PON_{diff} (PON_m-PON_f) feature a high seasonal variability as shown in Figure 2.5 for the transect 'GE' and Figure 2.6 for the transect 'UKBE'. At any moment of the year, both PON_m and PON_f show higher concentrations at the coast than offshore. That difference becomes, however, much less significant for PON_f in winter as biological activity is minimal everywhere. In spring and summer, PON_m concentrations are lower than in winter due to the low SPMC that are mainly the result of an enhanced flocculation and sinking due to the presence of fresh TEP (Fettweis et al., 2022). During the growing season, PON_f reaches the highest concentrations, especially in April and May at the coast and in March, April and September offshore.

As a result of this seasonal variability, PON_{diff} follows a coastal-offshore gradient similar to the one of PON_m during winter months, which is characterized by a strong decrease in concentration between the coast up to 80 km from the Elbe outlet and about 30 km from the Belgian coast. In the spring and summer, while PON_f increases and PON_m decreases, the resulting PON_{diff} is characterized by lower values (mostly negative values) across the transect. PON_{diff} shows minimum values from April to September between the coast and 80

16

km offshore from the Elbe outlet and 20 km from the Belgian coast. In April, when phytoplankton production is at the highest, more negative values of PON_{diff} occur between km 20 and km 80 from the Elbe outlet and 10 to 30 km from the Belgian coast. In that zone, although PON_f shows lower concentrations than at the coast, the PON_m concentration has dropped to such an extent that PON_{diff} shows its lowest value. Over the entire North Sea, this zone is visible as the dark red narrow area on Figure 2.4b, where $PON_{diff}<-40$ mg N l^{-1}).
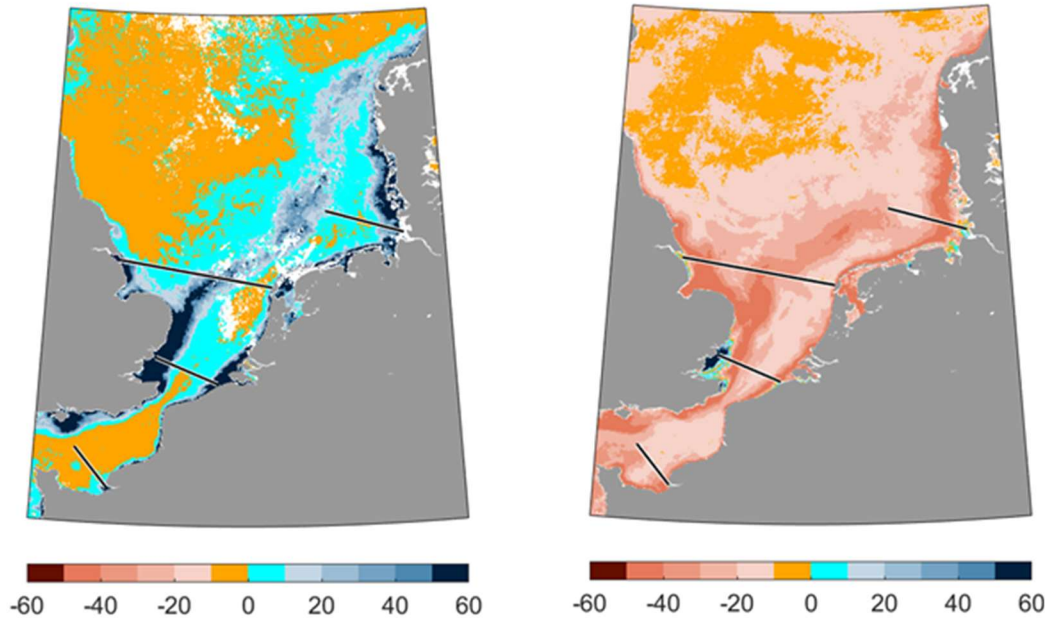
Figure 2.4: Surface PON_{diff} (PON_m-PON_f) concentration [mg N m^{-3}] in 2020, January (left) and April (right). Black lines are the transects of interest (see Figure 2.1).
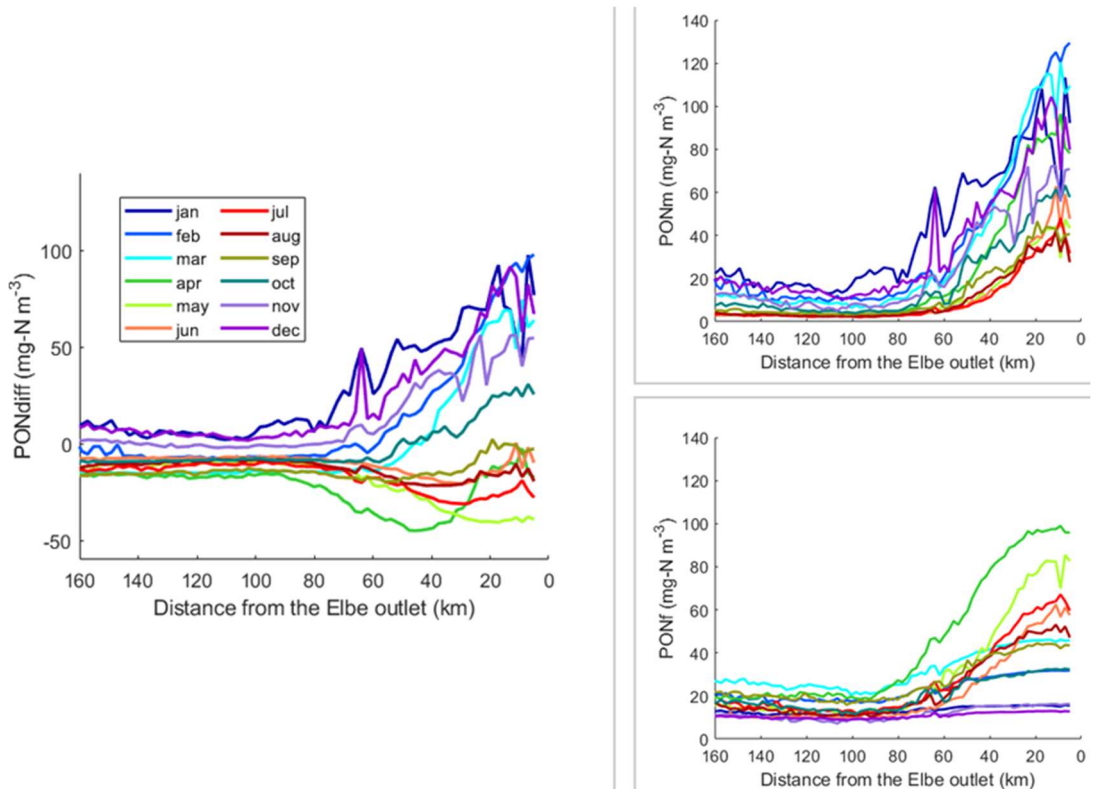

Figure 2.5 Monthly surface PON_{diff}, PON_m and PON_f concentrations [mg N m^{-3}] along the transect 'GE'. Each line features the multi-year mean values in the period 2017-2021.
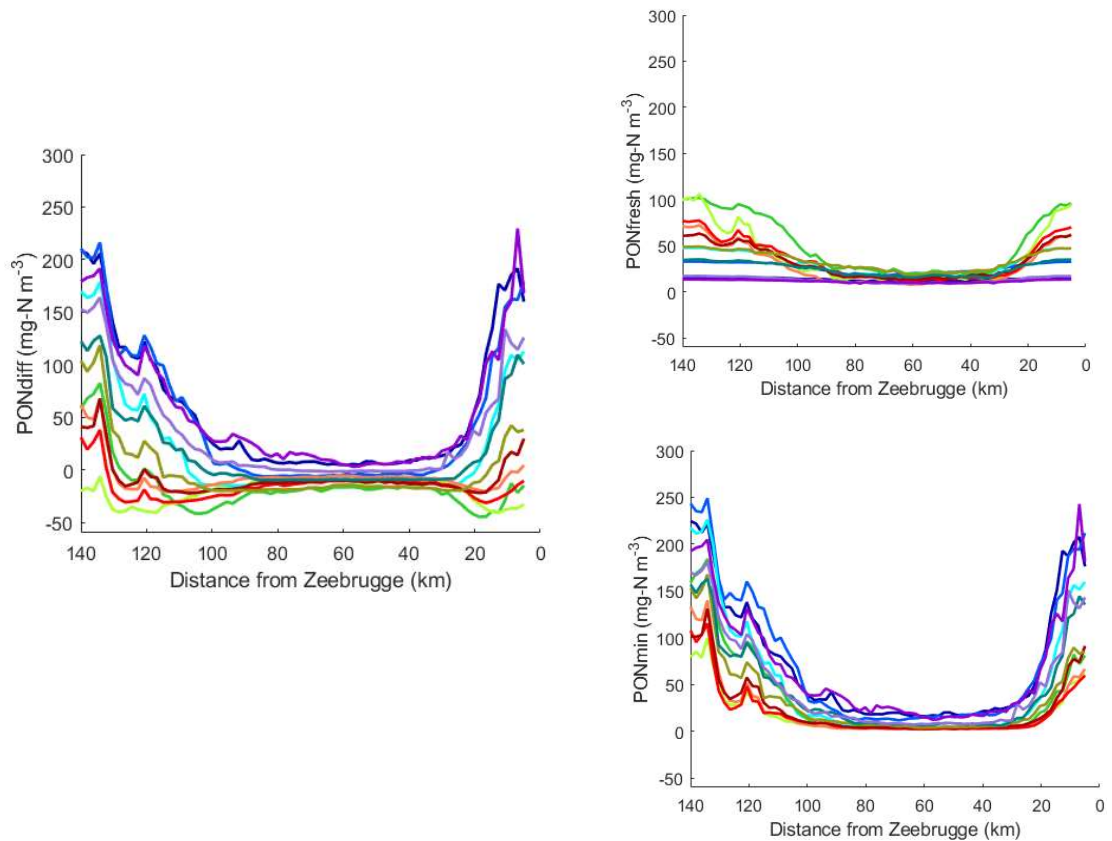
Figure 2.6 Monthly surface PON$_{diff}$, PON$_m$ and PON$_f$ concentrations [mg N m^{-3}] along the transect 'UKBE'. Each line features the multi-year mean values in the period 2017-2021. Color scale, see Figure 2.5.

Figure 2.7 shows the average winter (red) and spring (green) PON$_{diff}$ profiles over the four studied transects. The main characteristics of PON$_{diff}$ variability across the 'GE' transect are also observable in other coastal zones, whether featuring low turbidity like the Texel coast ('UKNL' transect), moderate turbidity like the Bay of Seine ('FR' transect), or high turbidity like the Belgian and the UK coasts along the Humber mouth (north of East Anglia) and the Thames mouth (south of East Anglia; 'UKBE' transect). In winter, PON$_{diff}$ is dominated by PON$_m$ and reflects well the SPM concentration. In spring, PONf concentration increases due to biological activity while PON$_m$ decreases concomitantly due to TEP accumulation in the bulk and settling of the flocs, which results in a considerable decrease in PON$_{diff}$ at the coast (toward negative values). As PON$_{diff}$ is derived from SPM concentration, the East Anglia plume and the Thames plume are visible respectively in the 'UKNL' and 'UKBE' transects, especially in winter. The fact that the East Anglia plume is visible in satellite images in winter suggests that the particles are small and have low settling velocities. It is unlikely that particles from the bottom be resuspended towards the surface along the trajectory of the plume, especially when bathymetry increases. In spring, the East Anglia plume is also visible with lower values of PON$_{diff}$ than in the surrounding waters, which suggests a higher phytoplankton production in the plume. Along the coastal-offshore transects, the annual variability of PON$_{diff}$ (shaded area) is lower than the spatial and seasonal variability in the period 2017-2021, suggesting that basin morphology and seasonal processes, such as phytoplankton production, mainly control the particle dynamics. This tends to be less obvious in offshore waters.
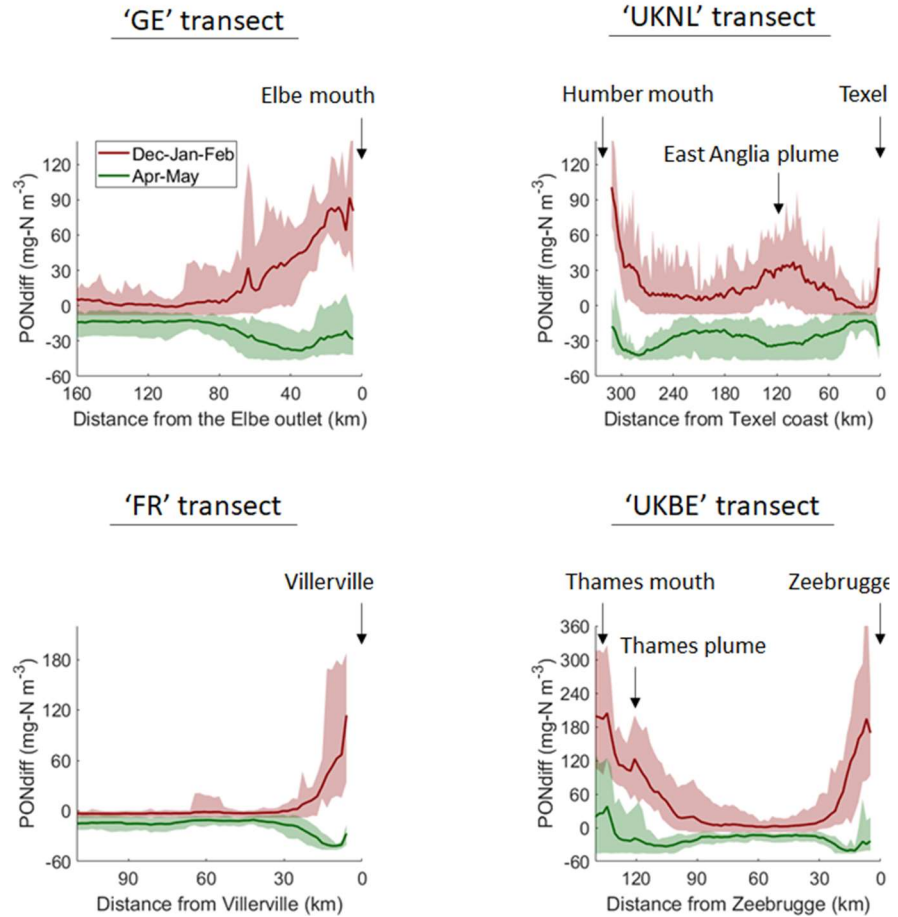
Figure2.7: Surface PON$_{diff}$ (PON$_m$-PON$_f$) concentration [mg N m^{-3}] in winter and spring along four transects. Lines show the multiyear mean values (2017-2021) and shaded areas illustrate the multiyear minimum and maximum values.

2.3.3. Variations of PON with bathymetry

In order to test the dependency of PON$_{diff}$ on basin morphology, PON$_{diff}$ is also represented as a function of the bathymetry along the transects (more specifically along each coastal-offshore sub-transects; Figure 2.8). In most studied cases, the winter decrease in PON$_{diff}$ mainly occurs within bathymetry 5-25 m. Also, the spring dip in PON$_{diff}$ occurs within bathymetry 5-25 m, with the exception of the German case where it occurs within bathymetry 10-30 m. It should be pointed out that in spite of the complexity of particle dynamics in coastal zones, PON$_{diff}$ values tend to stabilize in most cases around bathymetry 25 m, or 35 m in the German case, where SPM dynamics reach an offshore regime - except in the East Anglia plume (bathymetry 20-50 m in Figure 2.8d). This suggests that bathymetry 25-35 m be the location of the virtual 'line of no return', which may also depend locally on the river plume dynamic.

2.4. Discussion

Suspended particle composition illustrates well the gradual changes from coastal towards offshore waters. Coastal and offshore systems exhibit very different biogeochemical properties, including differences in SPM concentration, in the organic matter content of the SPM and in the dominance of mineral or fresh POM. While coastal areas are often characterized by high SPM concentrations and dominated by mineral-associated POM, the offshore systems often exhibit lower SPM concentrations and are dominated by fresh POM. The transition between coastal and offshore waters is marked by gradients in concentration
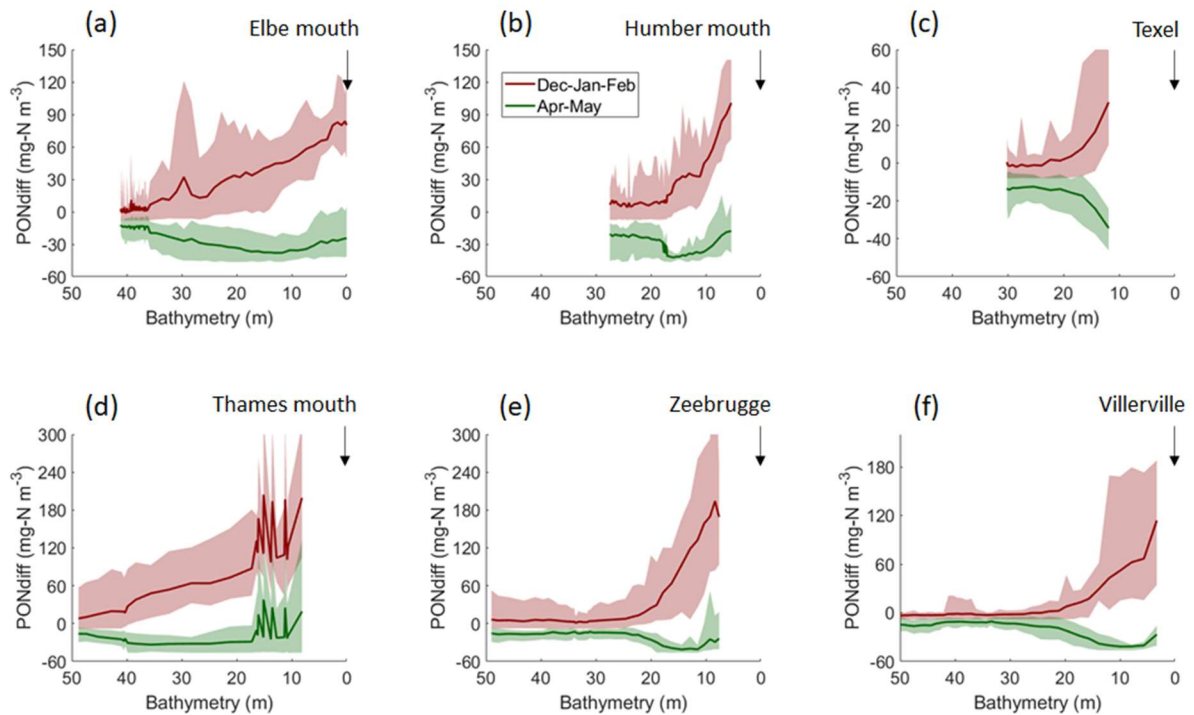
Figure 2.8: Surface PON$_{diff}$ (PON$_m$-PON$_f$) concentration [mg N m^{-3}] in winter and spring as a function of bathymetry (a. 'GE' transect; b. 'UKNL' transect, Humber plume; c. 'UKNL' transect, Texel coast; d. 'UKBE' transect, Thames plume; e. 'UKBE' transect, Belgian coast; f. 'FR' transect). Lines show the multiyear mean values (2017-2021) and shaded areas illustrate the multiyear minimum and maximum values.

of dissolved and particulate material, both mineral and organic in nature. Our results on SPM and PON dynamics unravel some characteristics of this coastal-offshore gradient. Satellite products of PON$_{diff}$ show across the North Sea a narrow area between coastal and offshore waters where PON$_{diff}$ is almost zero. This area corresponds with the maximum settling velocity zone as presented by (Maerz et al. 2016) and can be interpreted as the transition between land and ocean dominated areas.

2.4.1. Bathymetry and particle dynamics

The observed SPM concentration in the water column is the result of erosion/resuspension processes and phytoplankton production, on the one hand, and of settling processes, on the other hand. Turbulence is a major factor controlling the resuspension of fine-grained particles. Turbulence is due to both wind and tide dynamics causing shear stress at the surface and bottom boundaries of the water column. While tidal dynamics will force erosion of the bottom sediment, the influence of wind-induced turbulence through waves close to the bottom sediment will depend on bathymetry. Likewise, under a given turbulent energy, bathymetry determines whether resuspended particles may reach the surface of the water column. Thus, at the coast, both the shear stress on sediment and the particle resuspension to the surface increase, while they tend to decrease toward the offshore. The net downward flux of particles is a function of settling velocity and, hence, of their size, structure and density. These characteristics are controlled by flocculation that involves a combined process of aggregation, breakup and reshaping by turbulence (Ho et al 2022; Yu et al. 2023). While lower levels of turbulence will enhance flocculation, high levels of turbulence will result in floc breakup and, hence, decrease settling. By influencing the distribution of turbulent energy, bathymetry will therefore also play a role in the flocculation process. As

soon as seasonal irradiance permits which is potentially accelerated under higher temperature, phytoplankton production starts (Desmit et al. 2020). The accumulation of biomass is often maximum at the coast due to high nutrient availability and in spite of a higher turbidity. In this process also, bathymetry is thought to play a role in determining the critical depth for phytoplankton production, at least in vertically well-mixed water columns. As shown in the ocean and in turbid coastal systems (Engel et al. 2004; Logan et al., 2005 Fettweis et al. 2022), biological activity results in the production of transparent exopolymer particles (TEP). Freshly produced TEP have sticky properties by which they enhance flocculation of particles during the growing season. Fettweis et al. (2022) demonstrated that the flocs formed by TEP-particle collisions during the growing season tend to be larger and more resistant than the winter flocs. This explains the seasonal dynamics of SPMC, which exhibits much lower concentrations in summer than in winter on average (see Figure 2.3). The particle dynamics is not only visible in the SPMC and thus in the SPM composition but also in the size and density of the flocs. The floc sizes in the turbid nearshore are generally smaller than in the offshore. Also, the variation in floc size in the turbid nearshore can mainly be attributed to tides, while in the offshore seasonal effects, i.e. TEP production dominates the floc size variations. This points to stronger aggregates and particles of biological origin with lower density in the offshore, whereas in the nearshore the flocs can be classified as biomineral aggregates that contain various types of minerals as well as mineral-attached and fresh POM (Fettweis & Lee 2017; Spencer et al. 2021; Zhu et al. 2022). The PON_{diff} map in Figure 2.9 is shown that the offshore extension of the negative PON_{diff} (line of no return) corresponds well with the 20 m bathymetrical line along the coasta of the southern North Sea.
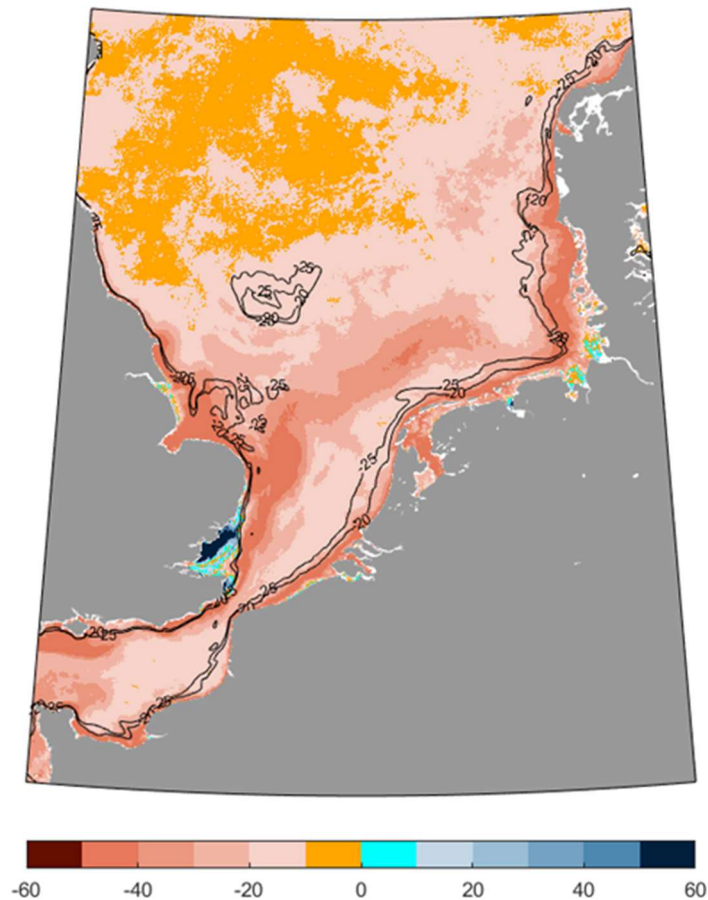

Figure 2.9 Surface PONdiff (PONm-PONf) concentration [mg N m^{-3}] in April 2020 with isolines (black) of bathymetry 20m and 25m.

2.4.2. Transition zone based on SPM composition

The transition zone between coastal and offshore waters (see Figure 2.4) was investigated along four transects as a function of the distance to the coast (Figure 2.7). It was also represented as a function of bathymetry because of the indirect, though central, influence of the latter on particle dynamics (Figure 2.8). From the results, we conclude that the transition zone tends to occur at all seasons within depths of 5-20 m in the studied transects (10-30 m in the German Bight). As particle net downward flux is higher within that transition zone, it is an area of sediment accumulation, as was described by Postma (1981). In the case the transition zone would overlap with a region of freshwater influence, the net transport of settled particles during a tidal cycle might also be directed toward the coast due to estuarine circulation (Maerz et al. 2016). Such occurrence would, thus, cause a net accumulation of particles in the coastal zone, shaping the strong horizontal gradients of SPM. In that case theoffshore extension of the transition zone could also be seen as the 'line of no return' introduced by Postma.

2.4.3. SPM and POM storage on the inner and offshore shelf

Analysing Figure 2.5 and 2.6, some hypotheses can be made on the influence of the transition zone on SPM and POM storage and export. The seasonal variability in PON_f is mainly due to phytoplankton production, and the seasonal variability in PON_m may be attributed to an increased settling of particles on average in the growing season. In the case of the German Bight (transect 'GE'), the most upstream values of PON_f concentration (multiyear mean of 2017-2021) increase by ~80 mg N m^{-3} (~15-20 mg N m^{-3} in the offshore) between December and April (March, offshore), illustrating the size of the spring bloom. Concomitantly, PON_m concentrations decrease by ~100 mg N m^{-3} (~13-17 mg N m^{-3} in the offshore) between the end of the winter and the summer, that is, between the seasons where particles show respectively the lowest and the highest median particle size due to the seasonal variability of fresh TEP (Fettweis et al. 2022). The SPM in winter is deposited and resuspended at tidal scale and no long term deposition of fine-grained sediments occurs in the benthic layer. In contrast during summer a significant part (about 50% in the Belgian zone) of the SPM is trapped in this benthic layer, and is not anymore continuously resuspended and deposited (Fettweis & Baeye, 2015). These vertical processes, which are mainly controlled by the seasonal variations in floc size, influence the horizontal fluxes of SPM and POM. The cross shore dispersion/transport of SPM is more pronounced in winter, which is reflected in a higher SPMC in the offshore zones. Associated to the SPM export in winter is the export of mainly mineral-attached and thus the refractory part of the POM. In spring and summer, the SPM has a higher probability to be embedded in the fluffy benthic layer, and the SPMC in the water column decreases. The bigger flocs are limiting the horizontal export towards the offshore. The export of POM towards the offshore in spring summer, which is more dominated by fresh POM, is thus also limited. In the coastal areas of the southern North Sea, such as the German Bight, the Belgian coastal area and the Seine Bay, the high turbidity area or the area influenced by land, is narrow, while along the East Anglia coast the SPM stretches out across almost the whole North Sea. The difference between both areas can be explained by a balance between hydrodynamic current patterns, which are more alongshore along the southern North Sea and more cross shore at the East Anglia coast and by the occurrence of estuarine circulation. Along the coasts of the southern North Sea, the currents are mainly directed alongshore, the low cross shore currents together with the estuarine circulation will limit the export of SPM and POM from the coasts of the southern North Sea. In contrast, along the East Anglia coast the currents are more cross shore directed and overtake the effects of estuarine circulation. The excess SPM and POM available and produced in the nearshore areas along the East Anglia coast are

exported and will be deposited in the Norwegian trench, while in the nearshore areas of the southern North Sea they will mainly be stored in marsh areas, such as the Wadden Sea and export to the offshore is small (Herman et al. 2018; Oost et al., 2021).

2.4.4. Location of dumping sites within the coastal to offshore gradients

Changes in coastal ecosystems are often correlated with changes SPM concentration and composition and thus with the POM content of the SPM (e.g. May et al., 2003; Capuzzo et al., 2015). The area where PON_{diff} exhibits a low or negative value across the transect during spring and summer is of particular interest. PON_{diff} shows minimum values from April to September between the coast and 30 km offshore the Belgian coast, see Figures 2.6 and 2.9. During winter the PON is dominated by the mineral-associated fraction, while in spring and summer the fresh PON dominates in the offshore region and becomes more important in the nearshore area. The turbid nearshore area very close to the coast is still dominated by the mineral-associated fraction in April. Two dumping sites (i.e. ZBO and OST) are located in this mineral-dominated PON area and we expect that the dumping of dredged material has only minor effects on the pelagic habitat. The other dumping sites (i.e. S1, S2 and NWP) are located in the transition zone, where PON_{diff} shows minimum values from April to September. The offshore end of this zone seems to correspond with the *Abra alba* benthic habitat zone (Van Hoey et al. 2007). The bathymetry and the SPMC control the SPM composition and when SPMC changes, pelagic ecosystems may also change in terms of nutrient cycling, primary production, phytoplankton species composition. Further investigation is needed to evaluate the effect of dumping of dredged material in these area on the pelagic ecosystem.
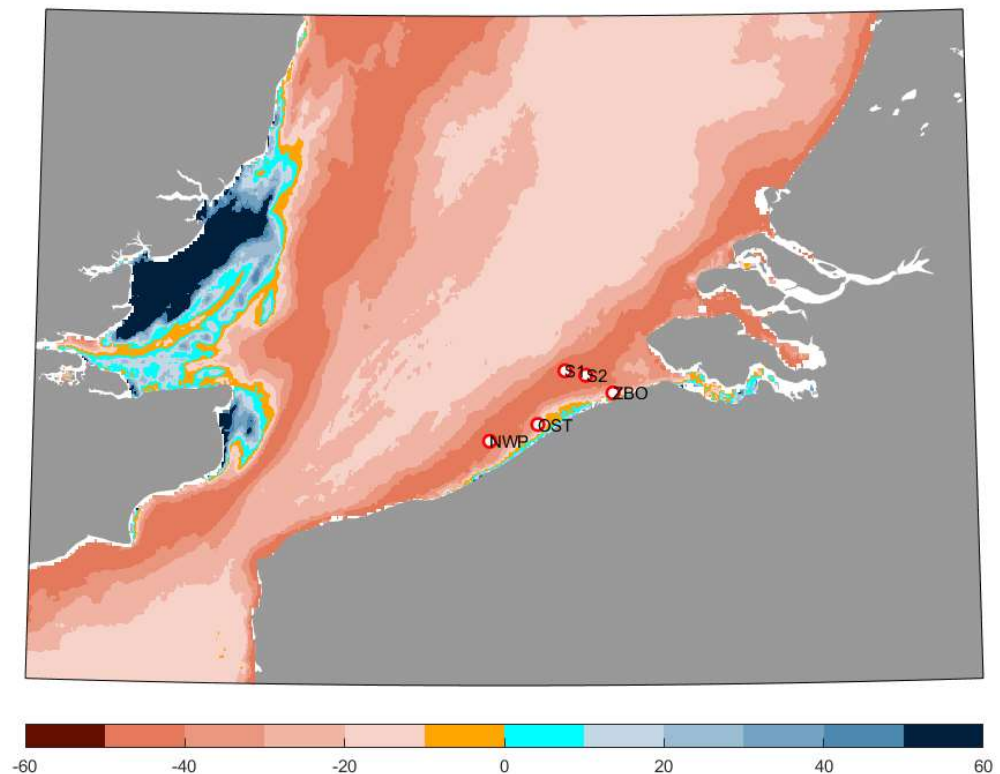

Figure 2.9: Surface PON_{diff} (PON_m-PON_f) concentration [mg N m^{-3}] in April 2020. The dots indicate the dumping sites (S1, S2, ZBO, OST and NWP) in the Belgian nearshore area.

2.5. Conclusions

The transition zone between coastal and offshore systems can be partly identified through particle dynamics. In the transition zone the settling of particles increases significantly at all seasons, making it an area of sediment accumulation. The scales of variability show that spatial and seasonal variabilities largely dominate the particle dynamics, suggesting that basin morphology and biological activity mainly control the processes at play. Bathymetry plays an important role in determining the turbulence and, hence, the settling rate of particles. Our study shows that the maximum net downward flux of particles mainly occurs within a range of bathymetry equal to 5-20 m. The seasonal production of phytoplankton considerably increases the flocculation and the particle settling. Due to tidal forcing, the sediment deposited in the transition zone can be transported toward the coast through estuarine circulation. In that case, the transition zone contributes to accumulating sediment at the coast and, thus, plays a similar role as the line of no return. As particulate organic matter is part of the SPM, the settling and accumulation of particles has an effect on the local storage of organic matter at the coast or its export flux toward the offshore. The coastal-offshore transition is a complex system subject to intense gradients and variability. In this study we aimed at reducing that complexity, and at deriving clearer information that may be useful in calculating carbon budgets or modelling the fate of organic matter across the land-ocean continuum.

3. Referenties

Adriaens R, Zeelmaekers E, Fettweis M, Vanlierde E, Vanlede J, Stassen P, Elsen J, Środoń J, Vandenberghe N. 2018. Quantitative clay mineralogy as provenance indicator for recent muds in the southern North Sea. Marine Geology, 398, 48-58. doi:10.1016/j.margeo.2017.12.011

Alldredge A, Passow U, Logan B. 1993. The abundance and significance of a class of large, transparent organic particles in the ocean. Deep Sea Research I 40, 1131–1140. doi:https://doi.org/10.1016/0967-0637(93)90129-Q

Baschek B, Schroeder F, Brix H, Riethmüller R, Badewien TH, Breitbach G, Brügge B, Colijn F, Doerffer R, Eschenbach C, Friedrich J, Fischer P, Garthe S, Horstmann J, Krasemann H, Metfies K, Merckelbach L, Ohle N, Petersen W, Pröfrock D, Röttgers R, Schlüter M, Schulz J, Schulz-Stellenfleth J, Stanev E, Staneva J, Winter C, Wirtz K, Wollschläger J, Zielinski O, Ziemer F. 2017. The coastal observing system for northern and arctic seas (COSYNA). Ocean Science 13, 379–410. doi:10.5194/os-13-379-2017

Becherer J, Flöser G, Umlauf L, Burchard H. 2016. Estuarine circulation versus tidal pumping: Sediment transport in a well-mixed tidal inlet. Journal of Geophysical Research Ocean 121: 6251–6270. doi:10.1002/2016JC011640

Becker GA, Dick S, Dippner JW. 1992. Hydrography of the German bight. Marine Ecology Progress Series 91, 9–18.

Blattmann TM, Liu Z, Zhang Y, Zhao Y, Haghipour N, Montluçon DB, Plötze M, Eglinton TI. 2019. Mineralogical control on the fate of continentally derived organic matter in the ocean. Science 366 742–745.

Brenon I, Le Hir P. 1999. Modelling the turbidity maximum in the Seine estuary (France): identification of formation processes. Estuarine, Coastal and Shelf Science 49, 525–544. doi:10.1006/ECSS.1999.0514

Capuzzo E, Stephens D, Silva T, Barry J, Forster RM. 2015. Decrease in water clarity of the southern and central North Sea during the 20th century. Global Change Biology 21, 2206–2214.

Desmit X, Nohe A, Borges AV, Prins T, De Cauwer K, Lagring R, Van der Zande D, Sabbe K. 2020. Changes in chlorophyll concentration and phenology in the North Sea in relation to de-eutrophication and sea surface warming. Limnology & Oceanography 65, 828–847. doi:10.1002/lno.11351

Du Z, Yu Q, Peng Y, Wang L, Lin H, Wang Y, Gao S. 2022. The Formation of Coastal Turbidity Maximum by Tidal Pumping in Well-Mixed Inner Shelves. Journal of Geophysical Research Ocean 127. doi:10.1029/2022JC018478

Dyer KR. 1989. Sediment processes in estuaries: Future research requirements. Journal of Geophysical Research 94(C10), 14,327–14,339.

Dyer KR, Moffat TJ. 1998. Fluxes of suspended matter in the East Anglia plume Southern North Sea. Continental Shelf Research 18, 1311-1331.

Eisma D. 1981. Supply and deposition of suspended matter in the North Sea. In: Nio S-D, Shüttenhelm RTE, Van Weering TCE (Eds.), Holocene Marine Sedimentation in the North Sea Basin. Blackwell Publishing Ltd., Oxford, UK.

Eisma D, Kalf J. 1979. Distribution and particle size of suspended matter in the Southern Bight of the North Sea and the Eastern Channel. Netherlands J. Sea Res. 13: 298–324. doi:10.1016/0077-7579(79)90008-5

Engel A, Endres S, Galgani L, Schartau M. 2020. Marvelous marine microgels: on the distribution and impact of gel-like particles in the oceanic water-column. Frontiers in Marine Science 7. doi:10.3389/FMARS.2020.00405/FULL

Engel A, Thoms S, Riebesell U, Rochelle-Newall E, Zondervan I. 2004. Polysaccharide aggregation as a potential sink of marine dissolved organic carbon. Nature 428: 929–932. doi:10.1038/nature02453

Ehrhardt M, Koeve W. 1999. Determination of particulate organic carbon and nitrogen. In Grasshoff K, Kremling K, Ehrhardt M (Eds.), Methods of seawater analysis (3rd ed., pp. 437–444). Wiley. doi:10.1002/9783527613984.ch17

Fettweis M, Houziaux J-S, Du Four I, Van Lancker V, Baeteman C, Mathys M, Van den Eynde D, Francken F, Wartel S. 2009. Long-term influence of maritime access works on the distribution of cohesive sediment: Analysis of historical and recent data from the Belgian nearshore area (southern North Sea). Geo-Marine Letters 29, 321-330. doi:10.1007/s00367-009-0161-7

Fettweis M, Monbaliu J, Baeye M, Nechad B, Van den Eynde D. 2012. Weather and climate induced spatial variability of surface suspended particulate matter concentration in the North Sea and the English Channel. Methods in Oceanography 3–4, 25–39. doi:10.1016/j.mio.2012.11.001

Fettweis M, Baeye M. 2015. Seasonal variation in concentration, size and settling velocity of muddy marine flocs in the benthic boundary layer. Journal of Geophysical Research Oceans, 120, 5648-5667. doi:10.1002/2014JC010644

Fettweis M, Lee BJ. 2017. Spatial and seasonal variation of biomineral suspended particulate matter properties in high-turbid nearshore and low-turbid offshore zones. Water, 9, 694. doi:10.3390/w9090694

Fettweis M, Riethmüller R, Verney R, Becker M, Backers J, Baeye M, Chapalain M, Claeys S, Claus J, Cox T, Deloffre J, Depreiter D, Druine F, Flöser G, Grünler S, Jourdin F, Lafite R, Nauw J, Nechad B, Röttgers R, Sotollichio A, Vanhaverbeke W, Vereecken H. 2019. Uncertainties associated with in situ long-term observations of suspended particulate matter concentration using optical and acoustic sensors. Progress in Oceanography, 178, 102162. doi:10.1016/j.pocean.2019.102162

Fettweis M, Schartau M, Desmit X, Lee BJ, Terseleer N, Van der Zande D, Parmentier K, Riethmüller R. 2022. Organic matter composition of biomineral flocs and its influence on suspended particulate matter dynamics along a nearshore to offshore transect. Journal of Geophysical Research Biogeosciences, 127, e2021JG006332

Flemming, B. W., and M. T. Delafontaine. 2000. Mass physical properties of muddy intertidal sediments: some applications, misapplications and non-applications. Cont. Shelf Res. 20: 1179–1197. doi:10.1016/S0278-4343(00)00018-2

Fugate DC, Friedrichs CT. 2002. Determining concentration and fall velocity of estuarine particle populations using ADV, OBS and LISST. Continental Shelf Research 22, 1867–1886. doi:10.1016/S0278-4343(02)00043-2

Gerritsen H, Boon JG, van der Kaaij T, Vos RJ. 2001. Integrated modelling of suspended matter in the North Sea. Estuarine, Coastal and Shelf Science 53, 581–594.

Hemingway JD, Rothman DH, Grant KE, Rosengard SZ, Eglinton TI, Derry LA, Galy VV. 2019. Mineral protection regulates long-term global preservation of natural organic carbon. Nature 570, 228–231. doi:10.1038/s41586-019-1280-6

Herman PMJ, van Kessel T, Vroom J, Dankers P, Cleveringa J, de Vries B, Villars N. 2018. Mud Dynamics in the Wadden Sea - Towards a Conceptual Model. Deltares Technical Report, 69pp.

Ho QN, Fettweis M, Spencer KL, Lee BJ. 2022. Flocculation with heterogeneous composition in water environments: A review. Water Research 213, 118147. doi:10.1016/j.watres.2022.118147

Huthnance JM. 1991. Physical Oceanography of the North Sea. Ocean & Shoreline Management 16, 199-231.

Jago CF, Bale AJ, Green MO, Howarth MJ, Jones SE, McCave IN, Millward GE, Morris AW, Rowden AA, Williams JJ. 1994. Resuspension processes and seston dynamics, southern North Sea, p. 97–113. In Charnock H, Dyer KR, Huthnance JM, Liss PS, Simpson JH, Tett PB [eds.], Understanding the North Sea System. Springer, Dordrecht; Chapman & Hall, for the Royal Society.

Jung AS, Bijkerk R, Van Der Veer HW, Philippart CJM. 2017. Spatial and temporal trends in order richness of marine phytoplankton as a tracer for the exchange zone between coastal and open waters. Journal of the Marine Biological Association UK 97, 477–489. doi:10.1017/S0025315416001326

Kopte R, Becker M, Holtermann P, Winter C. 2022. Tides, stratification, and counter rotation: The German Bight ROFI in comparison to other regions of freshwater influence. Journal of Geophysical Research: Oceans 127, e2021JC018236. https://doi.org/10.1029/2021JC018236

Lasareva EV, Parfenova AM. 2023. Influence of Organic Matter on the Transport of Mineral Colloids in the River-Sea Transition Zone, p. 1–20. In: Pereira L & Pardal M (Eds.), Oceanography - Relationships of the Oceans with the continents, their biodiversity and the atmosphere. IntechOpen. https://doi.org/10.5772/intechopen.110247.

Lauwaert B, Fettweis M, De Witte B, Van Hoei G, Timmermans S, Hermans L. 2019. Vooruitgangsrapport (juni 2019) over de effecten op het mariene milieu van baggerspeciestortingen (Vergunningsperiode 01/01/2017 – 31/12/2021). RBINS-ILVO-AMT-CD rapport. BL/2019/01, 28pp.

Lauwaert B, De Witte B, Festjens F, Fettweis M, Hermans L, Lesuisse A, Le H-M, Seghers S, Timmermans S, Vanavermaete D, Van Hoey G. 2021. Synthesis report on the effects of dredged material dumping on the marine environment (licensing period 2017-2021). RBINS-ILVO-AMT-AMCS-FHR report BL/2021/10, 67pp.

Logan BE, Passow U, Alldredge AL, Grossartt SM, Simont M. 1995. Rapid formation and sedimentation of large aggregates is predictable from coagulation rates (half-lives) of transparent exopolymer particles (TEP). Deep-Sea Research II, 42, 203–214. doi:10.1016/0967-0645(95)00012-F

Maerz J, Hofmeister R, Van Der Lee EM, Gräwe U, Riethmüller R, Wirtz KW. 2016. Maximum sinking velocities of suspended particulate matter in a coastal transition zone. Biogeosciences 13, 4863–4876. doi:10.5194/BG-13-4863-2016

Maggi F, Tang, FHM. 2015. Analysis of the effect of organic matter content on the architecture and sinking of sediment aggregates. Marine Geology 363, 102–111. doi:10.1016/j.margeo.2015.01.017

May CL, Koseff JR, Lucas LV, Cloern JE, Schoellhamer DH. 2003. Effects of spatial and temporal variability of turbidity on phytoplankton blooms. Marine Ecology Progress Series, 254, 111-128.

Nechad B, Ruddick K, Neukermans G. 2009. Calibration and validation of a generic multisensor algorithm for mapping of turbidity in coastal waters. In: Proceedings SPIE "Remote Sensing of the Ocean, Sea Ice, and Large Water Regions", SPIE Vol. 7473, 74730H.

Nechad B, Ruddick KG, Park Y. 2010. Calibration and validation of a generic multisensor algorithm for mapping of total suspended matter in turbid waters. Remote Sensing of Environment 114, 854-866. doi: 10.1016/j.rse.2009.11.022.

Neukermans G, Ruddick K, Loisel H, Roose P. 2012. Optimization and quality control of suspended particulate matter concentration measurement using turbidity measurements. Limnology and Oceanography: Methods, 10, 1011–1023. doi:10.4319/lom.2012.10.1011

Novoa S, Doxaran D, Ody A, Vanhellemont Q, Lafon V, Lubac B, Gernez P. 2017. Atmospheric Corrections and Multi-Conditional Algorithm for Multi-Sensor Remote Sensing of Suspended Particulate Matter in Low-to-High Turbidity Levels Coastal Waters. Remote Sensing 9, 61. doi:10.3390/rs9010061

Oost A, Alonso AC, Esselink P, Wang ZB, van Kessel T, van Maren B. 2021. Where mud matters. Towards a mud balance for the Trilateral Wadden Sea area: Mud supply, transport and deposition. Report, Wadden Academy, 154pp.

Otto L, Zimmerman JTF, Furnes GK, Mork M, Saetre R, Becker G. 1990. Review of the Physical Oceanography of the North Sea. Netherlands Journal of Sea Research 26, 161-238.

Pearson SG, Verney R, van Prooijen BC, Tran D, Hendriks ECM, Jacquet M, Wang Z B. 2021. Characterizing the composition of sand and mud suspensions in coastal and estuarine environments using combined optical and acoustic measurements. Journal of Geophysical Research Oceans 126, e2021JC017354. Doi:10.1029/2021JC017354

Postma H. 1954. Hydrography of the Dutch Wadden sea. Archives Néerlandaises de Zoologie 10, 405–511.

Postma H. 1981. Exchange of materials between the North Sea and the Wadden Sea. Marine Geology 40, 199–213. doi:10.1016/0025-3227(81)90050-5

Postma H. 1984. Introduction to the symposium on organic matter in the Wadden Sea. Netherlands Institute of Sea Research - Publication Series 10, 15–22.

Prandle D, Ballard G, Flatt D, Harrison AJ, Jones SE, Knight PJ, Loch SG, McManus JP, Player, R, Tappin A. 1996. Combining modelling and monitoring to determine fluxes of water, dissolved and particulate metals through the Dover Strait. Continental Shelf Research 16, 237-257.

Prandle D, Hydes DJ, Jarvis J, McManus J. 1997. The seasonal cycles of temperature, salinity, nutrients and suspended sediment in the southern North Sea in 1988 and 1989. Estuarine, Coastal and Shelf Science 45, 669–680.

Riebesell U. 1991. Particle aggregation during a diatom bloom II. Biological aspects. Marine Ecology Progress Series 69, 281–291.

Rijnsburger S, van der Hout C, van Tongeren O, de Boer G, van Prooijen BC, Borst WG, Pietrzak JD. 2016. Simultaneous measurements of tidal straining and advection at two parallel transects far downstream in the Rhine ROFI. Ocean Dynamics 66, 719-736.

Röttgers R, Heymann K, Krasemann H. 2014. Suspended matter concentrations in coastal waters: Methodological improvements to quantify individual measurement uncertainty. Estuarine, Coastal and Shelf Science 151, 148–155. doi:10.1016/j.ecss.2014.10.010

Schartau M, Riethmüller R, Flöser G, van Beusekom JEE, Krasemann H, Hofmeister R, Wirtz K. 2019. On the separation between inorganic and organic fractions of suspended matter in a marine coastal environment. Progress in Oceanography 171, 231–250.

Schwarz C, Cox T, van Engeland T, van Oevelen D, van Belzen J, van de Koppel J, Soetaert K, Bouma TJ, Meire P, Temmerman S. 2017. Field estimates of floc dynamics and settling velocities in a tidal creek with significant along-channel gradients in velocity and SPM. Estuarine, Coastal and Shelf Science 197, 221-235. doi: 10.1016/j.ecss.2017.08.041

Spencer KL, Wheatland JAT, Bushby AJ, Carr SJ, Droppo IG, Manning AJ. 2021. A structure–function based approach to floc hierarchy and evidence for the non-fractal nature of natural sediment flocs. Scientific Reports 11, 14012 (2021). doi:10.1038/s41598-021-93302-9

Stavn RH, Rick HJ, Falster AV. 2009. Correcting the errors from variable sea salt retention and water of hydration in loss on ignition analysis: Implications for studies of estuarine and coastal waters. Estuarine, Coastal and Shelf Science 81, 575–582. doi:10.1016/j.ecss.2008.12.017

van Beusekom JEE, Carstensen J, Dolch T, Grage A, Hofmeister R, Lenhart H, Kerimoglu O, Kolbe K, Pätsch J, Rick J, Rönn L, Ruiter H. 2019. Wadden sea eutrophication: Long-term trends and regional differences. Frontiers in Marine Science 6, 1–17. doi:10.3389/FMARS.2019.00370

Simpson JH, Brown J, Matthews J, Allen G. 1990. Tidal straining, density currents, and stirring in the control of estuarine stratification. Estuaries 13: 125–132. doi:10.2307/1351581

Van Hoey G, Vickx M, Degraer S. 2007. Temporal variability in the Abra alba community determined by global and local events. Journal of Sea Research 58, 144-155.

Wakelin SL, Holt JT, Blackford JC, Allen JI, Butenschön M, Artioli Y. 2012. Modeling the carbon fluxes

of the northwest European continental shelf: Validation and budgets. Journal of Geophysical Research Ocean 117, 5020. doi:10.1029/2011JC007402

Yu M, Yu X, Mehta AJ, Manning AJ. 2023. Persistent reshaping of cohesive sediment towards stable flocs by turbulence. Scientific Reports 13, 1760. doi:10.1038/s41598-023-28960-y

Zhu Y, Lin M, Shen X, Fettweis M, Zhang Y, Zhang J, Bi Q, Wi Z. 2022. Bio-mineral flocculation of kaolinite and microalgae: Laboratory experiments and stochastic modeling. Journal of Geophysical Research Ocean 127, e2022JC018591. Doi:10.1029/2022JC018591

COLOPHON

BEHEERSEENHEID VAN HET
MATHEMATISCH MODEL VAN DE NOORDZEE
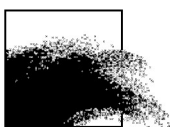
APPENDIX 1

Abstract & poster
ASLO Aquatic Sciences Meeting, 4–9 June 2023,
Palma de Mallorca (Spain)

From brown to blue water: Unraveling spatio-temporal variations in the organic matter content of suspended particulate matter

Markus Schartau, GEOMAR Helmholtz Centre for Ocean Research Kiel, Germany (mschartau@geomar.de)
Michael Fettweis, Royal Belgian Institute of Natural Sciences, Belgium (mfettweis@naturalsciences.be)
Xavier Desmit, Royal Belgian Institute of Natural Sciences, Belgium (xdesmit@naturalsciences.be)
Nathan Terseleer, Royal Belgian Institute of Natural Sciences, Belgium (nterseleerlillo@naturalsciences.be)
Rolf Riethmüller, Helmholtz Zentrum hereon, Germany (rolf.riethmueller@hereon.de)

The determination of biogeochemical fluxes across the land-ocean-continuum is challenging, because of the interaction between particulate organic matter (POM) and mineral particles and the extensive variability of their concentrations. Suspended particulate matter (SPM) consist of POM and of mineral particles. Some, rather recalcitrant, portion of the POM is associated with mineral particles of resuspended sediments whereas another fraction is produced and degraded on a seasonal scale. Analyses of the POM content of SPM along the transition from brackish towards clearer marine waters, or during periods of varying turbidity of a tidal cycle, disclose similar patterns: at high SPM concentrations, variations of the POM fraction of SPM remain small; towards off-shore waters, the POM content becomes highly variable but reveals a nonlinear increase with decreasing SPM concentration. A semi-empirical modelling approach was developed to describe these predominant changes of the POM content as a function of the SPM concentration. A prerequisite for obtaining valuable model estimates is the calibration of the model with field data, of e.g. loss on ignition (for POM), particulate organic carbon, nitrogen (POC, PON), or transparent exopolymer particles (TEP) measurements together with corresponding SPM concentrations. The model can then be applied to independent SPM data, e.g. derived from remote sensing. We will show how our data-model syntheses facilitate the unraveling of spatio-temporal variations of POM, POC, PON, and TEP, across the transition from the coast towards the ocean.

Interactions between phytoplankton, marine gels and suspended particulate matter in a dynamic, shallow coastal system before and during the phytoplankton spring bloom.

Auria Kallend[1], Jens H. Dujardin[1, 2], Michael Fettweis[3], Wim Vyverman[1], Maarten De Rijcke[2], Koen Sabbe[1], Xavier Desmit[3]
[1] Protistology and Aquatic Ecology, Universiteit Gent, Gent, BE ; [2] VLIZ, Oostende, BE ; [3] Operational Directorate Natural Environment, Royal Belgian Institute of Natural Sciences, Brussels, BE
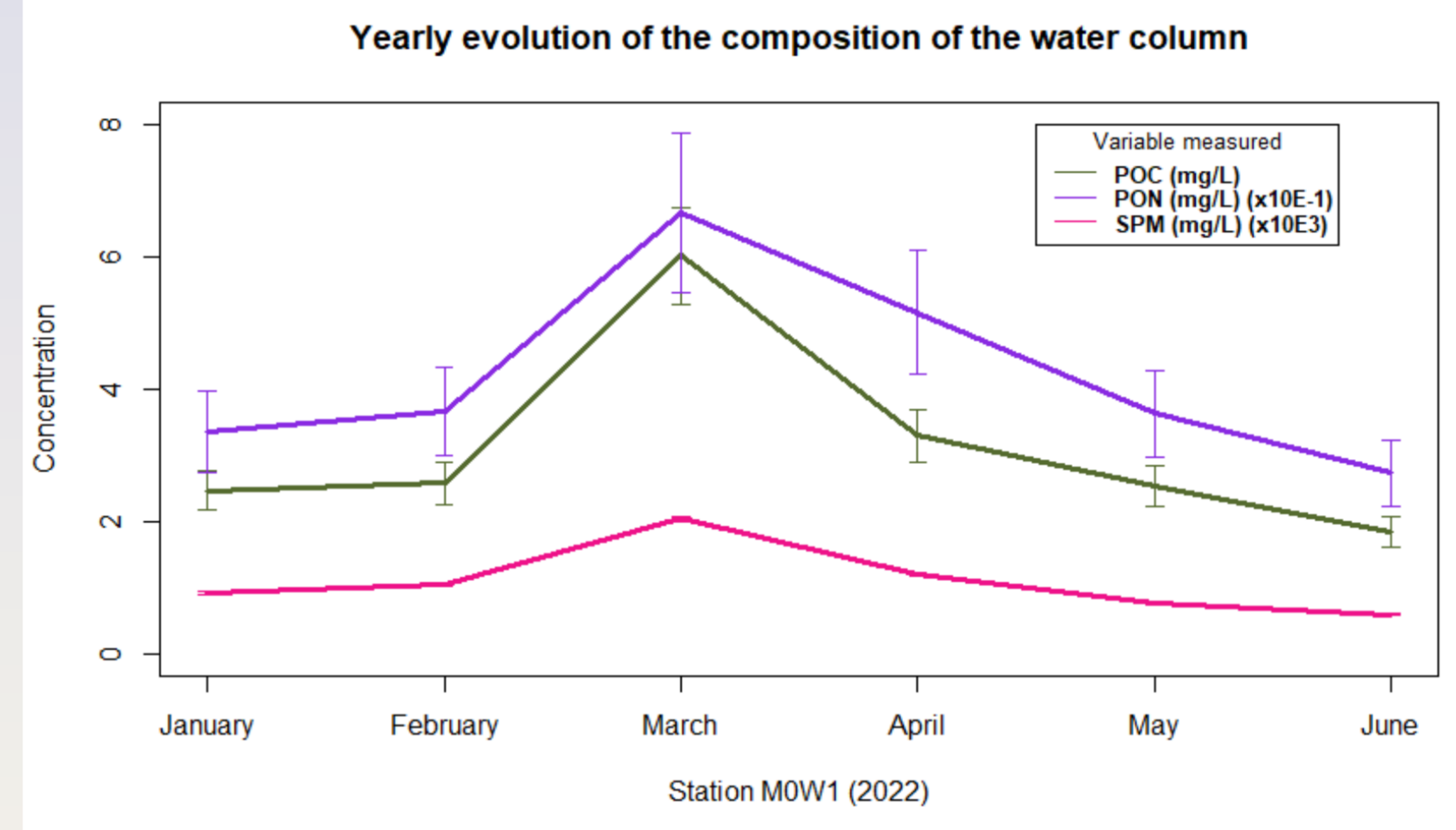
Introduction

Suspended Particulate Matter (SPM) is a key determinant of biological processes, ecosystem functioning and biogeochemical fluxes in coastal ecosystems. While SPM dynamics is primarily controlled by hydrodynamic forcing and the physical and chemical properties of the particles, it is becoming increasingly clear that biological activity also affects the size and settling of particle aggregates. The release of exopolymeric substances (EPS) by phytoplankton and the formation of sticky marine gels will stimulate flocculation, while bacterial mineralisation and grazing can break down the flocs. To date however, in contrast to the open ocean, little is known about the relative importance of physical and biological processes for SPM dynamics in highly productive yet turbid shallow coastal areas. We aim to assess the importance of interactions and feedback mechanisms between biological activity and the mineral particles for SPM dynamics and ecosystem functioning on the Belgian Continental Shelf (BCS).

Hypotheses

The cohesive and non-cohesive mineral fractions of the SPM differently affect flocculation processes. In winter, the flocs are mainly made of cohesive minerals, while in summer non-cohesive minerals may be integrated in the flocs due to the production of fresh marine gels. The fine grained non-cohesive minerals, which remain outside flocs in winter, settle slowly and remain in suspension longer, resulting in a background turbidity that is higher than in summer.

Method

- Samples are taken with Niskin bottles set on a rosette alongside a CTD sensor.
- Samples are taken hourly along a full tidal cycle (unless the weather was not allowing), i.e. 12 hours.
- A surface and a bottom cast are taken for each sampling time.
- In the Results section, we present data from the winter-spring 2022.
- Station M0W1 is located in the shallow, tidal coastal zone, close to the mouth of the river Scheldt and is therefore subject to eutrophication.
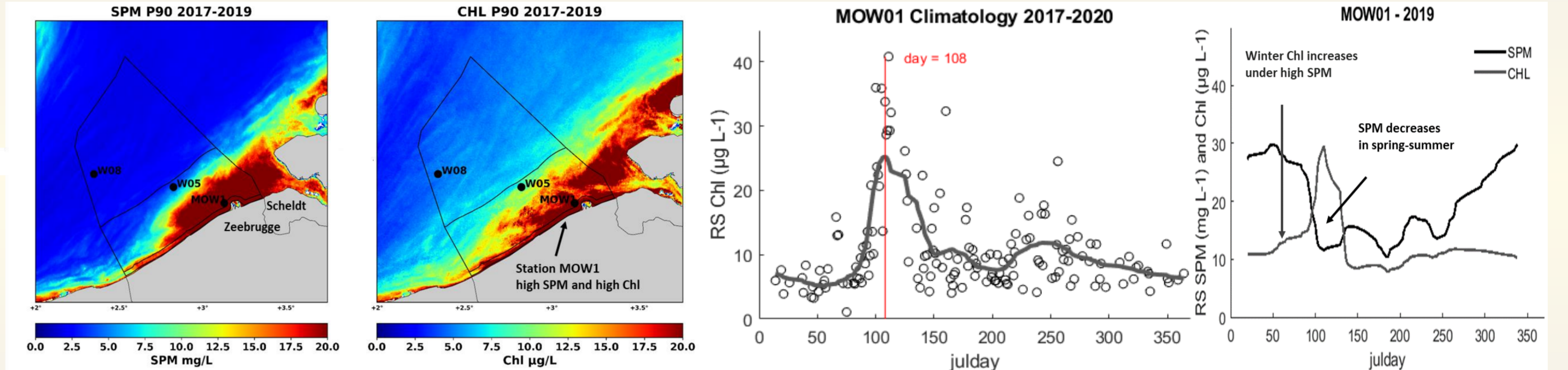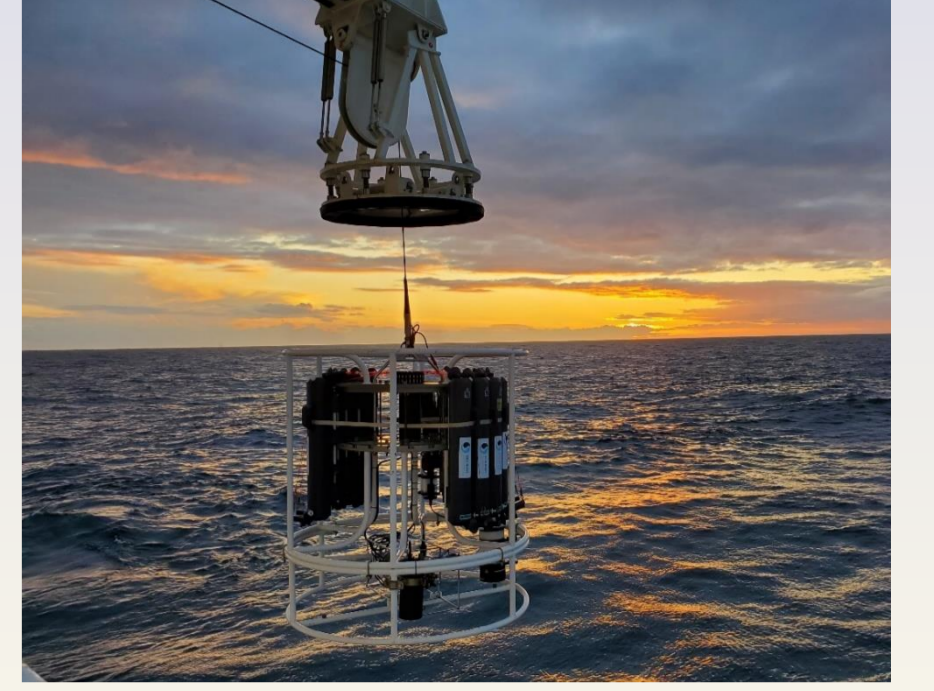
Figure 1: Multi year mean of P90 SPM, Chl a concentrations in the BCS and Climatolgy showing the Chl a max from 2017 to 2020.

- Analysis of the samples : suspended particulate matter (SPM), transparent exopolymers (TEP), exopolysaccharides (EPS, TEP precursors, exuded by phytoplankton), Coomassie stainable particles (CSP, which are exuded when the cells die), dissolved organic carbon, particulate organic carbon (POC) and nitrogen (PON), pigments (chlorophyll, phaeophytine), turbidity.
- The salinity and temperature *in situ* are also recorded by the CTD.

Preliminary results

- SPM, POC and PON are low in winter, increase in early spring (March) after which they gradually decline. Generally SPM is higher in winter than in spring[1]. It could be that the high values in March are caused by e.g. neap-spring tide variations. Because of the strong adhesion of OM (POC, PON and TEP, probably also CSP) to clay minerals, there is always a high OM concentration when SPM is high[1,2].
- There is a secondary pattern for TEP and CSP concentrations, which are high in the winter.
- TEP concentration peaks in March, while CSP gradually declines from winter to spring, with a minor peak in April.
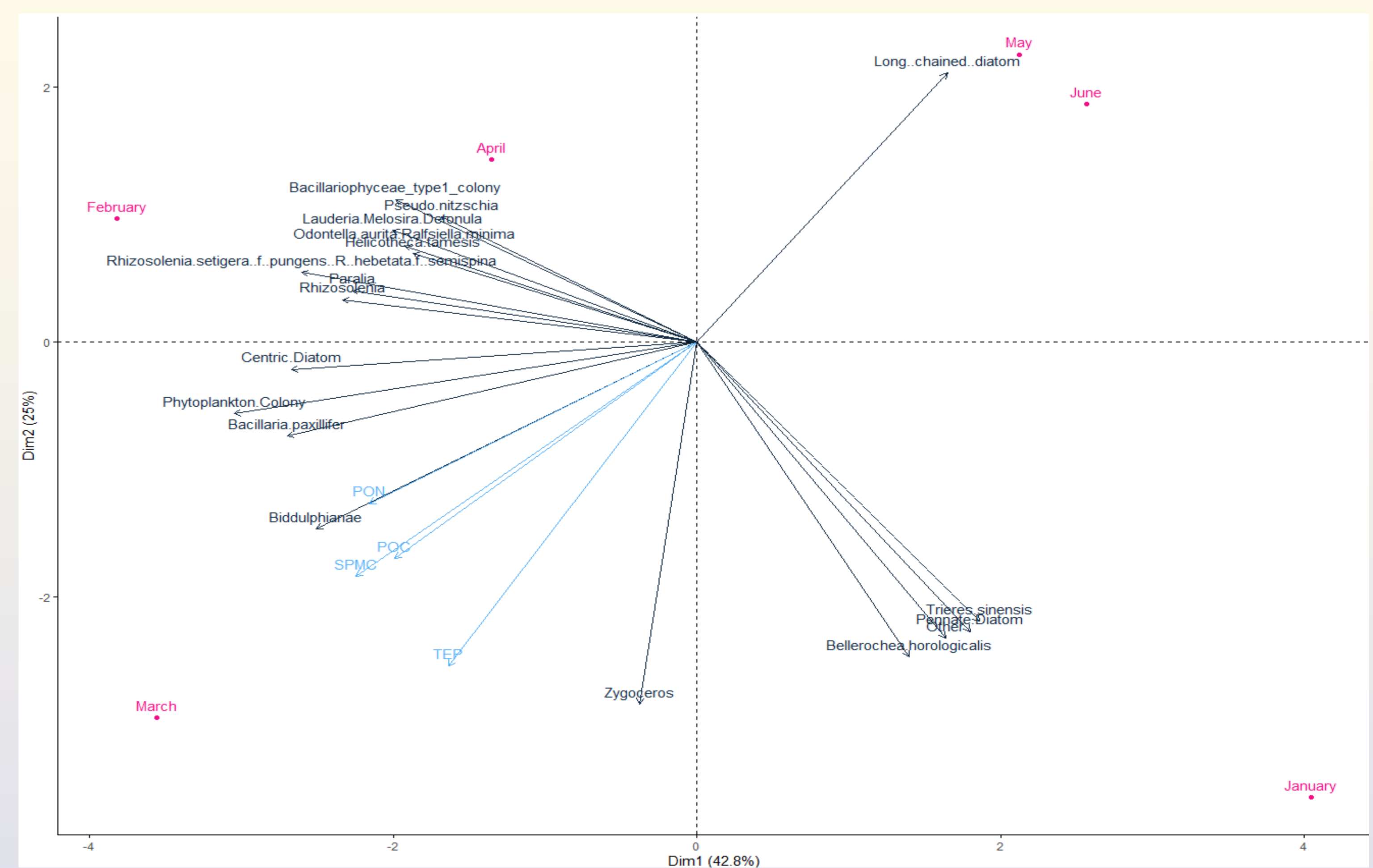

- The dominant species of the community follow the same pattern: *Bellerochea sp.* dominated community in the winter, *Rhizosolenia sp.* dominated community in the early spring and long chained diatoms in the late spring/early summer.
- There is a significant difference (*p*-value < 0,05) in the relative abundance of these taxa between their prominent season and the other seasons.
- There is a significant difference (*p*-value < 0,05) in the relative abundance between the dominant taxon and the other 2 for every season.
- The larger, less buoyant cells tend to sink during slack water, before being resuspended during maximum current velocity periods therefore they seem to disappear from the surface community at slack water.

Figure 2: Yearly evolution of the phytoplanktonic community composition

- The 1*st* axis of the PCA is composed of the late winter/early spring species (i.e. transition species), and the 2*nd* axis of the winter and early summer species (i.e. communities with stronger contrast).
- The chemical parameters (i.e. PON, POC, SPM and TEP) seem to be mostly correlated with the spring community.
- Each season is characterized by a community and a set of environmental conditions.

Figure 3: Principal component analysis of the relationship between phytoplankton species and the different chemical parameters measured

Conclusions

Observations presented in this poster are based on preliminary results. As the effort of analysing and processing the 18 months sampling of the BG-Part project is still ongoing, there is evidence that sediment-microgels shape the phytoplanktonic community in the Belgian part of the North Sea. In the upcoming 2,5 years the rest of the parameters from the BG-Part sampling campaigns will be analysed and experiments will be conducted to test the hypotheses of the project.

References
1 Fettweis et al. 2022 JGR Biogesciences, 10.1029/2021JG006332
2 Hemingway et al. 2019 Nature 570, 228-231

APPENDIX 2

Fettweis M, Riethmüller R, Van der Zande D, Desmit X. 2023. Water quality monitoring in coastal seas: How significant is the information loss of patchy time series? Science of the Total Environment 873, 162273.

Sample based water quality monitoring of coastal seas: How significant is the information loss in patchy time series compared to continuous ones?

Michael Fettweis [a],[*], Rolf Riethmüller [b], Dimitry Van der Zande [a], Xavier Desmit [a]

[a] OD Natural Environment, Royal Belgian Institute of Natural Sciences, rue Vautier 29, 1000 Brussels, Belgium
[b] Institute of Coastal Ocean Dynamics, Helmholtz-Zentrum Hereon, Max-Planck-Str. 1, 21502 Geesthacht, Germany

HIGHLIGHTS

- Suspended particulate matter and chlorophyll concentrations show high variability in tidal systems.
- Common monitoring programmes have been evaluated against continuous data series.
- Low-frequency sampling may cause high uncertainties in annual mean and trend estimates.
- Discrete time series are better suited for low turbide and less dynamic systems.
- Tidal turbid systems require continuous time series.

GRAPHICAL ABSTRACT
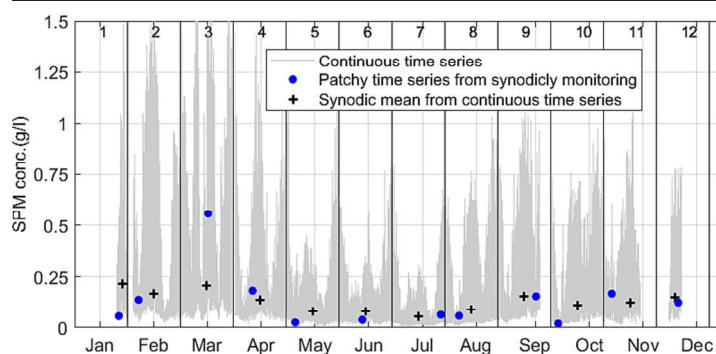
ABSTRACT

The high temporal and spatial variability of tidal dominated coastal areas poses a challenge for characterising water quality. Water quality monitoring relies often on information collected by water sampling from a vessel or by satellites, and covers limited time periods and therefore limited tidal and meteorological conditions. To assess the loss of information from discrete sampling, continuous time series of one year (suspended particulate matter (SPM) concentration, SPM flux and Chlorophyll a (Chl) concentration) were used. Eight different schemes of sampling into these time series were applied that are typical for many monitoring programs. They differ in the time between sampling events (synodic or half-synodic) and the duration of the sampling (tidal cycle, half a tidal cycle, one or more samples). The information loss was quantified by applying a bootstrap method to calculate the mean and standard deviation over the considered period. These were then compared with the true mean calculated from the continuous series. The probability to match the true mean within a certain margin depends on the sampling period and the season, but it is always low, especially if the allowed uncertainty is stringent (e.g., ±2.5 % about the true mean). For the SPM concentration this probability is lower than 10 % and for Chl concentration lower than 20 %. Similarly, conclusions arise for the detection of trends in a 20 year time series of SPM concentration with an artificial yearly increase of 0.5 %. None of the sampling schemes was able to assess statistical significant interannual trends with probabilities above 60 %. Further, the significant trends overestimated the increase by a factor 2 to 8. Here, present modus operandi is thus inadequate for basic trend detection, but may be acceptable for the more marine, lower turbid areas where higher probabilities were obtained in this study.

1. Introduction

The purpose of water quality monitoring in marine waters is multiple. From a policy perspective it may consist in identifying pollutant concentrations exceeding their threshold value, detecting harmful algae blooms,

evaluating the ecological status of an area or detecting trends. From a scientific perspective the data may be used to quantify the mean biogeochemical properties of a system, evaluating variations at different time scales, understanding the element cycles and their underlying processes and validating model predictions related to major trends such as global warming or the discharge of nutrients into the sea. These objectives require a long time series of water quality data that will also help policy to develop effective strategies for mitigation in case for example of eutrophication, effects of human activities at sea or accidental pollution (Lovett et al., 2007; Conley et al., 2009; Kirby and Law, 2010; Mack et al., 2020). Generally, measurements from a monitoring program that rely on water sampling from a vessel or on remote sensing data are limited to moderate and in the latter case cloud free meteorological and oceanographic conditions. It is thus essential to assess the representativeness of such a subsample of the data population and to evaluate the information loss provided by patchy and discrete sampling (e.g. Erkkilä and Kalliola, 2007; Anttila et al., 2012; Lin et al., 2022).

In this study, three water quality parameters are considered: turbidity, which is controlled by the concentration, size and composition of suspended particulate matter (SPM), the flux of SPM and chlorophyll *a* (Chl) concentration as a proxy for phytoplankton abundance. They are representative for key processes in the food web and element cycling on shelf seas on different time scales: a vertical resuspension-deposition pattern of SPM on the scale of tides and in many areas waves on the scale of low pressure passages, a directional pattern of horizontal SPM fluxes governed by variations in ebb-flood currents, and a seasonal pattern of Chl concentration that is controlled by primary production and grazing. Other particulate water quality parameters fit into these types of variability, such as particulate organic matter (POM) concentration, pollutants adsorbed to clay minerals and the transport of microplastics and pollutants. Turbidity is the oldest water quality parameter; the first standardised method used Secchi disks and dates back to the 19th century (Wernand, 2010). Today, water sampling, optical back- or side scatter sensors, acoustic backscatter sensors and satellites provide data on SPM concentration (e.g. Grabemann and Krause, 1989; Druine et al., 2018; Herman et al., 2018). Chl is correlated with the phytoplankton biomass and thus with the particulate organic matter (POM) pool; it can be obtained directly from water samples, indirectly by fluorometers (Roesler et al., 2017) and satellite observations (Harvey et al., 2015). The SPM concentration may further act as a proxy for the organic components, such as the content of POM in the SPM; and the concentration of particulate organic carbon (POC), particulate organic nitrogen (PON) and transparent exopolymer particles (TEP) (Keil et al., 1994; Ransom et al., 1998; Schartau et al., 2019; Fettweis et al., 2022), or for the occurrence of trace metals or organic pollutants adsorbed onto clay minerals and microplastics (Kowalska et al., 1994; Gaulier et al., 2019; Shen et al., 2023).

The data from water samples or from satellites provide a distorted image of the continuous variability as they consist of time series at low-frequent discrete time intervals, which are in contrast with high-frequent time series from buoys or landers that incorporate all relevant amplitudes in the variations. The study focuses on coastal areas in the North Sea, where the hydrodynamics are dominated by tides. The main frequencies of variability are quarter-diurnal (about 6.2 h), semidiurnal (12.4 h), half-synodic (14.7 days) and synodic (29.5 days). Further the effect of biology is responsible for seasonal variations. Additional variations have lower (interannual variations) or higher frequencies (turbulence) or occur irregularly such as variations caused by extreme weather events or human activities. The three parameters vary along all these time scales due to their fast response to changes in physical forces, whether caused by astronomical (tides, seasons), climatological or human effects or nutrient and light availability. The objectives of the study are to understand the effect of a sampling scheme and thus the frequency of the sampling on the information that is collected. We have used high-frequency data as a sufficient approximation to a continuous time series of SPM, SPM flux and Chl concentration from a tidally dominated coastal area to answer the significance of information loss in relation to lower-sampling schemes, and the effect of this sampling on the detection of interannual trends.

2. Method

2.1. Continuous time series

In order to evaluate the loss of information due to discrete sampling and the representativeness of a sampling scheme, we have used the 2013 high-frequency (Δt = 15 min) time series of calibrated Optical Backscatter Sensor (OBS) derived SPM concentration and ADCP derived current velocity data from MOW1 station located in the southern Bight of the North Sea (Fettweis et al., 2016). SPM flux has been calculated as the product of the SPM concentration and the current velocities and is expressed as kg/m^2s. The fluorescence data were recorded in spring 2016 and summer 2017 in the same station. Fluorescence was converted to Chl concentration (expressed in μg/l) using the factory specifications of the Eco-FL sensor (Sea-Bird Electronics, 2011). The data have been collected at the MOW1 coastal observatory located in the Belgian nearshore area (51°N 21.30′, 3°E 07.85′) at 2 m above the bed. The average water depth is about 12 m. Located some 5 km away from the shoreline it is situated within a coastal turbidity maximum area where SPM concentrations vary between 20 mg/l and >3000 mg/l at 2 m above the bed. The Belgian nearshore is characterised by semidiurnal tides with a mean tidal amplitude of 3.6 m. The tidal current ellipses are elongated and vary on average between 0.2 and 0.8 m/s during spring tide and 0.2 and 0.5 m/s during neap tide at 2 m above the bed. The strong tidal currents, the shallowness and the low freshwater discharges result in a well-mixed water column. The residual alongshore currents and the residual SPM fluxes at MOW1 are, respectively, in 53 % and 80 % of the time directed towards the NE, which occur during periods of prevailing SW winds.

Both the SPM concentration and flux time series from MOW1 consists of 27,849 data distributed over the four seasons, while the Chl concentration time series counts 12,574 data distributed over spring and summer. Although the Chl time series covers only 35 % of the year, it incorporates critical periods, that is, spring and summer but does not include other periods, such as the start of the bloom in February and the late summer/early autumn bloom. Therefore, a true annual mean cannot be derived from it. Fig. 1 shows the time series of SPM and Chl concentrations, and of SPM flux at MOW1 together with the tidal amplitude. Additionally, the mean over a certain period (can be synodic or half-synodic) is shown in the figure. This mean is considered as the true mean.

Additionally, the 2010 time series (Δt = 120 min) of turbidity (algae and non-algae) from the West Gabbard smart buoy (51°N 58.82′; 2°E4.97′) was used as an example of a location with lower turbidity. The turbidity is about 10 times lower than at MOW1 and the time series was used in this study only for trend detection. West Gabbard is located in well-mixed conditions in about 30 m water depth at 36 km offshore (https://wavenet.cefas.co.uk/SmartBuoy). The time series consists of 3906 data.

2.2. Simulation experiments with sampling schemes

Our approach simulated a number of in-situ water sampling schemes by picking and choosing data from the high-frequency time series according to in-situ monitoring programmes with monthly or two-weekly sampling occasions and earth reconnaissance satellite programmes with daily overflight repetitions-. In total, ten different sampling schemes with varying sampling frequency have been implemented (Table 1). The six in situ random schemes can be divided into synodic (Synodic) and half-synodic (Hsynodic) depending on the time between two successive sampling events. The samples are selected by a random number generator during every synodic or half-synodic periods. The time between two successive sampling events is on average the duration of the considered period, but may vary between 1 day and two times the considered period.

Secondly, we considered four non-random schemes with regularly-spaced sampling events to simulate the one-pixel time-series as collected by polar orbiting earth reconnaissance satellites, such as e.g. MODIS-AQUA, MERIS, Sentinel-3/OLCI (Alvera-Azcaráte et al., 2021). The satellite sampling schemes are divided into an ideal and a realistic one. In the ideal satellite scheme, a sample is taken daily at the same time (noon), simulating
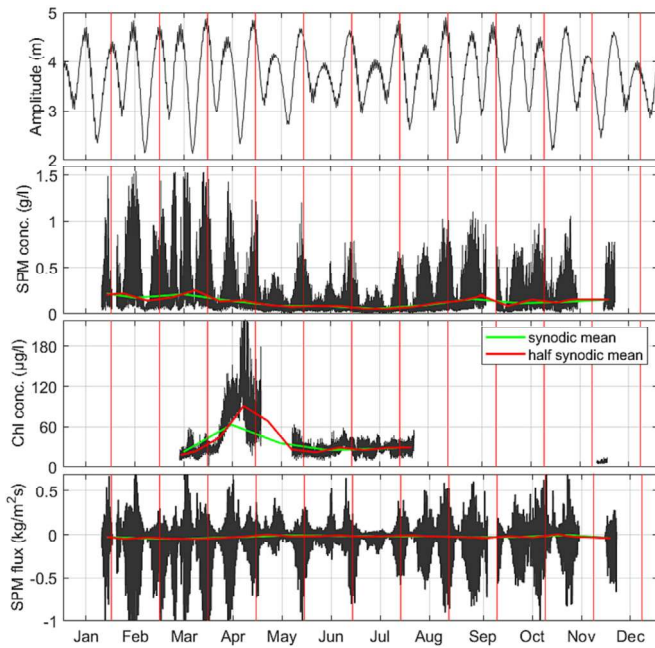
Fig. 1. Tidal amplitude, SPM concentration, Chl concentration and SPM flux in 2013 at 2 m above the bed at MOW1. The red vertical lines indicate synodic periods. Further are shown the SPM and Chl concentrations, and SPM flux mean and over synodic and half synodic periods. (For interpretation of the references to color in this figure legend, the reader is referred to the web version of this article.)

cloud-free conditions. In the realistic satellite scheme, the sample is also taken at the same time during the day, however, cloud coverage and solar inclination angle are taken into account. As a consequence the number of data available is considerably lower and equal to 92 on average per year over the period 1998–2020. The number of data points varies seasonally from one in December and January up to twelve in the summer months.

The total number of samples per year taken by the random schemes Synodic-1 and Hsynodic-1 amounts to 156 and 286 (corresponding to 13 hourly samples or a full tidal cycle for each of the 12 synodic or 22 half-synodic periods) respectively, and 72 and 132 (corresponding to 6 hourly samples or half a tidal cycle for each of the 12 synodic or 22 half-synodic period) for the random schemes Synodic-2 and Hsynodic-2. For the Synodic-3 and Hsynodic-3 the total number of samples equals 12 and 22 respectively. The synodic and half-synodic random sampling schemes 1 and 2

Table 1
Sampling schemes used in the analysis. During a tidal cycle 13 hourly samples are for schemes Synodic_1 and Hsynodic_1; 6 hourly samples (half a tidal cycle) for schemes Synodic_2 and Hsynodic_2 and one sample for schemes Synodic_3 and Hsynodic_3. The ideal satellite schemes take a sample once a day at noon. For the realistic satellite schemes the number of samples depends on the season and varies between 1 in winter and 12 in summer for synodic period and 1 till 7 for the half synodic period.

Sampling scheme		Period	Tidal cycle	Number of samples per period	Number of samples per year
Random "in situ"	Synodic_1	29.5 days	1	13	156
	Synodic_2	29.5 days	0.5	6	72
	Synodic_3	29.5 days	–	1	12
	Hsynodic_1	14.7 days	1	13	286
	Hsynodic_2	14.7 days	0.5	6	132
	Hsynodic_3	14.7 days	–	1	22
Satellite	Synodic_ideal	29.5 days	–	30	365
	Hsynodic_ideal	14.7 days	–	15	365
	Synodic_realistic	29.5 days	–	1–12	92
	Hsynodic_realistic	14.7 days	–	1–7	92

resolve the quarter-diurnal and/or semidiurnal tidal variabilities, while random schemes 3 and the satellite sampling schemes do not.

To quantify the degree of information loss of the reduced sampling schemes, we computed a number of monitoring key quantities, i.e. half-synodic, synodic and annual means for both the constructed reduced-sample and the high-frequency MOW1 data time-series. We assumed the high-frequency means to represent the "true" values with no error and quantified the information loss of discrete low-frequency sampling by the differences between the "true" means and the "discrete sampling" means in probabilities due to the standard deviations of the latter. These standard deviations were computed for each sampling scheme (except for the ideal satellite schemes) by a bootstrap method. The bootstrap method is a statistical technique for estimating quantities, such as the mean or the standard deviation, about a population by averaging estimates from multiple small data samples (Efron, 1979). We performed 1000 iterations with randomly altered sampling times to quantify the standard deviations of the annual, synodic and half-synodic means. The number of data available for the random sampling scheme varies between 1416 (half-synodic) and 2832 (synodic period). For the real satellite sampling schemes this number is 15 and 30, as the random selection only picks up the day in the period, while the time is always at noon.

In order to test if interannual trends can be detected from the data extracted by the sampling schemes, time series of 20 years of SPM concentration or turbidity were constructed based on the concatenation of 20 times the MOW1 or the West Gabbard time series. The first year is the original time series, the successive years each have a 0.5 % higher SPM concentration or turbidity than the previous year. The mean SPM concentration or turbidity in year 20 is thus about 10 % higher than from the original time series. The satellite schemes cannot be applied to such a time series as they would pick every year values at the same moments of the tide, which is not realistic. Therefore, the satellite sampling schemes were adopted for the trend analysis such that a time was randomly chosen for every year; all the data selected during this year have the same time. The trend was calculated by a linear regression. The slope of the regression gives the trend while the p value provides its statistical significance, which is set as $P < 0.05$.
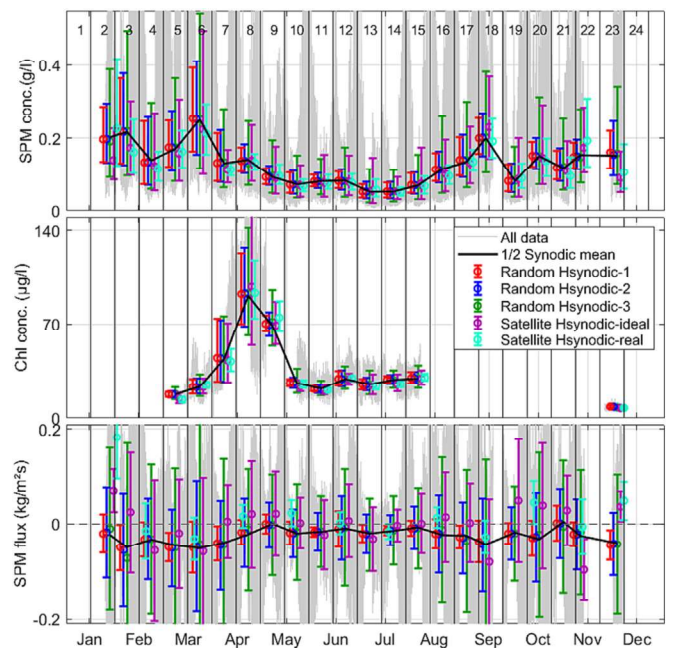

Fig. 2. True half synodic mean SPM and Chl concentrations and SPM fluxes (black line) together with corresponding means from the random and satellite half synodic sampling scheme at MOW1. The error bars display the standard deviations (see text) for the random and the satellite schemes.

3. Results

3.1. Periodic and annual mean derived from sampling schemes

As a first step we compared the half-synodic (Fig. 2) and synodic means (Fig. 3) computed for the high-frequency continuous data series and from the 1000 bootstrap subsampling of the above listed sampling schemes. The means of the 1000 bootstrap samplings are obviously close to the true means for all sampling schemes except for the satellite schemes in winter. However, the magnitudes of their standard deviations demonstrate the strong sensitivity of the individual means to altered picking times within each scheme. The magnitude of the standard deviations is determined by the number of samples involved and the variability in the high-frequency data. They are highest for the sampling schemes with the lowest number of samples (scheme 3) and lowest for the random sampling schemes with the highest number of samples (scheme 1) and show seasonal variations. For SPM concentration and flux they are higher in winter than in summer, as SPM concentration shows higher variability in winter. For Chl concentration the standard deviations are highest in spring, when the value changes fast during the spring bloom. The realistic satellite sampling schemes have more samples in spring and summer than in winter. Therefore, the satellite sampling in winter shows results closer to the random synodic and half-synodic sampling schemes-3. In contrast, in spring and summer, the standard deviation of the realistic satellite sampling scheme gets closer to the ones of the random schemes 1 and 2. This is because the number of data in the realistic satellite schemes is closer to the number of data in random schemes 1 and 2 depending on the satellite sampling considered (i.e., synodic or half-synodic).The standard deviation for the ideal satellite schemes is low during summer and slightly larger during winter for SPM concentration, while for Chl concentration highest standard deviations are occurring in spring.

Table 2
Probability (in %) of the sampling schemes to reproduce the true annual mean SPM concentration at MOW1 within ±2.5 %, ±5 %, ±10 % and ± 33 %. Further the mean of 1000 SPM concentration samplings (in mg/l) is given together with the multiplicative standard deviation.

Sampling scheme		SPM conc.	Standard dev.	±2.5 %	±5 %	±10 %	±33 %
Random	Synodic-1	132	1.47	5	11	20	61
	Synodic-2	133	1.54	5	10	18	56
	Synodic-3	132	2.12	3	6	11	35
	½ Synodic-1	130	1.43	6	11	22	66
	½ Synodic-2	130	1.50	5	10	19	60
	½ Synodic-3	131	2.10	3	5	11	36
Satellite	Synodic-ideal	118	–	–	–	–	–
	Synodic-real	124	1.32	7	15	28	78
	½ Synodic-ideal	120	–	–	–	–	–
	½ Synodic-real	121	1.40	6	11	23	69

3.2. Accuracy of the mean SPM concentration, SPM flux and Chl concentration

The annual mean for the station MOW1 has been calculated for SPM concentration by taking the mean of all synodic or half-synodic periods. This is considered as the true annual mean and equals 132 mg/l for the synodic and 130 mg/l for the half-synodic mean. The annual mean and the standard deviation derived from the sampling schemes using a bootstrap method is shown in Table 2 together with the probability that the true mean is obtained within a certain margin (for example ±2.5 %, 5 %, 10 % and 33 %). The results indicate that the probability of each scheme to match the true mean with statistical significance (< ±2.5 %) is low. The probabilities are similar for the random sampling schemes 1 (tidal cycle) and 2 (half a tidal cycle) but lower for scheme 3 (one sample). The
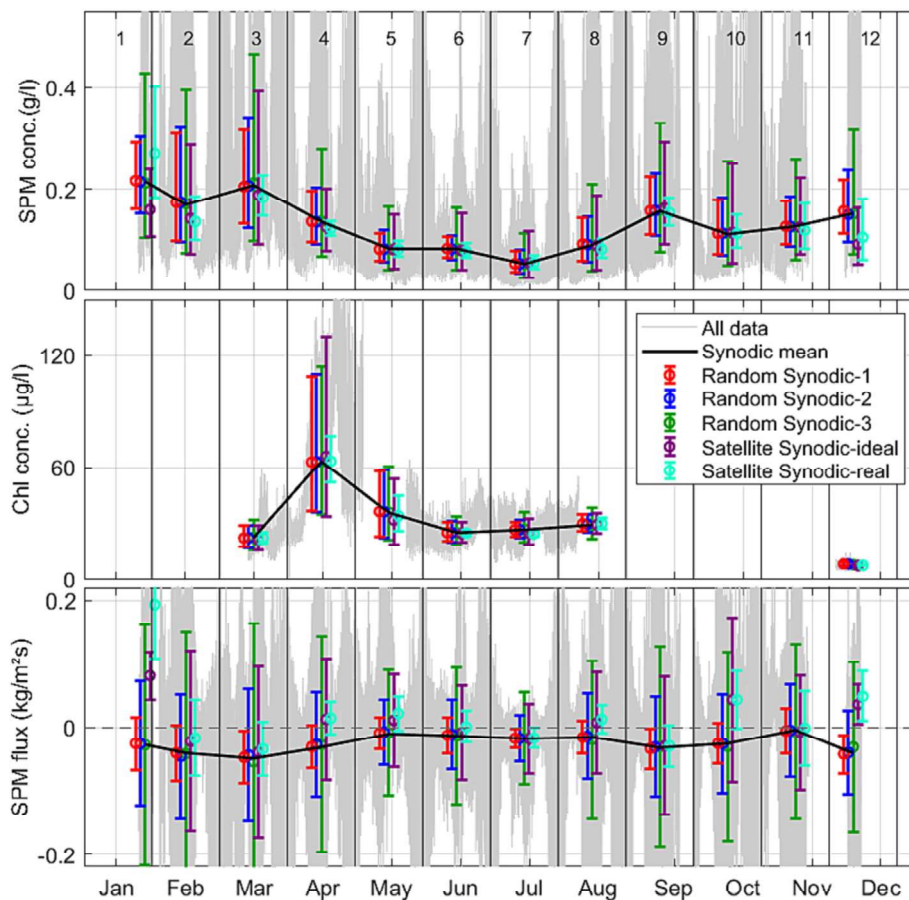

Fig. 3. The same as Fig. 2, but here for the synodic sampling period.

Table 3
Probability (in %) of the sampling schemes to reproduce the true mean Chl concentration over the period March till August at MOW1 within ±2.5 %, ±5 %, ±10 % and ±33 %. Further the mean of 1000 Chl concentration samplings (in µg/l) is given together with the multiplicative standard deviation.

Sampling scheme		Chl conc.	Standard dev.	±2.5 %	±5 %	±10 %	±33 %
Random	Synodic-1	34	1.35	7	13	26	74
	Synodic-2	34	1.37	6	12	25	72
	Synodic-3	34	1.49	5	10	20	61
	½ Synodic-1	37	1.21	10	21	40	91
	½ Synodic-2	37	1.23	9	19	37	88
	½ Synodic-3	37	1.38	6	12	24	70
Satellite	Synodic-ideal	33	–	–	–	–	–
	Synodic-real	33	1.16	13	26	50	97
	½ Synodic-ideal	36	–	–	–	–	–
	½ Synodic-real	37	1.13	16	32	59	99

satellite sampling schemes underestimate the true mean, an effect that is specific to polar-orbiting satellites that sample all individual stages of the semidiurnal and fortnightly harmonic components, but not all combinations of the two due to tidal aliasing (Eleveld et al., 2014).

The probability of a sampling scheme to match the true mean depends on the season. Concerning SPM concentration, it is up to about 50 % higher in summer than in the other seasons. The lower probabilities in winter, spring and autumn are caused by the higher variabilities and reinforced for the realistic satellite sampling schemes by the low number of satellite data during winter and autumn. In contrast to SPM concentration, Chl exhibits large changes in concentration in spring and summer due to primary production and grazing. The seasonal changes in Chl concentration respond to changes in drivers such as temperature or nutrient concentration. The probability of a sampling scheme to match the true mean Chl concentration is lowest during these periods. During spring the half-synodic sampling scheme performs better than the synodic one. The probability that the true mean (34 µg/l over the synodic and 37 µg/l over the half-synodic periods) over the period March till August is obtained within a certain margin is shown in Table 3. Similar as for SPM concentration, the results indicate that the probability of each scheme to match the true mean with statistical significance (< ±2.5 %) is low. However, the half-synodic schemes have up to 100 % higher probabilities during the period considered, which is dominated by the spring phytoplankton bloom.

The probabilities to match the true mean SPM flux are low for all sampling schemes. Only random scheme 1 is able to estimate most of the time the direction of the residual flux correctly within one standard deviation. All the other schemes exhibit very large uncertainties.

3.3. Interannual trends at MOW1 and West Gabbard

The trend over the re-built 20 year time series of SPM concentration at MOW1 has a true slope of 1.9×10^{-3} (mg/l day, p≈0). The random and satellite sampling schemes have been applied as described in Section 2.2. A linear regression was fitted through all data points obtained over the 20 year data series. A bootstrap method (number of iteration was 1000)

was applied to obtain a 2D frequency distribution of slope and P values for all sampling schemes. The probability of detecting a positive and significant trend is presented in Table 4, together with the corresponding mean slope value. The results at MOW1 show low probabilities for all sampling schemes. The satellite sampling schemes perform less good than the random ones, which is caused by the unequal distribution of the data points over the year. Reducing the number of samples to half a tidal cycle or just one sample per period decreases the probability of finding a significant regression. For random sampling scheme 3, probabilities are lower than 6 %. The histograms of slope versus P values are shown for MOW1 in Fig. 4. By reducing the number of samples in the random schemes, not only the probability to obtain a positive trend gets less significant, but also the probability to find a reverse slope increases from 14 % for the synodic (6 % for half-synodic) sampling schemes 1 to 35 % (resp. 29 %) for sampling schemes 3.

To check whether these results are also valid for more offshore stations showing lower SPM concentrations, the same method was applied onto the 2010 turbidity time series from West Gabbard surface buoy. The true trend over the 20 year turbidity time series has a slope of 0.68×10^{-4} (FTU/day, p≈0).The probability of detecting a positive and significant trend is also presented in Table 4 for West Gabbard, together with the mean slope value. The results show that the probabilities of finding the trend are significantly higher than at MOW1, but remain as low as at MOW1 for the random sampling scheme 3.The probability to find a reverse slope at West Gabbard is below 7 % for all sampling schemes.

Moreover, the slope is overestimated in all random and satellite sampling schemes by a factor 2 up to 7 at MOW1, and by a factor 3 up to 8 at West Gabbard. This suggests that when the sampling scheme reproduces a detectable trend its slope is often particularly pronounced. In contrast, when the sampling scheme leads to data with a weak slope (closer to the true slope in this case), the variability in the randomly sampled values may mask the trend and prevent its detection with statistical significance ($P < 0.05$).

4. Discussions

Ideally monitoring should resolve all relevant temporal and spatial scales. In this study we have focused mainly on the temporal scales by applying typical in situ and remote sensing sampling schemes to continuous time series of SPM and Chl concentration and SPM flux from a dynamic coastal area in order to evaluate the capacity of monitoring programmes to resolve temporal scales. Do typical monitoring sampling schemes yield sufficient information to reach the goals of the programmes, such as inter-annual trend detection? In the southern Bight of the North Sea and many other coastal areas, for example, the SPM and Chl concentrations decrease from the coast towards offshore. In the same manner the variability in concentration decreases from the coast towards the offshore (Fettweis et al., 2022). These features, together with the temporal variations that are caused by tides, spring-neap cycles, seasons and storms, define the monitoring efforts needed. It is clear that picking samples from a continuous time series leads to loss of information and this loss gets worse when the sampling intervals increase or when the main variabilities are not sampled. The frequency of the sampling determines the highest frequency about
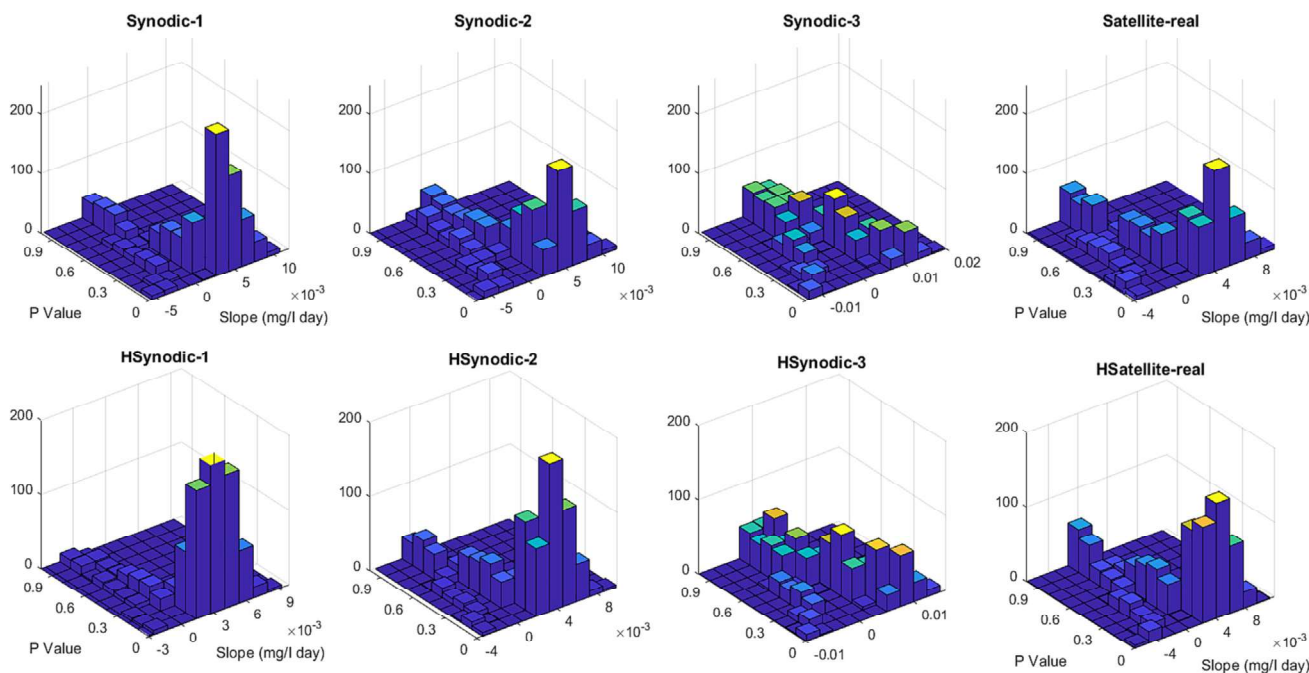
Table 4
Probability of detecting a positive and significant ($P < 0.05$) trend in a 20-year time series of SPM concentration at MOW1 and turbidity at West Gabbard. The mean slope for MOW1 (in mg/l day) and for West Gabbard (in FTU/day) is shown between brackets. The probability and mean slope value are calculated for all data and nine sampling schemes.

	MOW1		West Gabbard	
	Synodic	½ Synodic	Synodic	½ Synodic
All data	100 % (1.9×10^{-3})		100 % (0.68×10^{-4})	
Random-1	46 % (5.1×10^{-3})	61 % (4.0×10^{-3})	85 % (2.7×10^{-4})	87 % (1.8×10^{-4})
Random-2	26 % (6.3×10^{-3})	39 % (4.6×10^{-3})	73 % (2.9×10^{-4})	78 % (2.0×10^{-4})
Random-3	4 % (13.7×10^{-3})	6 % (10.0×10^{-3})	17 % (4.7×10^{-4})	12 % (3.2×10^{-4})
Satellite-ideal	58 % (3.1×10^{-3})		77 % (1.0×10^{-4})	
Satellite-real	29 % (5.5×10^{-3})	31 % (5.5×10^{-3})	64 % (1.9×10^{-4})	44 % (1.7×10^{-4})

Fig. 4. Trends in 20 year SPM concentration time series at MOW1 (every year SPM concentration increases by 0.5 %). The histograms show the slope of the trends (true slope is 1.9×10^{-3} mg/l day) and the *P* values obtained by a bootstrap method for the eight sampling schemes. The z-axis is the number of iterations (in total = 1000).

which we can get meaningful information from a set of data. In the case of tidal signals there are several frequencies that interfere. The highest frequencies are quarter- and semidiurnal and thus only the random sampling schemes 1 and 2 can provide information about them. The next lower ones are the half-synodic and the synodic frequencies. These schemes can only provide information on phenomena with periods longer than twice of the sampling frequency. This means that the proposed sampling schemes cannot resolve neap-spring variability, but they can provide information on seasonal variations.

Fig. 5. Probability of detecting a significant ($p < 0.05$) and correct trend (within ± 25 % of the true value) with the different sampling scheme as a function of a given yearly increase in SPM concentration at MOW1.

4.1. Detecting interannual trends with discrete sampling

Human activities (coastal management, dredged sediment disposal, sand mining, port developments, beach nourishments, bottom trawling, de-eutrophication, aquaculture) and climate change are changing or expected to change the SPM or Chl concentration at the temporal and spatial scales of these pressures. If these changes are small compared to the amplitudes of undisturbed natural variabilities, such as is the case for temporal trends related to global warming, coastal management or de-eutrophication, a consistent, long data record has to be available to detect their impacts (Henson et al., 2010; Fettweis et al., 2016; Desmit et al., 2020). Can the synodic, half-synodic or satellite sampling schemes be used to detect interannual trends?

The results indicate that none of the sampling schemes can be used to assess statistical significant interannual trends with probabilities higher than 61 % in a coastal turbidity maximum with large natural variability in SPM and Chl concentration such as at MOW1. The probabilities at West Gabbard are higher and the random sampling schemes 1 and 2 detect significant trends with a probability of up to 87 %, but remain low for the random sampling scheme 3. Further, in case a statistically significant trend was obtained, all sampling schemes overestimate the slope of the trend by a factor ranging from 2 to 8 at both sites.

How pronounced has a trend to be so that the sampling schemes can detect it with a high probability and with the correct trend value. Fig. 5 shows the probabilities of the eight sampling schemes to detect a trend within ± 25 % of the correct trend value at the turbid station MOW1. The results indicate that the yearly increase has to be between 1 and 2 % in order to obtain a probability of >60 % for random sampling schemes 1 and 2 and for the satellite sampling schemes. Random sampling schemes 3 will detect trends with similar probability if the yearly increase is between 3 and 4 %. These results imply that high-frequency time series are needed in coastal waters to resolve vertical (resuspension-deposition) and horizontal (transport) variations and to detect statistically significant ($P < 0.05$) long-term trends. Similar conclusions were formulated by Blauw et al. (2012) for phytoplankton monitoring in dynamic coastal areas. Our trend experiments were built on linear increasing signals; in reality long-term changes are seldom linear and their detection therefore even more difficult.
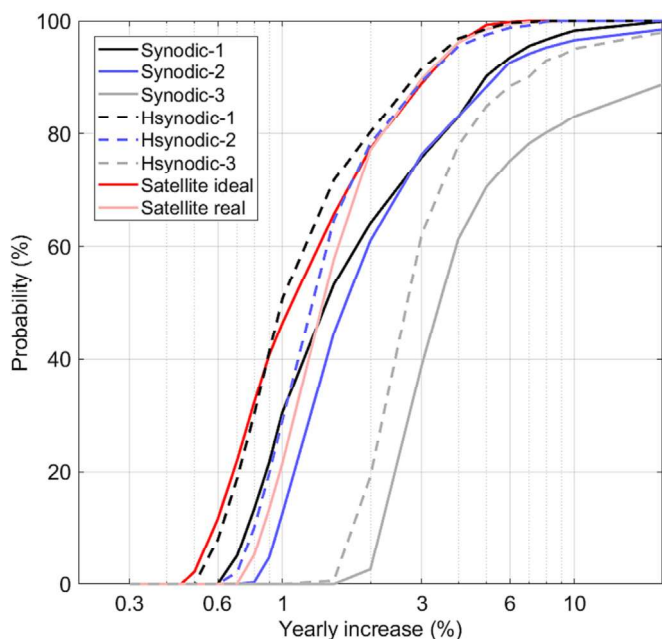
How sound are interannual trend estimates derived from patchy time series? Gohin et al. (2019) detected trends in Chl concentration in the English channel over six yearly averaged data when only the growth period (March–October) was considered, however, these authors increased the number of data points by applying a kriging interpolation technique to create daily values out of the spatial and temporal patchy satellite data. Capuzzo et al. (2015) have divided the North Sea into five hydrodynamic regions. For the region that includes the high turbidity area along the Belgian-Dutch coastline, no significant trend has been found in SPM concentration over a period of 20 years, in contrast with offshore regions with lower turbidity or regions with long-term high-frequent time series such as in the East Anglia plume region. Similar results were found by Desmit et al. (2020) who only found significant trends in Chl concentration in stations with low turbidity values, but for example not in the Belgian nearshore area. OSPAR, 2010 assessment combines the monitoring programmes from different countries into large-scale areas. They conclude that the different sampling strategies, sampling protocols and the spatial heterogeneity hampers comparability of the monitoring results and of the detection of interannual trends. These results confirm our conclusions that the sampling scheme needs to be adapted to the temporal variability of the parameters. They also underline that coastal zones are often undersampled, despite the fact that these land-sea transition zones are highly dynamic, very productive and exhibit large variability in organic and inorganic particles composition and concentration (Levin et al., 2001; Talley et al., 2003; Blauw et al., 2018; Fettweis et al., 2022).

4.2. What is the gain of using discrete sampling in a tidal system?

Are water samples of SPM and Chl concentration of any interest in a highly turbid coastal area when sampled on a low frequency with regard to tidal and neap-spring frequencies? If such sampling is the only form of monitoring, the interest is limited. A low frequency measurement will only detect if the water is turbid, oligotrophic or eutrophic, a feature that could instead be easily derived from remote sensing products. However, when such sampling accompanies other forms of observation, they are of interest as they are needed to calibrate the sensors used in long-term continuous time series (e.g., turbidity, acoustic backscatter, fluorometer, remote sensing). As discussed above, continuous sensor measurements provide periodic mean values with low uncertainty and a reliable determination of interannual trends. The relationship between sensor outputs (turbidity, acoustic backscatter or fluorescence) and the SPM or Chl concentration should be established using mass concentration derived from water samples (Roesler et al., 2017; Fettweis et al., 2019). Finally, low frequency samplings of SPM and Chl concentration are of interest when they can be combined with other water parameters sampled simultaneously, that escape detection by automated sensors or satellites. In the case SPM and Chl are correlated with other constituents (e.g., POC, PON, TEP), a sound analysis of the relationships between constituents can be made without necessarily resolving all variabilities. In recent analyses, Schartau et al. (2019) and Fettweis et al. (2022) have successfully modelled POC, PON and TEP concentrations from SPM concentrations along the coastal-offshore transect of eutrophic coastal zones with no special consideration for the tidal complexity of these parameters. SPM and Chl concentration can then be seen as indicator parameters as they are correlated or covarying with the concentration of these constituents.

4.3. True mean of SPM and Chl concentration and SPM flux

In our approach, the true mean over a specific period was derived from continuous sensor measurements. This mean value was considered "true" for the purpose of testing the performance of different sampling schemes. However, if our conclusion is using continuous sensors in turbid tidal systems, then we must ask how true is the "true" mean value? The drawback of sensor-derived continuous time series is that the quality or certainty of the data and thus any statistics based on it also depends on factors that are only to a certain level avoidable. Long-term observations of SPM and Chl concentration, for example, are the result of a complex ladder of operations that involve field, laboratory and modeling methods (Roesler et al., 2017; Fettweis et al., 2019). Each step contributes its own random and systematic errors to the overall uncertainties of the sensor derived SPM or Chl concentration. Systematic errors related to the functioning of the sensors, the environment, the collection and processing of calibration samples and faulty human operations are detectable and sometimes correctable. As long as protocols for sample analysis and sensor calibration are carefully followed, uncertainties for SPM concentration can be confined within ± 5 %, otherwise they may reach up to ± 20 % (Fettweis et al., 2019). Specific effects such as non-photochemical quenching and large natural variability in the relationship between fluorescence and Chl concentration may lead to even higher uncertainty for Chl than for SPM (Roesler et al., 2017). This means that a "true" mean, as assumed here, is always associated with an uncertainty that should be included in the analysis. Furthermore the monitoring data are also associated with uncertainties that can reach up to 40 % for satellite data (He et al., 2020; Wei et al., 2021) and up to a 10–15 % for SPM (Fettweis et al., 2019) and 20–25 % for Chl samples (Kratzer et al., 2022).

5. Conclusion

The intent of our analysis was to provide researchers and policy makers with information on how to select appropriate sampling schemes depending on the variability of their system in order to derive meaningful results. This may help improve existing monitoring efforts. As our approach is system-dependent one should first quantify the variabilities in their area with regard to the parameters they want to monitor, second specify the information they want to obtain (tidal, monthly or annual mean, long term trends, calibration data…) and then define an appropriate monitoring scheme.

The effectiveness of different sampling schemes in resolving temporal variations relies on the sampling intervals and the number of samples taken per sampling occurrence. The analysis has shown that in highly turbid and dynamic coastal areas patchy time series obtained from low-frequency monitoring programmes do not provide sufficient information to calculate mean values or interannual trends with statistical significance as they do not resolve the main tidal variability. The performance of the sampling scheme is better at offshore sites, where the tidal dynamic is less important and the SPM and Chl concentration variabilities are lower. Still, when a significant ($p < 0.05$) trend is detected in a randomly sampled data series in a high turbid coastal station, there is a 6 to 35 % probability that it is reversed compared to the "true" trend. If, however, the detected trend is correct its slope may be overestimated by a factor 2 to 8 (whether inshore or offshore). Measurements taken at fixed times during a day, such as from satellites, introduce a bias in the data due to tidal aliasing, resulting in an underestimation of the mean concentrations.

In tidal turbid systems, SPM and Chl concentrations and SPM flux would better be monitored at high frequency using sensors to capture the whole range of variabilities. This can be achieved by instrumented buoys or benthic landers who resolve variations related to tides, meteorological conditions and seasons. However, sensor measurements do not yet offer the same guarantee of quality-assured data and in situ sampling remains needed for calibration. There is increasing evidence that climate change, eutrophication and de-eutrophication are altering the water quality and the underlying biogeochemical processes in coastal zones. Continuous sensor measurements may help detect and unravel these simultaneous decadal changes through the study of SPM and Chl long-term trends, with implications for the fate of coastal organic matter and the carbon cycle.

Still, it needs to be acknowledged that this work focuses on the temporal aspect of monitoring highly dynamic waters. Coastal systems are also often characterised by strong spatial gradients of Chl and SPM which would require an adequate distribution of in-situ stations to obtain a synoptic overview of the aquatic system which is often very difficult or even impossible to maintain. Sampling a limited number of locations in a non-homogeneous area can result in a bias and over-representation of certain water types. In

such areas the spatial coverage provided by satellite observations, can support the continuous in-situ observations to provide a more representative assessment.

CRediT authorship contribution statement

Conceptualization: Michael Fettweis, Rolf Riethmüller, Dimitry Van der Zande, Xavier Desmit.

Formal analysis: Michael Fettweis, Rolf Riethmüller, Dimitry Van der Zande, Xavier Desmit.

Funding acquisition: Michael Fettweis, Xavier Desmit.

Methodology: Michael Fettweis, Rolf Riethmüller, Xavier Desmit.

Software & visualization: Michael Fettweis.

Writing original manuscript: Michael Fettweis, Rolf Riethmüller, Xavier Desmit.

Writing review & editing: Rolf Riethmüller, Dimitry Van der Zande, Xavier Desmit.

Data availability

The long-term sensor data from MOW1 can be accessed through doi:10.24417/ bmdc.be:dataset:1250. The turbidity time series of West-Gabbard has been downloaded from CEFAS: https://wavenet.cefas.co.uk/SmartBuoy/Map

Declaration of competing interest

The authors declare that they have no known competing financial interests or personal relationships that could have appeared to influence the work reported in this paper.

Acknowledgements

References

Alvera-Azcaráte, A., Van der Zande, D., Barth, A., Troupin, C., Martin, S., Beckers, J.-M., 2021. Analysis of 23 years of daily cloud-free chlorophyll and suspended particulate matter in the Greater North Sea. Front. Mar. Sci. 13 (19), 2657. https://doi.org/10.3389/fmars.2021.707632.

Anttila, S., Ketola, M., Vakkilainen, K., Kairesalo, T., 2012. Assessing temporal representativeness of water quality monitoring data. J. Environ. Monit. 14, 589. https://doi.org/10.1039/C2EM10768F.

Blauw, A.N., Benincà, E., Laane, R.W.P.M., Greenwood, N., Huisman, J., 2012. Dancing with the tides: fluctuations of coastal phytoplankton orchestrated by different oscillatory modes of the tidal cycle. PLoS ONE 7 (11), e49319. https://doi.org/10.1371/journal.pone.0049319.g001.

Blauw, A.N., Benincà, E., Laane, R.W.P.M., Greenwood, N., Huisman, J., 2018. Predictability and environmental drivers of chlorophyll fluctuations vary across different time scales and regions of the North Sea. Prog. Oceanogr. 161, 1–18. https://doi.org/10.1016/j.pocean.2018.01.005.

Capuzzo, E., Stephens, D., Silva, T., Barry, J., Forster, R.M., 2015. Decrease in water clarity of the southern and central North Sea during the 20th century. Glob. Chang. Biol. 21, 2206–2214. https://doi.org/10.1111/gcb.12854.

Conley, D., Paerl, H., Howarth, R., Boesch, D., Seitzinger, S., Havens, K., Lancelot, C., Likens, G., 2009. Controlling eutrophication: nitrogen and phosphorus. Science 323 (5917), 1014–1015. https://doi.org/10.1126/science.1167755.

Desmit, X., Nohe, A., Borges, A.V., Prins, T., De Cauwer, K., Lagring, R., Van der Zande, D., Sabbe, K., 2020. Changes in chlorophyll concentration and phenology in the North Sea in relation to de-eutrophication and sea surface warming. Limnol.Oceanogr. 65, 828–847. https://doi.org/10.1002/lno.11351.

Druine, F., Verney, R., Deloffre, J., Lemoine, J.-P., Chapalain, M., Landemain, V., Lafite, R., 2018. In situ high frequency long term measurements of suspended sediment

concentration in turbid estuarine system (Seine Estuary, France): optical turbidity sensors response to suspended sediment characteristics. Mar. Geol. 400, 24–37. https://doi.org/10.1016/j.margeo.2018.03.003.

Efron, B., 1979. Bootstrap methods: another look at the jackknife. Ann. Stat. 7 (1), 1–26. https://doi.org/10.1214/aos/1176344552.

Eleveld, M.A., van der Wal, D., van Kessel, T., 2014. Estuarine suspended particulate matter concentrations from sun-synchronous satellite remote sensing: tidal and meteorological effects and biases. Remote Sens. Environ. 143, 204–215. https://doi.org/10.1016/j.rse.2013.12.019.

Erkkilä, A., Kalliola, R., 2007. Spatial and temporal representativeness of water monitoring efforts in the Baltic Sea coast of SW Finland. Fennia - Int.J.Geogr. 185, 107–132.. https://fennia.journal.fi/article/view/3715.

Fettweis, M., Baeye, M., Cardoso, C., Dujardin, A., Lauwaerts, B., Van den Eynde, D., Van Hoestenberghe, T., Vanlede, J., Van Poucke, L., Velez, C., Martens, C., 2016. The impact of disposal of fine grained sediments from maintenance dredging works on SPM concentration and fluid mud in and outside the harbor of Zeebrugge. Ocean Dyn. 66, 1497–1516. https://doi.org/10.1007/s10236-016-0996-1.

Fettweis, M., Riethmüller, R., Verney, R., Becker, M., Backers, J., Baeye, M., Chapalain, M., Claeys, S., Claus, J., Cox, T., Deloffre, J., Depreiter, D., Druine, F., Flöser, G., Grünler, S., Jourdin, F., Lafite, R., Nauw, J., Nechad, B., Röttgers, R., Sottolichio, A., Vanhaverbeke, W., Vereecken, H., 2019. Uncertainties associated with in situ long-term observations of suspended particulate matter concentration using optical and acoustic sensors. Prog. Oceanogr. 178, 102162. https://doi.org/10.1016/j.pocean.2019.102162.

Fettweis, M., Schartau, M., Desmit, X., Lee, B.J., Terseleer, N., Van der Zande, D., Parmentier, K., Riethmüller, R., 2022. Organic matter composition of biomineral flocs and its influence on suspended particulate matter dynamics along a nearshore to offshore transect. J. Geophys. Res. Biogeosci. 127, e2021JG006332. https://doi.org/10.1029/2021JG006332.

Gaulier, C., Zhou, C., Guo, W., Bratkič, A., Superville, P.-J., Billon, G., Baeyens, W., Gao, Y., 2019. Trace metal speciation in North Sea coastal waters. Sci. Total Environ. 692, 701–712. https://doi.org/10.1016/j.scitotenv.2019.07.31.

Gohin, F., Van der Zande, D., Tilstone, G., Eleveld, M.A., Lefebvre, A., Andrieux-Loyer, F., Blauw, A.N., Bryère, P., Devreker, D., Garnesson, P., Hernández Fariñas, T., Lamaury, Y., Lampert, L., Lavigne, H., Menet-Nedelec, F., Pardo, S., Saulquin, B., 2019. Twenty years of satellite and in situ observations of surface chlorophyll-a from the northern Bay of Biscay to the eastern English Channel. Is the water quality improving? Remote Sens. Environ. 233, 11134. https://doi.org/10.1016/j.rse.2019.111343.

Grabemann, I., Krause, G., 1989. Transport processes of suspended matter derived from time series in a tidal estuary. J. Geophys. Res. 94 (C10), 14373–14379. https://doi.org/10.1029/JC094iC10p14373.

Harvey, E.T., Kratzer, S., Philipson, P., 2015. Satellite-based water quality monitoring for improved spatial and temporal retrieval of chlorophyll-a in coastal waters. Remote Sens. Environ. 158, 417–430. https://doi.org/10.1016/j.rse.2014.11.017.

He, J., Chen, Y., Wu, J., Stow, D.A., Christakos, G., 2020. Space-time chlorophyll-a retrieval in optically complex waters that accounts for remote sensing and modeling uncertainties and improves remote estimation accuracy. Water Res. 171, 115403. https://doi.org/10.1016/j.watres.2019.115403.

Henson, S.A., Sarmiento, J.L., Dunne, J.P., Bopp, L., Lima, I., Doney, S.C., John, J., Beaulieu, C., 2010. Detection of anthropogenic climate change in satellite records of ocean chlorophyll and productivity. Biogeosciences 7, 621–640. https://doi.org/10.5194/bg-7-621-2010.

Herman, P.M.J., van Kessel, T., Vroom, J., Dankers, P.J.T., Cleveringa, J., de Vries, B., Villars, N., 2018. Mud Dynamics in the Wadden Sea – Towards a Conceptual Model. Report 11202177-000-ZKS-0011, Deltares, The Netherlands.

Keil, R.G., Montiuçon, D.B., Prahl, F.G., Hedges, J.I., 1994. Sorptive preservation of labile organic matter in marine sediments. Nature 370, 549–552. https://doi.org/10.1038/370549a0.

Kirby, M.F., Law, R.J., 2010. Accidental spills at sea – risk, impact, mitigation and the need for co-ordinated post-incident monitoring. Mar. Pollut. Bull. 60, 797–803. https://doi.org/10.1016/j.marpolbul.2010.03.015.

Kowalska, M., Güler, H., Cocke, D.L., 1994. Interactions of clay minerals with organic pollutants. Sci. Total Environ. 14, 223–240. https://doi.org/10.1016/0048-9697(94)90030-2.

Kratzer, S., Harvey, E.T., Canuti, E., 2022. International intercomparison of in situ chlorophyll-a measurements for data quality assurance of the Swedish Monitoring Program. Front.Remote Sens. 3, 866712. https://doi.org/10.3389/frsen.2022.866712.

Levin, L.A., Boesch, D.F., Covich, A., Dahm, C., Erséus, C., Ewel, K.C., Kneib, R.T., Moldenke, A., Palmer, M.A., Snelgrove, P., Strayer, D., Weslawski, J.M., 2001. The function of marine critical transition zones and the importance of sediment biodiversity. Ecosystems 4, 430–451. https://doi.org/10.1007/s10021-001-0021-4.

Lin, H., Yu, Q., Wang, Y., Gao, S., 2022. Identification, extraction and interpretation of multi-period variations of coastal suspended sediment concentration based on unevenly spaced observations. Mar. Geol. 445, 106732. https://doi.org/10.1016/j.margeo.2022.106732.

Lovett, G.M., Burns, D.A., Jenkins, J.T., Mitchell, M.J., Rustad, L., Shanley, J.B., Likens, G.E., Haeuber, R., 2007. Who needs environmental monitoring? Front. Ecol. Environ. 5, 253–260. https://doi.org/10.1890/1540-9295(2007)5[253:WNEM]2.0.CO;2.

Mack, L., Attila, J., Aylagas, E., Beermann, A., Borja, A., Hering, D., Kahlert, M., Leese, F., Lenz, R., Lehtiniemi, M., Liess, A., Lips, U., Mattila, O.-P., Meissner, K., Pyhälahti, T., Setälä, O., Strehse, J.S., Uusitalo, L., Willstrand, W.A., Birk, S., 2020. A synthesis of marine monitoring methods with the potential to enhance the status assessment of the Baltic Sea. Front. Mar. Sci. 7. https://doi.org/10.3389/fmars.2020.552047.

OSPAR, 2010. Quality status report 2010. https://qsr2010.ospar.org/en/index.html.

Ransom, B., Kim, D., Kastner, M., Wainwright, S., 1998. Organic matter preservation on continental slopes: importance of mineralogy and surface area. Geochim. Cosmochim. Acta 62, 1329–1345. https://doi.org/10.1016/S0016-7037(98)00050-7.

Roesler, C., Uitz, J., Claustre, H., Boss, E., Xing, X., Organelli, E., Briggs, N., Bricaud, A., Schmechtig, C., Poteau, A., D'Ortenzio, F., Ras, J., Drapeau, S., Haëntjens, N., Barbieux,

M., 2017. Recommendations for obtaining unbiased chlorophyll estimates from in situ chlorophyll fluorometers: a global analysis of WET Labs ECO sensors. Limnol.Oceanogr. Methods 15, 572–585. https://doi.org/10.1002/lom3.10185.

Schartau, M., Riethmüller, R., Flöser, G., van Beusekom, J.E.E., Krasemann, H., Hofmeister, R., Wirtz, K., 2019. On the separation between inorganic and organic fractions of suspended matter in a marine coastal environment. Prog. Oceanogr. 171, 231–250. https://doi.org/10.1016/j.pocean.2018.12.011.

Sea-Bird Electronics, 2011. Calculating Calibration Coefficients for WET Labs ECO-AFL and ECO-FL Fluorometer, ECO-NTU Turbidity Meter, and ECO-FL-NTU Fluorometer/Turbidity Meter. APPLICATION NOTE NO. 62. . https://www.seabird.com/eco-fluorometer/product?id=60429374754.

Shen, X., Huo, H., Zhang, Y., Zhu, Y., Fettweis, M., Bi, Q., Lee, B.J., Maa, J.P.-Y., Chen, Q., 2023. Effects of organic matter on the aggregation of anthropogenic microplastic particles in turbulent environments. Water Res. 232, 119706. https://doi.org/10.1016/j.watres.2023.119706.

Talley, D.M., North, E.W., Juhl, A.R., Timothy, D.A., Conde, D., deBrouwer, J.F.C., Brown, C.A., Campbell, L.M., Garstecki, T., Hall, C.J., Meysman, F.J.R., Nemerson, D.M., Souza Filho, P.W., Wood, R.J., 2003. Research challenges at the land–sea interface. Estuar. Coast. Shelf Sci. 58, 699–702. https://doi.org/10.1016/j.ecss.2003.08.010.

Wei, J., Wang, M., Jiang, L., Yu, X., Mikelsons, K., Shen, F., 2021. Global estimation of suspended particulate matter from satellite ocean color imagery. J. Geophys. Res. Oceans 126 (8), e2021JC017303. https://doi.org/10.1029/2021JC017303.

Wernand, M.R., 2010. On the history of the secchi disk. J.Eur.Opt.Soc.Rapid Publ. 5, 10013s.

APPENDIX 3

Escobar S, Bi Q, Fettweis M, Monbaliu J, Wongsoredjo S, Toorman E. 2023. A 2DH flocculation model for coastal domains. Ocean Dynamics 73, 333-358.

A dynamic 2DH flocculation model for coastal domains

Sebastian Escobar[1,2] · Qilong Bi[1,3] · Michael Fettweis[4] · Samor Wongsoredjo[1] · Jaak Monbaliu[1] · Erik Toorman[1]

Abstract
A dynamic two-dimensional depth-averaged (2DH) parameterization for flocculation of cohesive sediments is proposed based on the kinetic model by Winterwerp (J Hydraul Res 36:309–326, 1998). The aim is to achieve a realistic representation of the suspended sediment field by accounting for flocculation, also taking into consideration its dependence on advection, turbulent diffusion, and turbulent shear. This formulation is evaluated in a sand-mud model of the Belgian Coast and the Western Scheldt. Results indicate that it can reproduce known sediment transport patterns: modelled floc size and suspended sediment concentrations are in the range of measurements. When evaluating the model results spatially, the extent and shape of the coastal sediment plumes are similar to the observed suspended particle matter (SPM) maps from the PROBA-V satellite. Therefore, the use of the presently proposed flocculation model has added value to improve sediment transport calculations in coastal areas.

1 Introduction

Studies by Lee et al. (2011), Shen et al. (2018), and Shen et al. (2019) showed that size-varying flocs can be modelled through single-class and multiple-class flocculation equations. These allow examining complicated particle-size distributions, predicting better their settling velocities, and can optionally account for biological processes that enhance aggregation or breaking. These models are based on population balance equations (PBE) (Hulburt and Katz 1964; Randolph 1964), on extensive studies of floc density, strength, form, and fractal features (von Smoluchowski 1917; Tambo and Watanabe 1979; Weitz and Oliveria 1984; Maggi et al. 2007), and on flocculation kinetics (Tambo and Watanabe 1984; Dyer 1989; van Leussen 2011). Yet these models are not efficient for application to large-scale coastal studies. The many scales involved and complex interactions between primary particles and their aggregates, plus stability and computational time considerations, make them only applicable to small or idealized geometries like Quasi-1D

vertical frameworks and 3D schematized estuarine domains, or to controlled study cases like mixing tanks and settling column experiments (Bi et al. 2020).

Winterwerp (1998) proposed a flocculation model, which directly calculates the mean floc size assuming that the floc density is proportional to the size to a certain power, similar to fractal theory (Kranenburg 1994; Chapalain et al. 2019). This model is particularly popular, and its use in literature is extensive (Winterwerp 2002; Tarpley et al. 2019; Horemans et al. 2020; Zhang et al. 2020). Authors generally take advantage of its mathematical simplicity because it consists of a single ordinary differential equation, which facilitates its use in idealized estuaries and experiments. However, Kuprenas et al. (2018) found that this model can yield unreasonably large floc sizes when turbulent shear or suspended particle matter (SPM) fall outside of the range of calibration parameters.

It is not uncommon therefore that coastal modelling studies ignore or try to parametrize the flocculation dynamics to get better values of the sediment settling velocity, and thus more realistic SPM results. The most straightforward method is to calibrate the sediments settling velocity, which is taken as a parameter and its values fine-tuned to match SPM time series. However, this process is very subjective and a wide range of settling velocity values are often found in the literature of the same geographical area (Van den Eynde 2018;

Responsible Editor: Sandro Carniel

✉ Sebastian Escobar
s.escobar@hrwallingford.com

Extended author information available on the last page of the article

Bi and Toorman 2015; Cox et al. 2019). Moreover, seasonal variation of the settling velocity is well documented (Fettweis and Baeye 2015; McAnally and Mehta 2000; Maerz et al. 2016; Duy Vinh et al. 2018; Chang et al. 2006), which means that such calibrations should also involve seasonality. Another alternative is the use of empirical settling velocity equations that are a function of hydrodynamics and sediment transport. For example, the Soulsby et al. (2013) formula is a function of the instantaneous turbulent shear and suspended sediment concentration. Satellite data can also be used and assimilated to the settling velocity parameter by algorithms taken from computational science disciplines (Margvelashvili et al. 2013; Wang et al. 2018, 2020). These methods are promising, especially with rapid advances in remote sensing technologies, but they are limited by the temporal frequency of satellite data, and by its sensitivity to cloudiness, and because satellite data only provide information in the water surface.

We propose a comprehensive two-dimensional depth-averaged (2DH) flocculation formulation based on Winterwerp (1998). This model introduces new terms such as turbulent drift to account for the relative velocity of the sediment fraction to the flow, turbulence inertia correction, which emulates turbulence growth and decay rates, and data-based modifications of the breaking source term. The aim is to achieve a model that can deal with the many across-scales exchanges of mass and energy happening in the coastal zone (e.g., throughout offshore, nearshore, inter-tidal zones, and between the bed and the water column), along with floc-scale processes. Lastly, this flocculation model is assessed in a real setup of the Belgian Coast by comparison with field and satellite data.

2 Materials and methods

2.1 Model formulation

The following kinetic model for tracking the evolution of the floc size is proposed:

$$\frac{\partial d}{\partial t} + (u + u_D)\frac{\partial d}{\partial x} + (v + v_D)\frac{\partial d}{\partial y} = A - B \tag{1}$$

t is the independent time variable, d is the mean floc size, u and v are the depth-averaged velocity components along x and y directions, and A and B are the aggregation and breakage source terms.

This model accounts for the dispersive velocity of floc particles through the turbulent drift (u_D, v_D), which is obtained

from the turbulent mass flux term in the sediment mass balance equation:

$$\begin{pmatrix} u_D \\ v_D \end{pmatrix} = -\frac{1}{C}\frac{v_t}{\sigma}\nabla C \tag{2}$$

C is the total mass concentration of the suspended sediment, v_t the eddy viscosity, and σ the turbulent Schmidt number. Usually, the sediment diffusivity is assumed equal to the turbulent eddy viscosity, and thus the Schmidt number is taken as 1. Nevertheless, studies by Toorman (1997) and Toorman et al. (2002) indicate that a value of 0.7 produces better results for high-turbidity flows based on the work by Turner (1973).

Different from the original work by Winterwerp (1998), in this formulation, the influence of volumetric concentration (ϕ) on the breakage term (B) is considered. This follows observations by Manning and Dyer (1999) that point to a negative correlation of the sediment concentration with floc size.

$$\begin{aligned} A &= k_a \phi d^{(4-n_f)} G \\ B &= k_b \phi \frac{(d-d_p)^{(3-n_f)}}{d_p} d^2 G^{3/2} \end{aligned} \tag{3}$$

G is the turbulent shear rate, and d_p the primary particle, defined as the smallest possible particle size of the clay units, which are compact microflocs of the order of 10 to 20 μm in size (based on LISST data, Sect. 2.2.2). n_f is the pseudo-fractal dimension of the sediment particles' population; k_a and k_b are calibration constants.

Flocs undergo changes in their structure, strength, composition, and electrolyte concentration as their size changes (Chakraborti et al. 2003; Khelifa and Hill 2006; Maggi et al. 2007; Son and Hsu 2009). Therefore, the flocs' population pseudo-fractal dimension, rather than constant, is to be considered a function of the floc size. Following this reasoning, a formula similar to the one proposed by Maggi et al. (2007) is used:

$$n_f = n_{max}\left(\frac{d}{d_p}\right)^{-\beta} \tag{4}$$

$n_{max} = 2.5$ is the maximum pseudo-fractal dimension corresponding to microflocs (the strongest basic aggregates found in the environment, which rarely break up into primary clay particles), and the parameter $\beta = 0.09$, based on observed mean flocs sizes of micro-, macro-, and megafloc populations in the Belgian coastal area (Lee et al. 2012).

The turbulent shear rate is usually defined as $G = \sqrt{\frac{\epsilon}{v}}$, with ϵ being the turbulence kinetic energy dissipation, and

ν the fluid kinematic viscosity (Saffman and Turner 1956). For applications with turbulence models different from the $k - \epsilon$, such as this work, Toorman (2020) proposed the following formula based on extrapolation of direct numerical simulations data:

$$G = \frac{1}{2}\frac{u_*^2}{\nu} \tag{5}$$

Where $u_* = \sqrt{\tau_b/\rho_w}$ is the friction velocity, τ_b the bed shear stress, and ρ_w the water density. Note that with this formula the shear rate is computed at the vicinity of the bed level, where u_* and τ_b occur.

Equation (5) implies that G becomes 0 when $u_* = 0$ m/s. In reality, there always remains turbulence in the water column because of the inertia of the dissipation. To account for this memory effect, Toorman (2020) proposes the relaxation equation:

$$G = G_{eq} + (G_{t-\Delta t} - G_{eq})exp(-\Delta t/T_r) \tag{6}$$

Where G_{eq} is the turbulent shear rate calculated with Eq. (5), $G_{t-\Delta t}$ is the turbulence shear rate at a previous time step, and T_r is the relaxation time parameter, to be calibrated based on the time lag between shear rate and suspended sediment concentration peaks.

In addition to the flocculation model, the settling velocity is modified from Dietrich (1982) formula to be valid over a wider range of particle Reynolds numbers (Toorman 2022).

$$
\begin{aligned}
log\left(\frac{w_s}{w_0}\right) &= b_2(log(1 + d_*))^2 \\
&\quad + b_3(log(1 + d_*))^3 + b_4(log(1 + d_*))^4 \\
d_* &= (g'/\nu^2)^{1/3}d \\
g' &= (\rho_f/\rho_w - 1)g \\
\rho_f &= \rho_w + (\rho_s - \rho_w)\left(\frac{d}{d_1}\right)^{n_F-3} \\
w_0 &= g'd^2/18\nu
\end{aligned}
\tag{7}
$$

Where $b_2 = -0.33$, $b_3 = -0.056$, and $b_4 = 0.018$ are empirical constants, d_* the non-dimensional mean floc diameter, and g' is the specific gravity of sediment particles. ρ_f and ρ_s are respectively the floc bulk and the dry sediment density, g the gravity acceleration, w_s the settling velocity of the sediment, and w_0 the Stokes settling velocity (theoretically characteristic of spherical particles settling with very small Reynolds numbers).

2.1.1 Numerical solution

A MATLAB implementation of Eqs. (1) to (7) was used to prove the model's functioning on simplified cases. This con-

sisted of a solver for a single zero-dimensional point that receives input shear rate and concentration signals, and outputs the mean floc size after solving Eq. (1). The solution of (1) is based on Press et al. (1992) 4th-order step-varying Runge–Kutta algorithm, which adjusts the timestep between 0.5 and 5 s depending on the temporal rate of change of the mean floc size. The reason for using this solver is that the source terms in (3) have many time-varying inputs (e.g., the instantaneous floc size, the turbulent shear rate, and the volumetric sediment concentration) which can be subject to abrupt changes. Furthermore, non-stiff ODE solvers (e.g., Euler, or a constant step Runge–Kutta method) can easily become unstable under these conditions. For a pair of input turbulent shear rate and sediment concentraion signals, the solution steps are:

1. Calculate the pseudo-fractal dimension (4).
2. Calculate the instantaneous value of the aggregation and breakage source terms (3).
3. Solve Eq. (1) numerically with the Press et al. (1992) algorithm.

The results (Fig. 1) show the expected pattern where aggregation takes place during low shear, and breakage during high shear. Also, they show the modulation of the shear rate caused by (6). A more realistic test was carried out using measurements from the MOW1 station as input data (see Section 2.2.2). This is shown in Fig. 2; the model equations reproduce the growth and breakage phases of microflocs and macroflocs (20 to 200 μm), and it does not match the largest measured particles, which even grow larger than the scale of the LISST measurements. But these may be biological megaflocs, loose structures of minerals and phytoplankton, or phytoplankton aggregates, because the data was taken are during the spring, which is the diatom growing season (Nohe et al. 2020). Further, these megaflocs occur more frequently during lower tidal amplitudes (18–19/04/2009) than at the beginning of the time series.

2.2 Application: the Belgian Coast

Having tested the model in simplified conditions, the next step is using the newly formulated flocculation model in a more realistic model of the Belgian Coast.

2.2.1 Study area

The study area covers the Belgian Coast and the Western Scheldt (Fig. 3). Water-depth values range from 0 to 30 m, the bottom topography consists of sandbanks (e.g., Wenduine bank and Paardenmarkt), beaches, tidal flats, shoals (e.g., Vlakte van de Raan, Rassen and Bankje van het Zouteland), and tidal channels in the foreshore and within the Western

Fig. 1 Flocculation model results for a synthetic input tide signal (third row). These results were obtained with parameters $k_a = 1600$, $k_b = 60$, $d_p = 10\mu$m, $\phi = 0.003$ ml/m, $n_{max} = 2.5$, and $\nu = 1.E-6$ m^2/s. $Tr = 3600.0$ s. The shear velocity, not shown in the figure but used to calculate G, is estimated with Nikuradse friction law assuming a roughness height of $k_s = 0.03$ m
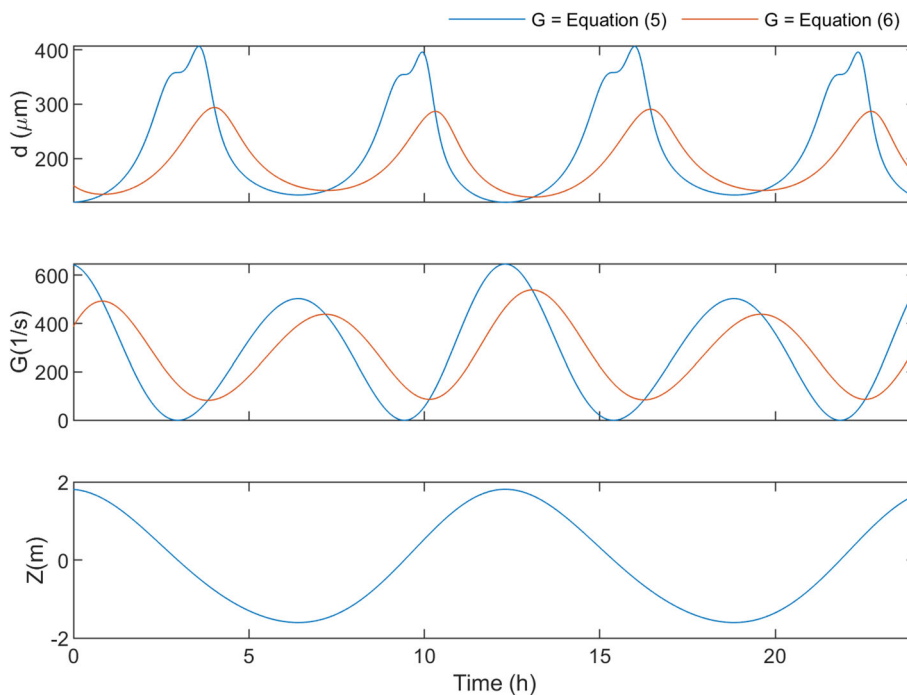

Scheldt estuary. Near the port of Zeebrugge is situated a coastal turbidity maximum area with SPM concentrations between 0.1 g/l and more than 3 g/l near the bed (Baeye et al. 2011; Fettweis et al. 2012). Studies by Baeye et al. (2012) around this area revealed bed boundary level changes of up to 0.2 m during spring-neap tide cycles, suggesting the occurrence of lutoclines and possibly of fluid mud layers.

Tides of the Belgian Coast are of the semi-diurnal type, with approximately two high and low water cycles per day.

The maximum tidal range is 4.8 m during spring tide and 3.1 m during neap tides. Offshore, the predominant harmonic constituent is M2 (principal lunar). The harmonic constituent S2 (principal solar) is also relevant because its superposition with M2 causes spring-neap cycles approximately every 15 days. The nearshore tidal current ellipses are elongated and vary between 0.2 and 0.8 m/s during spring tide and 0.2 and 0.5 m/s during neap tide at 2 m above the bed. The large tidal range and the low freshwater discharges result in a well-mixed water column (Fettweis et al. 2016; Brand et al. 2019).

Fig. 2 Flocculation model results compared with LISST-measured floc volume concentration at the MOW1 station. These results were obtained with parameters $k_a = 1800$, $k_b = 20$, $d_p = 20\mu$m, $n_{max} = 2.5$, and $\nu = 1.E-6$ m^2/s. G, not shown in the figure, calculated from velocity measurements and assuming a Nikuradse friction law with a roughness height of $k_s = 0.03$ m
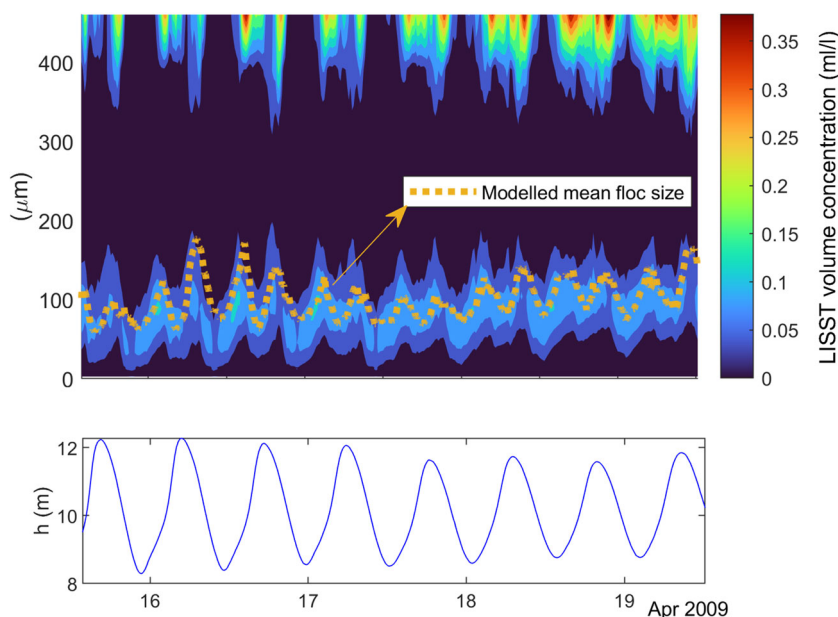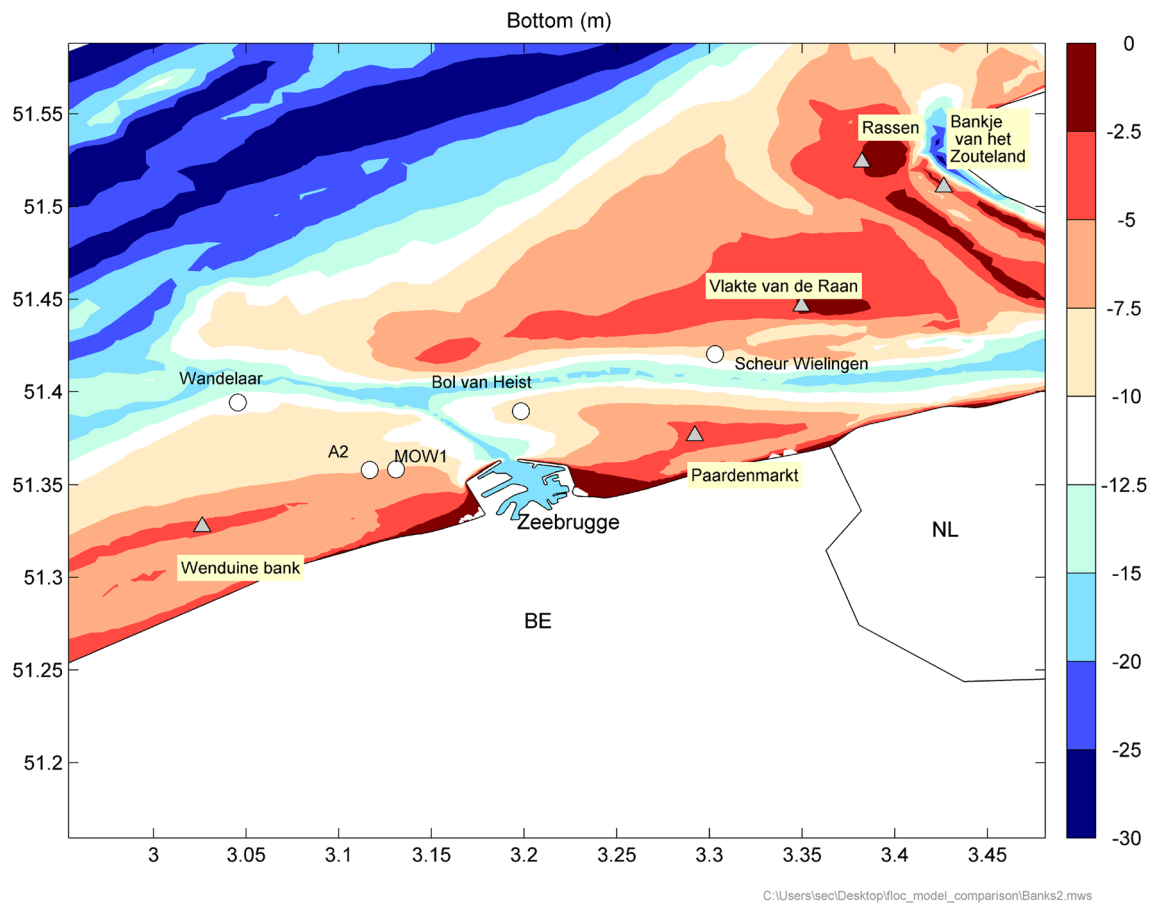
Fig. 3 Study area. The color contours show the water depth below mean sea level in m. Circle markers show the position of measurement stations, and the triangles indicate the position of known banks and shoals

The most frequent waves along the Belgian Coast, occurring approximately 30% of the time, propagate almost parallel to the shoreline, with north-east direction, a time-averaged significant wave height of 0.8 m, and a typical wave period of about 6 s.

2.2.2 Available data for calibration and validation

Data from the Flemish banks monitoring network (Meetnet Vlaamse Banken) was used for the assessment of modelled free surface water levels, flow velocities, significant wave height, and mean wave period.

Current velocity and SPM concentration were collected with a tripod at station MOW1 (Fig. 3). The instrumentation suite consisted of a point velocimeter (5-MHz ADVOcean velocimeter), a downward-looking ADP profiler (3 MHz SonTek Acoustic Doppler Profiler), and a Sequoia LISST-100X, used to measure the particle size distribution and volume concentration. The data were collected every 15 min for the LISST, and ADV, while the ADP was set to record a profile every 1 min; later on, averaging was performed to a 15-min interval (Fettweis et al. 2019).

Spatial information from the PROBA-V satellite mission was also used with the purpose of validation. This data are surface SPM concentration maps retrieved by Knaeps et al. (2017).

Modelled concentration results are brought to the reference level of the measurements and the satellite data with the Van den Eynde (2018) conversion algorithm.

2.3 Implementation in the TELEMAC modelling system

The setup consists of a layered array of nested meshes (Fig. 4) that run in the TELEMAC software (Hervouet 2000). The largest mesh (in spatial extension) covers the North Sea (NSG) and simulates hydrodynamics (waves and currents). Smaller meshes, nested in the NSG model, cover the Belgian Coast and the Western Scheldt (BCG). These smaller meshes take their seawards boundary conditions (depth, current velocity, and directional spectra of wave action) from the NSG model. This setup is inspired in modelling studies by Van den Eynde (2018); Komijani and Ortega (2016); Zhang et al. (2020).
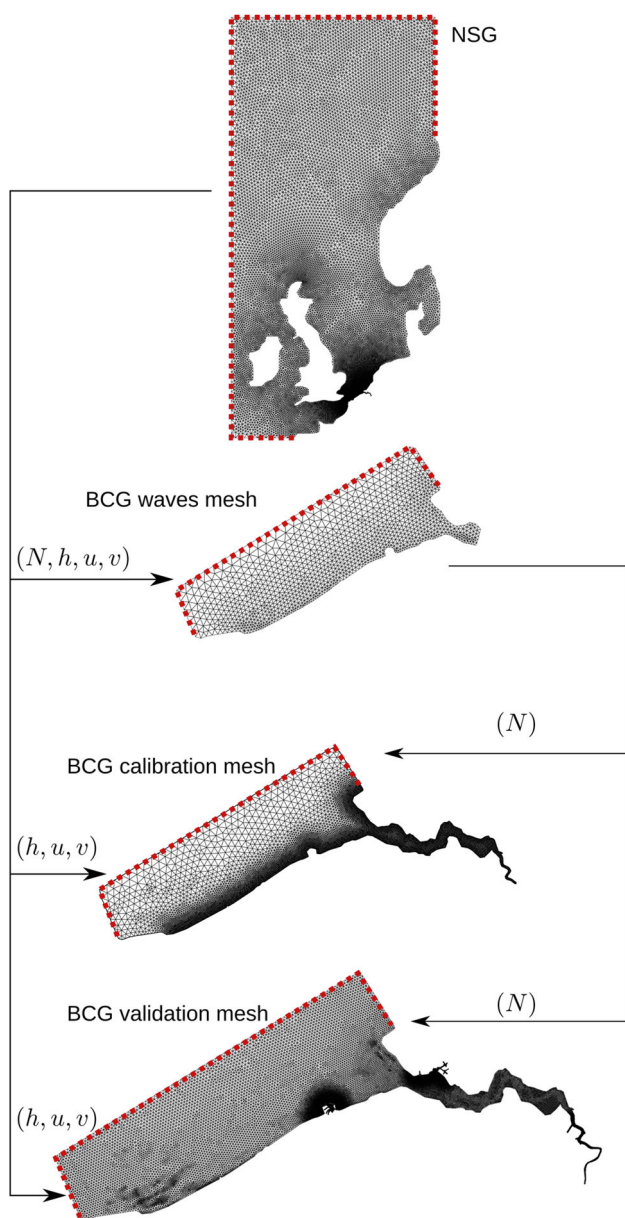
Fig. 4 Mesh layering of the North Sea and the Belgian Coast models. The dashed red lines indicate the models' offshore open boundaries. The North Sea (NSG) provides boundary directional spectra of wave action (N), the boundary depth (h), and boundary flow velocities (u, v) for meshes of the Belgian Coast (BCG). Different meshes of the Belgian Coast are used for wave calculations, for calibration of parameters, and for validation

The NSG and BCG models' timesteps are 5 s, with a coupling period of 300 s for the waves module (Sect. 2.3.2). The NSG has 20,603 nodes with edge lengths between 90 and 900 m. The BCG mesh used during calibration has 8633 nodes (edge lengths from 321.5 to 6.2 km). The BCG mesh used during validation has 24,394 nodes (67.9 to 2.0 km edge lengths). A differential approach is used for speeding up the waves calculation on the BCG model (Breugem et al. 2019);

thus, the BCG mesh of the waves module (see Section 2.3.2) has only 5434 nodes (edge lengths between 321.5 and 6.2 km) and excludes the Western Scheldt part of the study area. To minimize any transient effects of these initial conditions, a warming up time of 25 days was simulated and only the results after this period are considered for analysis.

Free surface elevation of the NSG model is prescribed from the TPXO8 global tides database (Dushaw et al. 1997). It considers eight primary (M2, S2, N2, K1, O1, P1, Q1), two long period (Mf, Mm), and three non-linear (M4, MS4, MN4) harmonic constituents. The initial hydrodynamics conditions are set to zero flow velocity and water level throughout the domain. The wave boundary conditions of the NSG model are based on a spectrum discretized in 12 directions and 25 frequencies following the discretization function $f_n = f_1 q^{n-1}$, with minimal frequency $f_1 = 0.04$ Hz and frequential ratio $q = 1.1007$. Horizontal wind velocities are interpolated spatially (inverse distance weighting) and temporally (linear) from the ECMWF ERA-Interim dataset (Berrisford et al. 2009). The boundary condition for the NSG model is a zero spectrum of wave action, and for the BCG model the boundary spectrum is imposed from results of the NSG model; thus, the same spectral discretization is used. The boundary condition at the sediment bed, for all models run during this work, is the dynamic friction law Bi and Toorman (2015).

The bathymetries of these meshes were generated from multiple datasets: The NSG uses data from EMODNET (Thierry et al. 2019) and the BCG model is made of data collected during the NEVLA project (Maximova et al. 2009). Along the foreshore, the data belongs to AMDK (2017), and on the western boundary of the model, we used data from SHOM (2015). The vertical datum of all grids is the mean sea level.

2.3.1 Hydrodynamics module

Hydrodynamics are computed by the TELEMAC-2D module which solves the shallow water equations of continuity (8) and momentum balance (9, 10) (Hervouet 2000).

$$\frac{\partial h}{\partial t} + \frac{\partial (hu)}{\partial x} + \frac{\partial (hv)}{\partial y} = 0 \tag{8}$$

$$\frac{\partial hu}{\partial t} + u\frac{\partial hu}{\partial x} + v\frac{\partial (hv)}{\partial y} = -g\frac{\partial Z}{\partial x} + F_x + \frac{1}{h}\nabla \cdot (h\nu_t\nabla u) \tag{9}$$

$$\frac{\partial hv}{\partial t} + u\frac{\partial hu}{\partial x} + v\frac{\partial (hv)}{\partial y} = -g\frac{\partial Z}{\partial y} + F_y + \frac{1}{h}\nabla \cdot (h\nu_t\nabla v) \tag{10}$$

h is the water depth, g is the gravity acceleration, Z the elevation of the free water surface, F is a source term that encompasses wind (Flather 1979), Coriolis, and the time-space varying friction induced forces. From Bi and Toorman (2015) friction law, we calculate time-space-varying bed

roughness and bed shear stress directly from the hydrodynamics with a Nikuradse roughness height of 0.03 m.

The turbulent eddy viscosity (ν_t) is modelled with the Smagorinsky formulation:

$$\nu_t = C_{s2}\Delta_{xy}^2 \left(2\bar{S}\bar{S}\right)^{1/2}$$
$$\bar{S} = \frac{1}{2}\left(\frac{\partial u}{\partial y} + \frac{\partial v}{\partial x}\right) \tag{11}$$

with $C_{s2} = 0.01$, $\bar{S}$ is rate of strain tensor, and Δ_{xy} is the spatial grid size.

2.3.2 Waves module

Evolution of the directional spectrum of wave action (12) is calculated in TOMAWAC (Benoit et al. 1997; Breugem et al. 2019).

$$\frac{\partial N}{\partial t} + \dot{x}\frac{\partial N}{\partial x} + \dot{y}\frac{\partial N}{\partial y} + \dot{k}_x\frac{\partial N}{\partial k_x} + \dot{k}_y\frac{\partial N}{\partial k_y} = Q(x, y, k_x, k_y, t) \tag{12}$$

N is the wave action density, k_x and k_y wave number vector components along the x and y directions respectively, and Q the source terms (e.g., wind-driven wave generation, whitecapping, bottom friction, wave breaking). The dot over the variables denotes the time transfer rates of each variable that are given by the linear wave theory; more details can be found in the TOMAWAC user manual (Fouquet 2020).

In this work, the following processes are taken into account: wind-driven wave generation (Komen et al. 1996), white-capping dissipation (Komen et al. 1984), bottom friction (Hasselmann et al. 1973), quadruplet interactions (Hasselmann et al. 1985), and depth-induced breaking (Battjes and Janssen 1978).

2.3.3 Sediment transport module

Suspended sediment concentration and bed evolution are calculated in the GAIA module (Tassi et al. 2023), with the advection–diffusion (13) and Exner (14) equations. We assumed that the sediment suspension can be characterized by two sediment classes. One sediment class is sand with constant grain size of 200 μm, and the other is a cohesive sediment fraction with variable mean floc diameter calculated with Eq. (1). Both sand and mud classes can be transported via the suspended load, and their mass concentrations are

---

Algorithm 1 Erosion law.

if $f_m < f_{m,s}$ **then**

$$\tau_{ce} = \tau_{ce,s} + x_1 f_m$$
$$E_s = E_{0s}(1 - f_m)\left(\frac{\tau_b}{\tau_{ce}} - 1\right)^a \tag{16}$$
$$E_m = E_{0s}f_m\left(\frac{\tau_b}{\tau_{ce}} - 1\right)^a$$

else if $f_m > f_{m,m}$ **then**

$$\tau_{ce} = \tau_{ce,m}$$
$$E_s = E_{0m}(1 - f_m)\left(\frac{\tau_b}{\tau_{ce,m}} - 1\right) \tag{17}$$
$$E_m = E_{0m}f_m\left(\frac{\tau_b}{\tau_{ce,m}} - 1\right)$$

else

$$\tau_{ce} = \frac{\tau_{ce,s} + x_1 f_{m,m}}{f_{m,m} - f_{m,s}}(f_{m,m} - f_m) + \frac{f_m - f_{m,s}}{f_{m,m} - f_{m,s}}\tau_{ce,m}$$
$$E_s = (1 - f_m)\left(E_{0s} + \frac{(f_m - f_{m,s})(E_{0m} - E_{0s})}{f_{m,m} - f_{m,s}}\right)$$
$$\left(\frac{\tau_b}{\tau_{ce}} - 1\right)^{\left[a + \frac{1-a}{f_{m,m} - f_{m,s}} - (f_m - f_{m,s})\right]} \tag{18}$$
$$E_m = f_m\left(E_{0s} + f_m\frac{(f_m - f_{m,s})(E_{0m} - E_{0s})}{f_{m,m} - f_{m,s}}\right)$$
$$\left(\frac{\tau_b}{\tau_{ce}} - 1\right)^{\left[a + \frac{1-a}{f_{m,m} - f_{m,s}} - (f_m - f_{m,s})\right]}$$

end if

  $\triangleright E$ is the erosion flux, The variable f defines the sediment class fraction, E_0 is the Partheniades constant, and the subindexes s and m denote sand and mud particle classes respectively. $f_{m,s} = 30\%$ and $f_{m,m} = 50\%$ are respectively the thresholds for non-cohesive and cohesive regimes of erosion. $\tau_{ce,s}$ and $\tau_{ce,m}$ are the critical shear stress for erosion of sand and mud respectively. $x_1 = 0.5$ N/m^2, per (Bi and Toorman 2015).

---

solved with (13).

$$\frac{\partial C_j}{\partial t} + (u, v) \cdot \nabla C_j = \epsilon_s\nabla^2 C_j + \frac{E_j - D_j}{h} \tag{13}$$

$$(1 - n)\frac{\partial Z_f}{\partial t} + \nabla \cdot Q_s = \frac{\sum D_j - E_j}{\rho_s} \tag{14}$$

The index j notes the sediment class, and $\epsilon_s = \nu_t/\sigma$ is the sediment diffusivity, with σ the turbulent Schmidt number taken as 0.70, as in (2). E and D are the erosion and deposition fluxes. n is the sediment bed porosity, Z_f is the elevation of the bed, and Q_s is the bedload transport rate of sand.

The bed shear stress (τ_b) of the combined wave-current field was computed with the Soulsby and Clarke (2005) formula. The deposition flux (15) was calculated using the

suspension capacity theory by Toorman (2000, 2003), and the erosion flux (Algorithm 1) with a hybrid erosion law proposed by Waeles et al. (2007); Le Hir et al. (2011), and adapted by Bi and Toorman (2015), which empirically combines three erosion regimes: sandy bed, mixed bed, and muddy bed.

$$D_j = w_s C_j \quad max \left\{ 0, \quad 1 - \frac{\tau_b U R_{f_L}}{(1 - \rho_w / \rho_f) g h w_s C_j} \right\}$$

$$R_{f_L} = \frac{0.25}{1 + \left(\frac{0.1 u_*}{w_s} \right)^2} \quad (15)$$

w_s is the sediment settling velocity solved with Eq. 7, U is the norm of the flow velocity vector, and R_{f_L} is the flux Richardson number, assuming the sediment suspension is saturated (Toorman 2000).

Initial conditions are a mean floc diameter of 40 μm throughout the domain, the winter average surface SPM concentration map from Fettweis et al. (2007), and the relative sand content from maps of Rijkswaterstaat (Ministry of Infrastructure and Water Management, the Netherlands), RBINS-MUMM (Scientific Service Management Unit of the Mathematical Model of the North Sea, Belgium) and Stephens and Diesing (2015). The initial sediment bed is assumed to have two vertical layers with a thickness of 0.1 m and 0.3 m respectively. Boundary conditions offshore are free tracer flux for the suspended concentration of sand, mud, and the floc size variables.
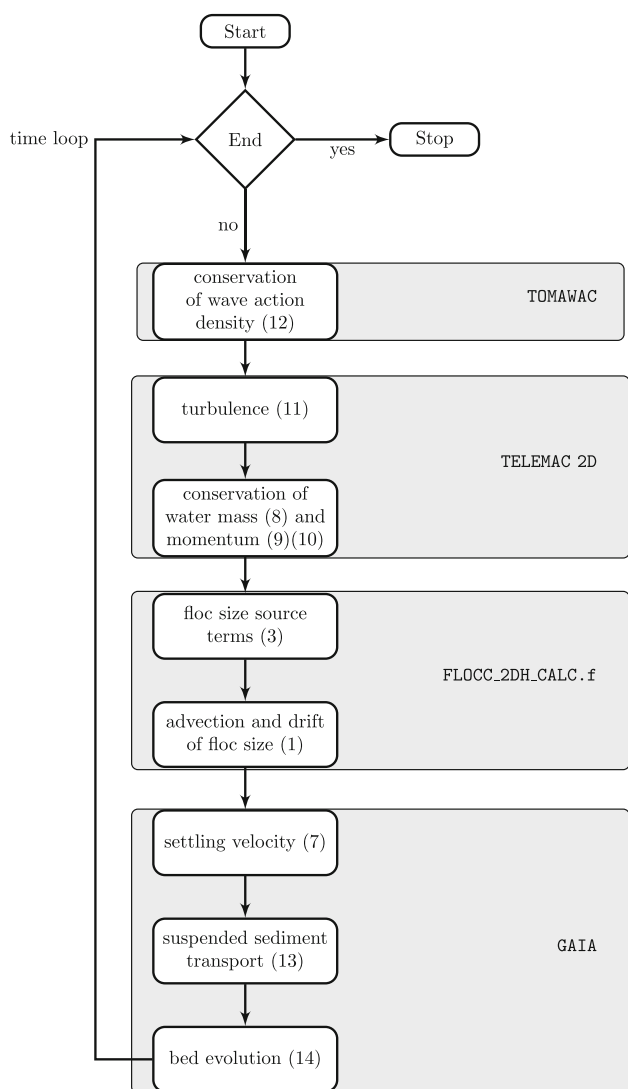
Fig. 5 Computational loop in TELEMAC. The proposed flocculation model has been coded in a new subroutine (FLOCC_2DH_CALC.f) of the TELEMAC software
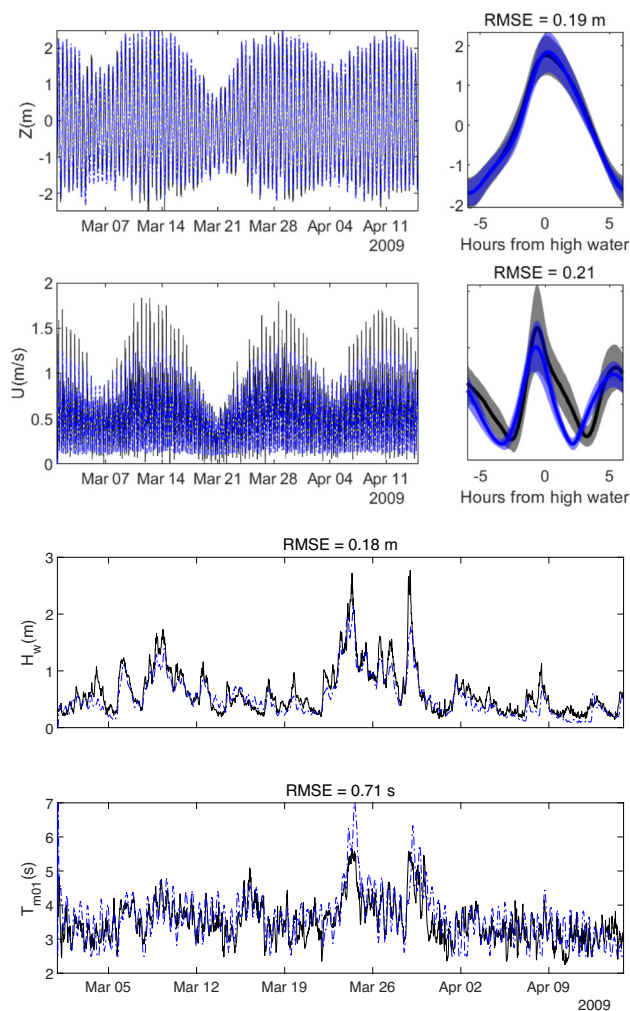

Fig. 6 Hydrodynamics at Bol Van Heist station. The black solid lines are measurements from the Flemish Banks Monitoring Network, and the blue lines are results from the BCG model. In the ensemble averages (first and second rows, right column), the solid lines are temporal means and the shaded areas are the standard deviation

Fig. 7 Model calibration. The black and blue colors represent LISST-measured and modelled values respectively. The lines correspond to the time mean of the data and the shaded areas represent the standard deviation. The data belongs to a time interval from 01/03/2009 to 20/04/2009 at the MOW1 station
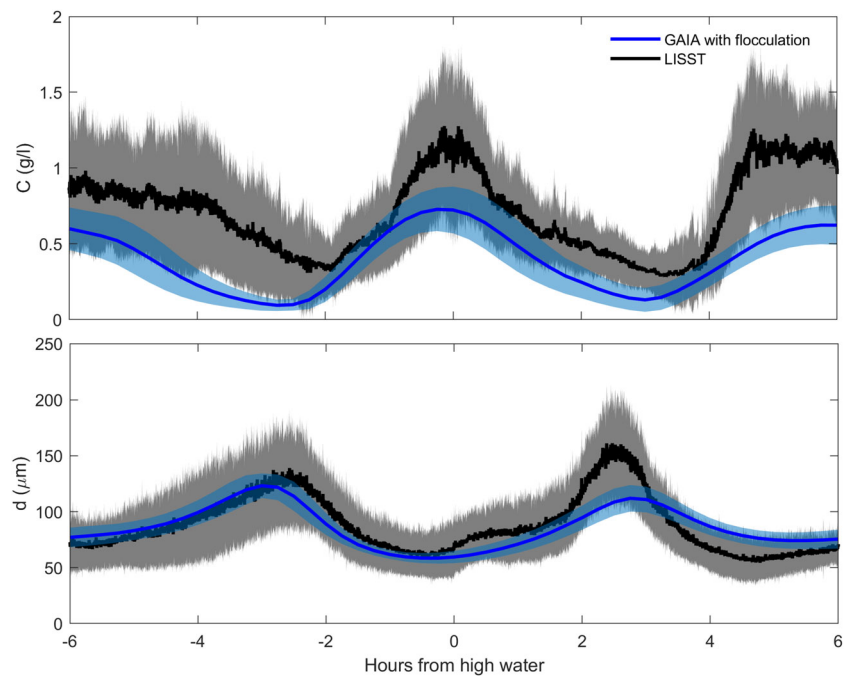
2.4 Computational loop in TELEMAC

Equations (1) to (7) were coded in a new subroutine of TELEMAC called `FLOCC_2DH_CALC.f`. The computational loop is in Fig. 5, subroutine `FLOCC_2DH_CALC.f` is called after the solution of the flow variables in TOMAWAC and TELEMAC 2D, and before the solution of the suspended sediment transport in the GAIA module. Due to the source terms stiffness, time integration is done through the 4th order step-variable Runge–Kutta method designed and implemented in FORTRAN by Press et al. (1992).

3 Results

3.1 Model calibration

Hydrodynamics Modelled free surface levels and flow velocities agree with the available measurements. Figure 6 (first and second rows) shows that the error is a small fraction of the range of variation of the free surface level and the flow velocities. The root mean square error (RMSE) is 0.19 m for the water level, and 0.21 m/s for the flow velocity. Wave model results (Fig. 6, third and fourth rows) are also acceptable with RMSE values of 0.18 m and 0.71 s for the significant wave height and the mean wave period respectively.

Comparison of modelled hydrodynamics and measurements at other locations yielded similar results. These can be seen in Appendix 2.

Suspended sediment concentration and mean floc diameter
Modelled suspended sediment concentration and mean floc diameter were compared with field data from the MOW1 station. The comparison period spans between 01/03/2009 and 20/03/2009, and the time information was clustered over one high-low-water cycle to facilitate visualization. Figure 7 shows the best fitting model results after calibration (see

Table 1 Parameter values of the calibrated model Belgian Coast model

Parameter	Value
time step (Δt)	5 s
Top layer thickness	0.1 m
Bottom layer thickness	0.3 m
Top layer mud concentration	680.0 kg/m^3
Bottom layer mud concentration	900.0 kg/m^3
E_{0s}	0.008 kg/m^2/s
E_{0m}	0.002 kg/m^2/s
$\tau_{ce,s}$	0.05 N/m^2
$\tau_{ce,m}(1)$	0.02 N/m^2
$\tau_{ce,m}(2)$	0.04 N/m^2
d_p	20 μm
k_a	1800
k_b	30
T_r	3600 s

$\tau_{ce,m}(1)$ and $\tau_{ce,m}(2)$ are the critical bed shear stresses for erosion of mud for the top and bottom sediment layers respectively

Appendix 1), which were obtained with the parameter values listed in Table 1.

Based on Fig. 7 (first row), the sediment model has a moderate success at reproducing the suspended sediment concentration. Results peak during flood and ebb, and concentration troughs take place during slack waters. This pattern is consistent with the measured data. However, in quantitative terms, the model results underestimate the measurements. Modelled concentrations do not reach neither the same peaks (1.26 g/l during flood, and 1.10 g/l during ebb), nor the same troughs (0.38 g/l and 0.28 g/l during slack waters from low to high and from high to low water respectively). Also, the sediment model has a phase lead of approximately

20 min during ebb, and 1 h during slack waters. The RMSE obtained for the suspended sediment concentration is 0.29 g/l.

The floc size dynamics in Fig. 7 (second row) show that the flocculation model results overlap with the measured mean floc size. Modelled and measured data are within the band of macroflocs and megaflocs (Fettweis et al. 2012; Shen et al. 2018), with values ranging between 70 and 150 μm for the measurements, and 40 to 290 μm for the simulations. Also, the model qualitatively follows the same temporal pattern as the measurements, displaying two peaks within a tidal cycle, one at slack water from ebb to flood, and a higher peak at slack from flood to ebb. The difference between the two floc size peaks is explained by tidal asymmetry, which causes

Fig. 8 Validation of model results. Top row, LISST-measured SPM concentration (black star markers) and modelled suspended sediment concentrations with flocculation (blue line), without flocculation and constant values of $w_s = 3.5$ m/s and $w_s = 2.0$ m/s (green and red lines respectively). Second row, LISST-measured mean floc size and modelled mean floc diameter. Third row, modelled free surface level (solid line) and significant wave height (dashed line). Fourth row, wind speed and direction (trigonometric convention) 10 m above the mean sea level. The simulation "GAIA with flocculation" uses the flocculation formulation proposed in this work. The simulation "GAIA without flocculation 1" assumed a constant settling velocity of 3.5 mm/s, and "GAIA without flocculation 2" assumed a constant settling velocity of 2.0 mm/s
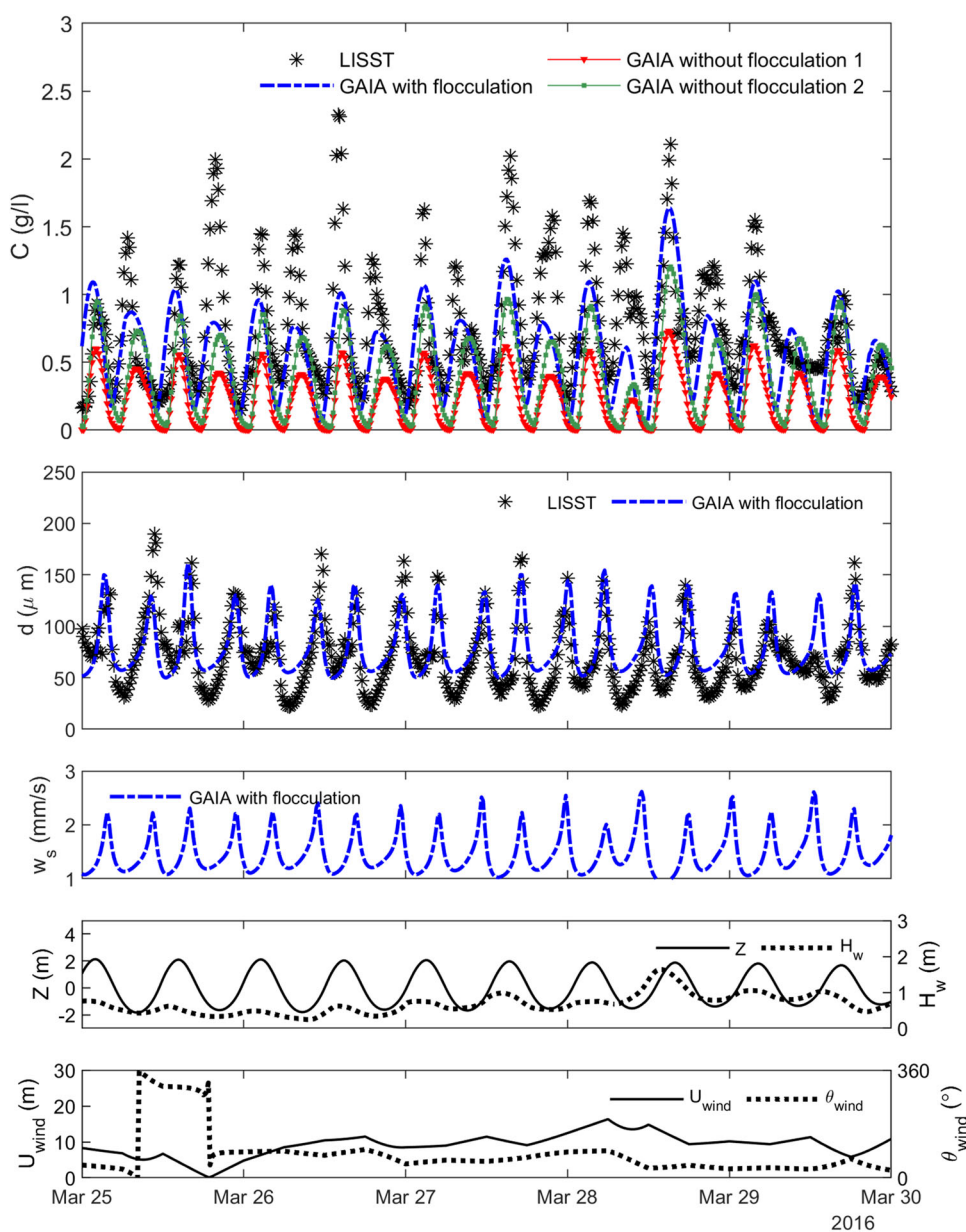
flow velocities—and turbulent shear—to be higher from ebb to flood than in the transition from flood to ebb (Bolle et al. 2010). Model deviations are generally a phase-lead, which causes floc size peaks to happen approximately 40 min earlier than in measurements, plus gaps in amplitude up to 100 μm. The RMSE obtained for mean floc diameters was 23 μm.

3.2 Model validation

Comparison with field data The validation period spans between 20/03/2016 and 30/03/2016. The modelled sediment concentration (Fig. 8, first row) matches in time with the measurements. The model follows the current-driven concentration peaks, although it deviates between 24/03/2016 and 29/03/2016, when U_{wind} is high (up to 15 m/s, see Fig. 8 fifth row) and the effect of waves becomes more important (Fig. 8, fourth row). Figure 8 also shows the results obtained without activating the flocculation equations, and with constant settling velocities of 3.5 mm/s and 2 mm/s (Fig. 8, first row), values previously used by Van den Eynde (2018). Without flocculation the concentration magnitudes are smaller, even showing nil concentrations throughout the totality of the ebb phase. Also, there is a shift in the concentration, whereby erosion and deposition cycles take place at a faster rate. This is corrected in the simulation with flocculation due to it accounting for the variability in the floc size. RMSE values of suspended sediment concentration were 0.39 g/l for the simulation with flocculation, 0.69 g/l without flocculation and w_s = 3.5 mm/s, and 0.55 g/s for the one without flocculation and w_s = 2.0 mm/s.

The mean floc diameters match overall in amplitude and phase (Fig. 8, second row). The RMSE obtained for the mean floc size was 78.02 μm. The modelled settling velocity (Fig. 8, third row) shows a pattern with increasing values

for the aggregation phase, and lower values during breakage. The range of values of the settling velocity is within 1 to 2.2 mm/s, and it is smaller than conventional ranges (e.g., 2.0 to 3.5 mm/s) found in the literature of the study area (Van den Eynde 2018; Bi and Toorman 2015).

Comparison with satellite data Comparison between satellite data and model results focused exclusively on the suspended sediment concentration because it is impossible to retrieve a particle size measure from satellite data. There were seven images with low cloudiness for comparison available between 01/03/2016 and 17/05/2016. Figure 9 shows extracted time series from these images and model results at the MOW1 station. Model results, with and without flocculation, are in the same range of values of the satellite SPM data. However, they do not show the same patterns. When the model runs without flocculation, the resulting suspended sediment concentration does not display the same seasonal decreasing trend induced by the flocculation equations. The maximum RMSE, between results and satellite data at the MOW1 station, is 0.014 g/l (during 12/04/2016 11:20) for the simulation with flocculation, 0.028 g/l (during 12/03/2016 11:20) for without flocculation and w_s = 3.5 mm/s, and 0.056 g/l (during 12/03/2016 11:20) for the one without flocculation and w_s = 2.0 mm/s.

The modelled large-scale sediment concentration patterns were also assessed. Figure 10 displays a PROBA-V image and model results with timestamp 01/05/2016 11:00. There are three major plumes that the model with flocculation reproduces qualitatively well: The first over Wenduine bank, second over Paardemarkt, and the third at the Western Scheldt delta, over Vlakte van de Raan shoal. These modelled plumes have approximately the same longshore extent and shape as the observed, although they are more confined to the
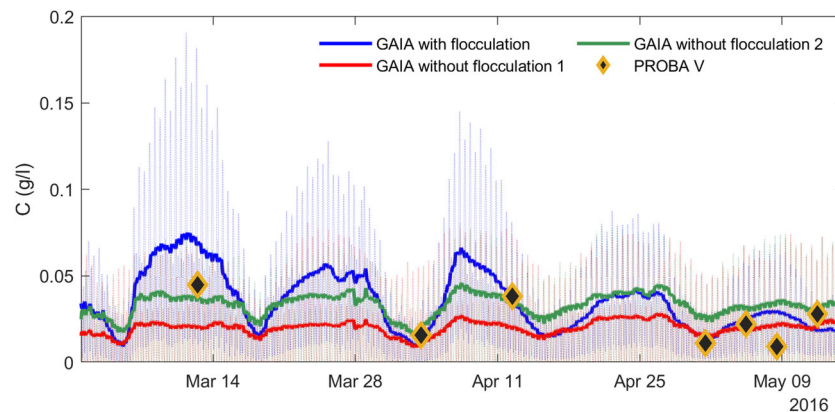

Fig. 9 PROBA-V satellite-retrieved SPM and near-surface sediment concentration retrieved from model results at the MOW1 station. The thin lines are the data extracted from GAIA, and the thick lines are the same data but filtered with a moving average window of 24 h. The simulation "GAIA with flocculation" uses the flocculation formulation proposed in this work. "GAIA without flocculation 1" assumed a constant settling velocity of 3.5 mm/s, and "GAIA without flocculation 2" assumed a constant settling velocity of 2.0 mm/s

Fig. 10 Spatial comparison of PROBA-V satellite-retrieved SPM (top) and modelled near-surface sediment concentration achieved with the proposed flocculation setup (bottom). The timestamp is 01/05/2016 11:00. Arrows indicate the current flow velocity direction. The numbered labels over the bottom map designate known banks and shoals: 1, Wenduine bank; 2, Paardenmarkt; 3, Vlakte van de Raan; 4, Rassen; 5, Bankje van het Zouteland
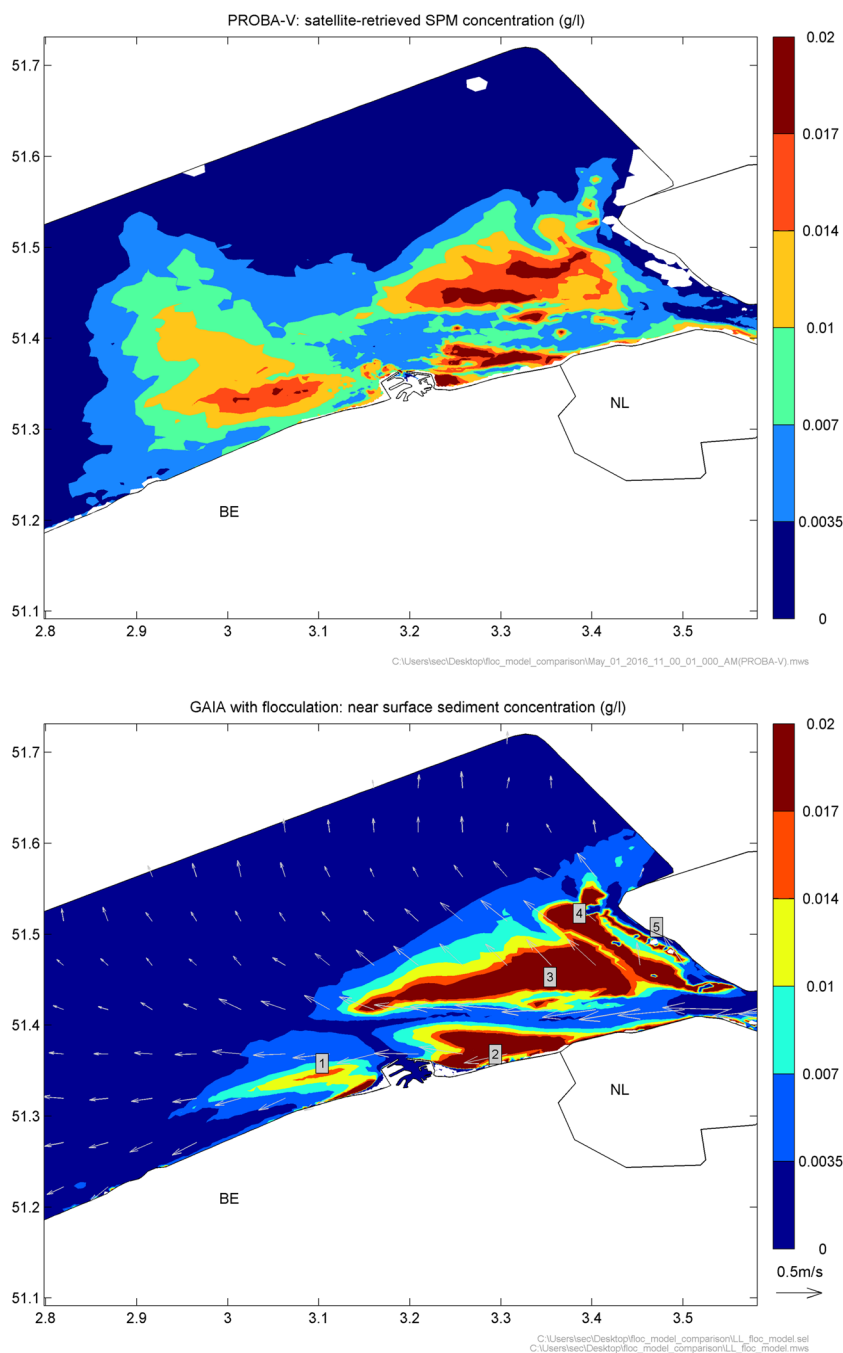

nearshore. A hypothesis that could explain the differences offshore is related with the biological processes. The satellite image was taken during spring, and in the middle of the growing season of phytoplankton Nohe et al. (2020), so the drifting plume observed off the coast may be partly made of biological SPM, which cannot be taken into account with the present model. We infer that the sediment plumes seen in Fig. 10 are mostly caused by local erosion because they overlap with the shallow and the mud-rich areas of the Western Scheldt and the Belgian Coast. Also, these plumes could

not be the result of remote transport since hydrodynamics at that time were calm, with spring tide currents up to 0.6 m/s, small wavelets (significant wave height $H_w < 0.5$ m), and light air ($U_{wind} \leq 1$ m/s).

When the flocculation equations are deactivated (Fig. 11), the sediment plumes are more localized, and the transport of sediment away from the originating shoals and banks of Paardenmarkt, Vlakte van de Raan Rassen, and Bankje van het Zouteland mostly limited. Also, different from the model with flocculation, and the satellite SPM data (Fig. 10), the

Fig. 11 Modelled near-surface sediment concentrations, without flocculation and with constant settling velocities. Top, the settling velocity was assumed 3.5 mm/s. Bottom, the settling velocity was assumed 2.0 mm/s. The timestamp is 01/05/2016 11:00. Arrows indicate the current velocity. The numbered labels over the maps designate known banks and shoals: 1, Wenduine bank; 2, Paardenmarkt; 3, Vlakte van de Raan; 4, Rassen; 5, Bankje van het Zouteland
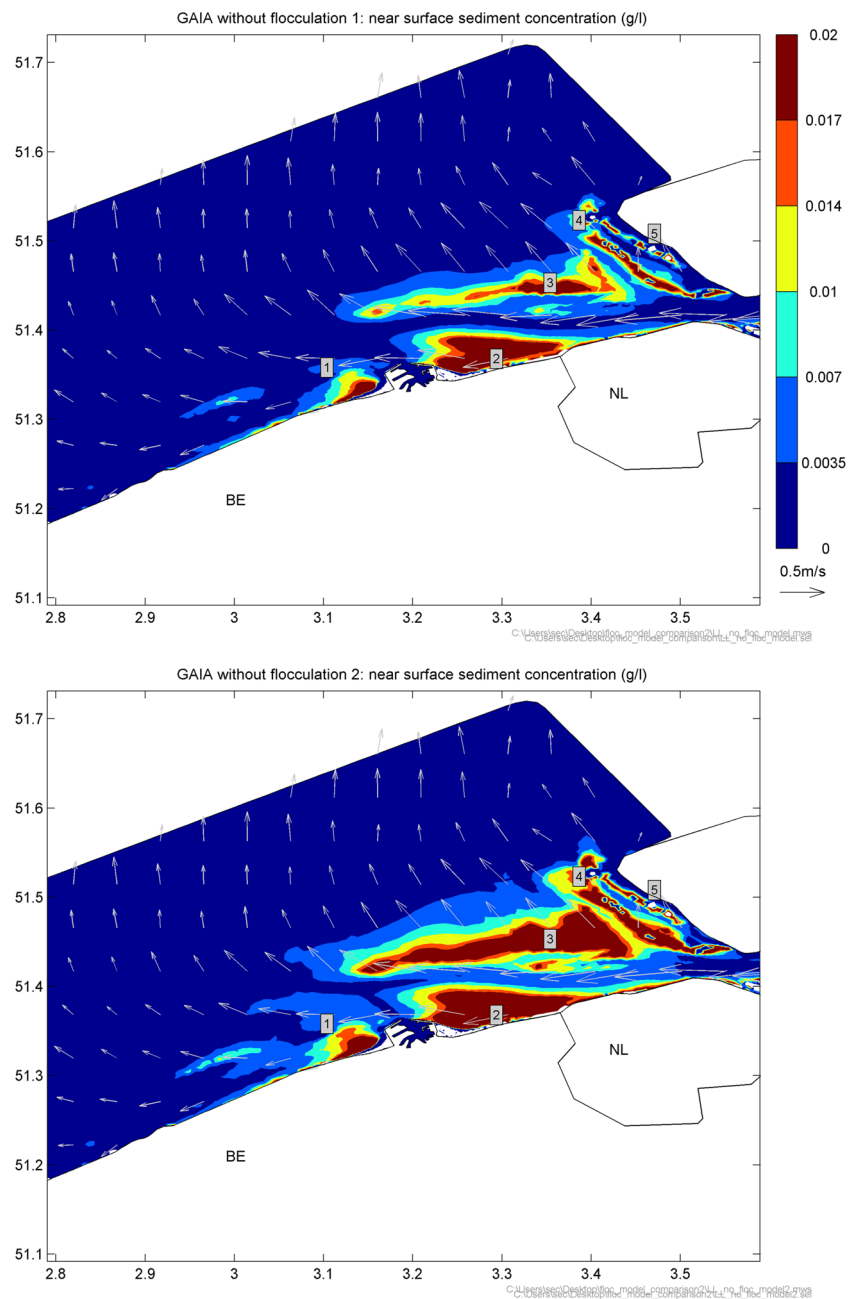
plumes near Wenduine bank are on a narrow band on the beach. These results highlight the main limitation of conventional models where settling velocity is a constant, and that they do not properly reproduce the spatial and temporal variability of the suspension.

4 Discussion

The model presented in this work incorporates flocculation processes in the 2DH framework. Application to the Belgian Coast indicates that it is able to reproduce the suspended sediment concentration and mean floc size dynamics of the study area with moderate success. Its main feature is that the settling velocity is a function of morphodynamics (bed shear stress and suspended sediment concentration), which is an improvement with respect to the conventional approach of using a constant settling velocity value. This can be seen in Figs. 10 and 11, where the simulation with flocculation has a better spatial agreement with the satellite-retrieved SPM. In Fig. 12, it can also be seen that the simulation with flocculation agrees more in phase and magnitude with the measurements.
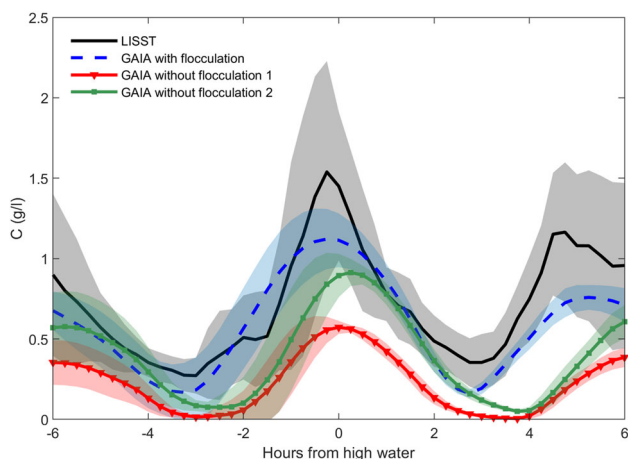
Fig. 12 Ensemble averaged concentration pattern at the MOW1 station. The black color represent LISST-measured values, the blue color represents the results of the flocculation model, and the green and red colors represent model results obtained without active flocculation and assuming constant settling velocities of 3.5 mm/s and 2 mm/s respectively. The lines are the temporal means, and the shades symbolize the standard deviation. The data belongs to the period between 20/03/2016 and 30/03/2016

The spatial patterns caused by the flocculation model are as follows: zones with the highest bed shear stresses and flow velocities have the smallest suspended flocs and lowest settling velocities. Conversely, zones with lower shear have the largest flocs and highest settling velocities. This can be observed in Fig. 13 along the navigation canal, where the flow is fast and with high shear ($\tau_b \approx 1.1$ N, $\|u\| \approx 1$ m/s), and in consequence particles are small with low settling velocity values ($50\,\mu$m, 0.001 m/s). In contrast, in the northwest, where flow velocity values are small ($\|u\| = 0.25$ m/s), floc size and settling velocity are the largest ($200\,\mu$m, 0.0026 m/s). The spatial aspect of the floc size and settling velocity is also dependent on the suspended sediment concentration. This SPM-dependence of the model may be further improved by linking empirically the coefficients k_a and k_b terms to salinity, the bed composition, organic matter content, and other aspects of the physical and biological environment which may affect electrolyte concentrations and flocculation kinetics (Fettweis and Lee 2017).

Differences between model results, and measurements and the satellite data used for model validation arise from the following limitations:

1. The floc size is multimodal, whereas the proposed model simulates the mean floc size, which makes the match of modelled results and measurements difficult to assess (Benson 2005). Moreover, Lee et al. (2012) found out, in the same study area of this work, that the estimated settling fluxes with a single discrete aggregate group had up to 45% errors against the reference settling flux of

a continuous multimodal floc size distribution (FSD). Also in the Belgian Coast, Shen et al. (2018) proved that introducing additional size groups into FSD model equations improves the prediction of settling and deposition of cohesive sediments. This explains why the presented model underestimates the low and peak values of suspended sediment concentration. Because by modelling only the mean floc size, suspended particles fall with the mean settling velocity and not the size-specific one.

2. The sediment fraction used in this work is entirely mineral; therefore, it is a simplification of the sediments found in nature. Sediments consist of inorganic and organic matter, and both groups of particles are very heterogenous (Ho et al. 2022; Tran and Strom 2017). Also, the composition of the SPM changes with concentration; it becomes more organic when the concentration decreases. This occurs along a nearshore to offshore gradient; hence, the particles are more organic and flocculation hardly occurs in the low turbid offshore (Maerz et al. 2020; Alldredge and Silver 1988; Turner 2015). So, by not accounting for the organic part of sediments, the presented model cannot reproduce well the offshore extent of the turbidity plumes.

3. Throughout this work, we assumed a 2D depth-averaged framework. Because of this, it was necessary to then assume that the suspension followed a Rouse profile. This was later used to transfer modelled depth-averaged concentrations to the near-bed, where measurements were available, and to the near-surface, where satellite data were available for comparison. This chain of decisions is debatable since Rouse profiles are valid for steady flows, which by definition are less variegated than the combined wave-current conditions taking place at the Belgian Coast (Bolle et al. 2010; Smolders et al. 2019; Vanlede et al. 2019).

4. LISST measurements of floc size have their own uncertainties because they assume spherical particles. The LISST sensor emits a laser beam and detects light scattering by particles. The intensities of scattered light are then inverted to estimate particle size distributions assuming spherical shapes; this influences the FSD and the mean floc size estimated from it because natural flocs have irregular shapes (Shen et al. 2019; Spencer et al. 2021). Also, the presence of particles outside the size range of the LISST introduce further uncertainties in the FSD Andrews et al. (2010); Graham et al. (2012).

The above listed limitations are not unique to this work. They are commonly acknowledged in flocculation studies (Shen et al. 2019; Soulsby et al. 2013; Nohe et al. 2020; Fettweis et al. 2022), and the necessity of further knowledge to better model and measure natural floc systems is a usual con-

Fig. 13 Modelled floc size (top) and settling velocity (bottom) during 01/05/2016 11:00. Gray arrows and black contours symbolize flow velocity and bed shear stress respectively
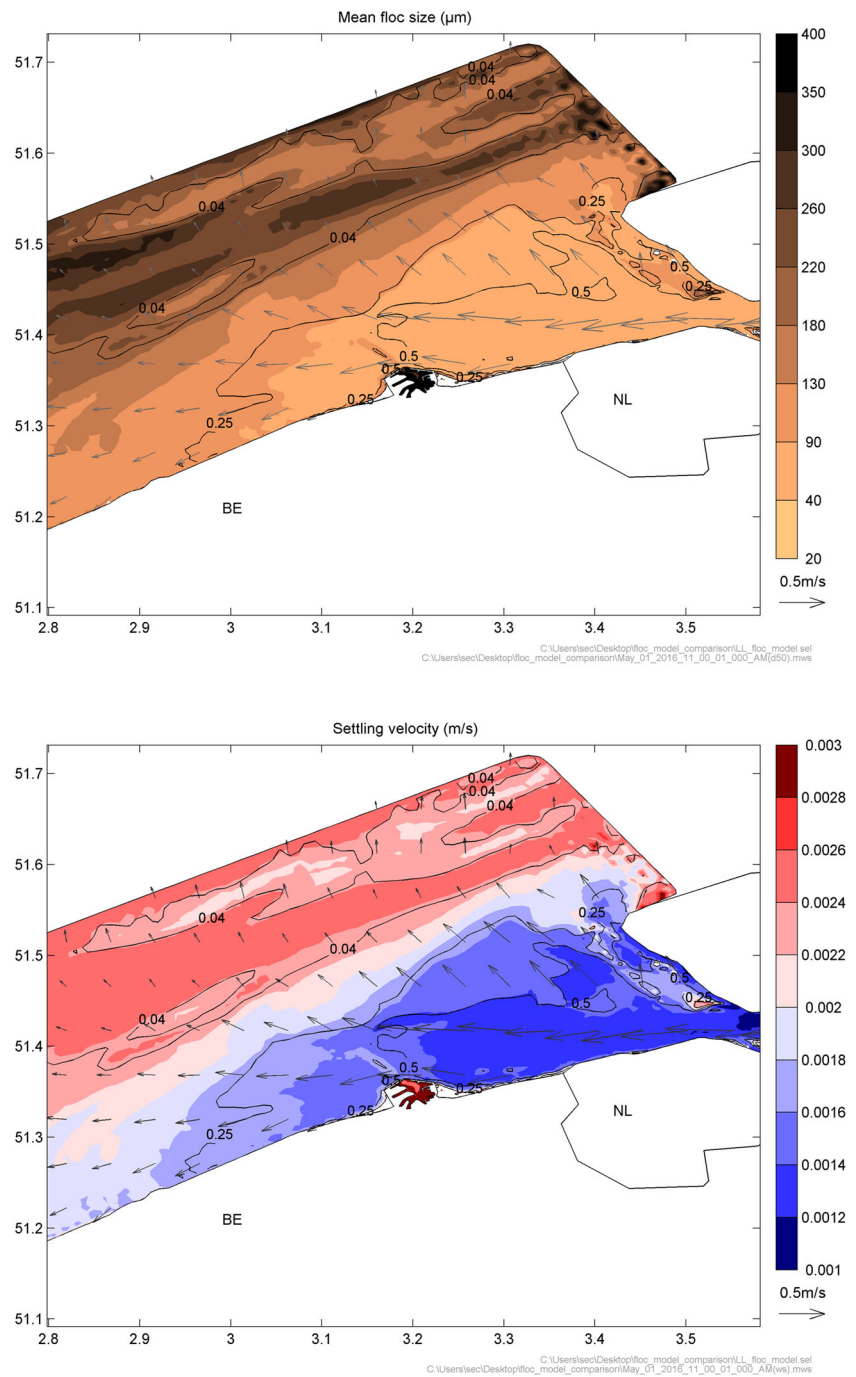
clusion (Benson 2005; Ho et al. 2022; Spencer et al. 2021; Fettweis et al. 2019). In this context, the newly proposed flocculation formulation, and its implementation in an open-source software as TELEMAC, is a valuable step towards modelling flocs' transport in large coastal domains. Moreover, being a 2DH model with only one additional differential Eq. 1, it has a good balance between computational time and accuracy, which is a plus with respect to more complex 3D and/or FSD models. Further developments of the proposed model are the inclusion of seasonal biological processes, and

salinity effects, which would improve results offshore and make this model applicable to estuarine waters.

5 Conclusion

A new kinetic formulation of the flocculation process, based on Winterwerp (1998) model, was implemented and assessed in a realistic application to the Belgian Coast with moderate success. Results are in the range of measured floc sizes and

suspended sediment concentrations of the study area. The model can also mimic spatial suspension patterns observed in satellite-retrieved suspended particle matter concentration maps, with modelled and observed sediment plumes matching spatially in longshore extent and location. The proposed flocculation model can therefore improve sediment transport calculations in coastal areas.

Author Contributions Conceptualization, E.T.; investigation, S.E., Q.B. and S.W.; writing—original draft preparation, S.E.; writing—review and editing, S.E., Q.B., E.T., J.M. and M.F; supervision, E.T., J.M.; All authors have read and agreed to the published version of the manuscript.

Declarations

Appendix A: Flocculation and sediment model calibration

A total of 19 Simulations were run with the flocculation equations activated. These simulations start on 01/03/2009 00:00 and have a duration of 45 days. The initial 25 days are considered warm-up time and discarded from any analysis. Only the remaining time interval was used.

The first simulation was called "standard". It used the parameter values listed in in Table 2. The ensuing simulations consisted on progressive but not cumulative variations of the parameter values of the standard simulation (Table 2). The characteristic parameters of each of these simulations are listed on Table 3, column "Characteristic parameters". The suspended sediment concentration and the mean floc size variables, at the MOW1 station, were extracted from all simulations' results and used for sensitivity analysis and for choosing the best performing set of parameters.

The sensitivity analysis consisted of qualitative comparisons of the calibration simulations with the standard. These results can be seen in Figs. 14 and 15. The summarized patterns are listed in Table 3 (column "Response"). In general,

Table 2 Parameter values of the "standard" simulation, which was the baseline throughout the calibration process

Parameter	Value
time step (Δt)	5 s
Top layer thickness	0.1 m
Bottom layer thickness	0.3 m
Top layer mud concentration	680.0 kg/m^3
Bottom layer mud concentration	900.0 kg/m^3
E_{0s}	0.006 kg/m^2/s
E_{0m}	0.002 kg/m^2/s
$\tau_{ce,s}$	0.05 N/m^2
$\tau_{ce,m}(1)$	0.02 N/m^2
$\tau_{ce,m}(2)$	0.04 N/m^2
d_p	20 μm
k_a	1600
k_b	30
T_r	900 s

the suspended sediment concentration is more sensible to parameters that are directly linked to sediment availability and erodibility. For example, increasing values of the bottom layer thickness and the Partheniades constants lead to larger overall concentrations. Conversely, larger values of the constant a, and lower values of the thresholds for non-cohesive and cohesive erosion, lead to lower sediment concentration values. The parameters associated with the mean floc size are less sensible regarding the suspended sediment concentration, but they do cause some important variations. Large values of the aggregation constant and the relaxation time decrease the suspended sediment concentration.

The mean floc size is more responsive to parameters linked directly to the aggregation source term. The aggregation constant plays a major role, and increasing its value causes the floc size to increase. Raising values of the relaxation time also lead to larger flocs and a slightly less peaked floc size curve. On the other hand, directly-related sediment parameters are only sensible if they cause acute decreases on the sediment concentration. That is, large values of a and low thresholds for non-cohesive and cohesive erosion cause larger floc sizes.

Regarding the critical bed shear stress, the results were not conclusive and it is difficult to assign a straightforward sensitivity to this parameter. The reason for this is that by having two vertical sediment layers, the model response to variations is consequence of the combination of critical bed shear stresses of both layers. For example, in simulations "tau ce m0015" and "tau ce s001" the critical bed shear stresses of the top layer decreased, either because the critical bed shear stress of the mud or the sand fractions were reduced. This caused the top layer to wash away and only the bottom layer remained. However, this resulted in

Ocean Dynamics

Table 3 Sensitivity analysis. Calibration runs are qualitatively compared with the standard simulation. The characteristic parameters are the changes relative to the standard, the arrows indicate an increase (↑) or decrease (↓) relative to the standard parameters. The response column evaluates the results relative to the standard, the arrows indicate an increase (↑) or decrease (↓) relative to the standard results

Simulation	Characteristic parameters	Response C (g/l)	d (μm)
standard	—	—	—
E0S0008	$E_{0s} = 0.008$ kg/m²/s ↑	↑	↑
E0V00016	$E_{0m} = 1.6E-4$ kg/m²/s ↓	↓	↑
Erosion law NS 05	a = 0.5 ↓	↓	↑
Erosion law NS 1 5	a = 1.5 ↑	↑	↑
tau ce m0015 ‡	$\tau_{ce,m}(1) = 0.015$ N/m² ↓ $\tau_{ce,m}(2) = 0.025$ N/m² ↓	—	—
tau ce m004‡	$\tau_{ce,m}(1) = 0.04$ N/m² ↑	—	—
tau ce s001‡	$\tau_{ce,s} = 0.01$ N/m² ↓	—	—
tshld 15 25	$f_{m,s} = 0.15$ ↓ $f_{m,m} = 0.25$ ↓	↑	↑
tshld 25 35	$f_{m,s} = 0.25$ ↓ $f_{m,m} = 0.35$ ↓	↑	↑
Top thickness 0.2	Top layer thickness = 0.2 m ↑	↓	↑
Bottom thickness 0.5	Bottom layer thickness = 0.5 m↑	↑	↑
Tr3600	$T_r = 3600$ s ↑	↓	↑
Tr3600 ka1800	$T_r = 3600$ s ↑ $k_a = 1800$ ↑	↓	↑
Tr3600 ka1800 E0S0008	$T_r = 3600$ s ↑ $k_a = 1800$ ↑ $E_{0s} = 8E-3$ kg/m²/s ↑	↑	↑
Trvar3600 ka1800	$T_r = \frac{3600}{(1+100\frac{s}{m}u_*)^2}$ s $k_a = 1800$ ↑	↓	↑
Trvar 900	$T_r = \frac{900}{(1+1\frac{s}{m}u_*)}$ s	↓	↑
ka2080	$k_a = 2080$ ↑	↓	↑
kb60	$k_b = 60$ ↓	-	-

‡ Non-conclussive result

lower suspended sediment concentrations because the bottom layer had larger critical bed shear stresses for the mud fraction.

The best performing simulation was chosen by ranking the RMSE of both the suspended sediment concentration and the mean floc size, which were calculated for each simulation and with respect to measurements at the MOW1 station (see Table 4). The best simulation was "Tr3600 ka1800 E0S0008", and its parameter values were used in Sections 3.1 and 3.2.

Fig. 14 Model calibration simulations in direct connection with the suspended sediment concentration. $\tau_{ce,m}(1)$ and $\tau_{ce,m}(2)$ are the critical bed shear stresses for erosion of mud for the top and bottom sediment layers respectively. The arrows on the figure legend indicate an increase (↑) or decrease (↓) in the parameter values relative to the standard simulation. LISST-measurements (black solid line) are included for reference
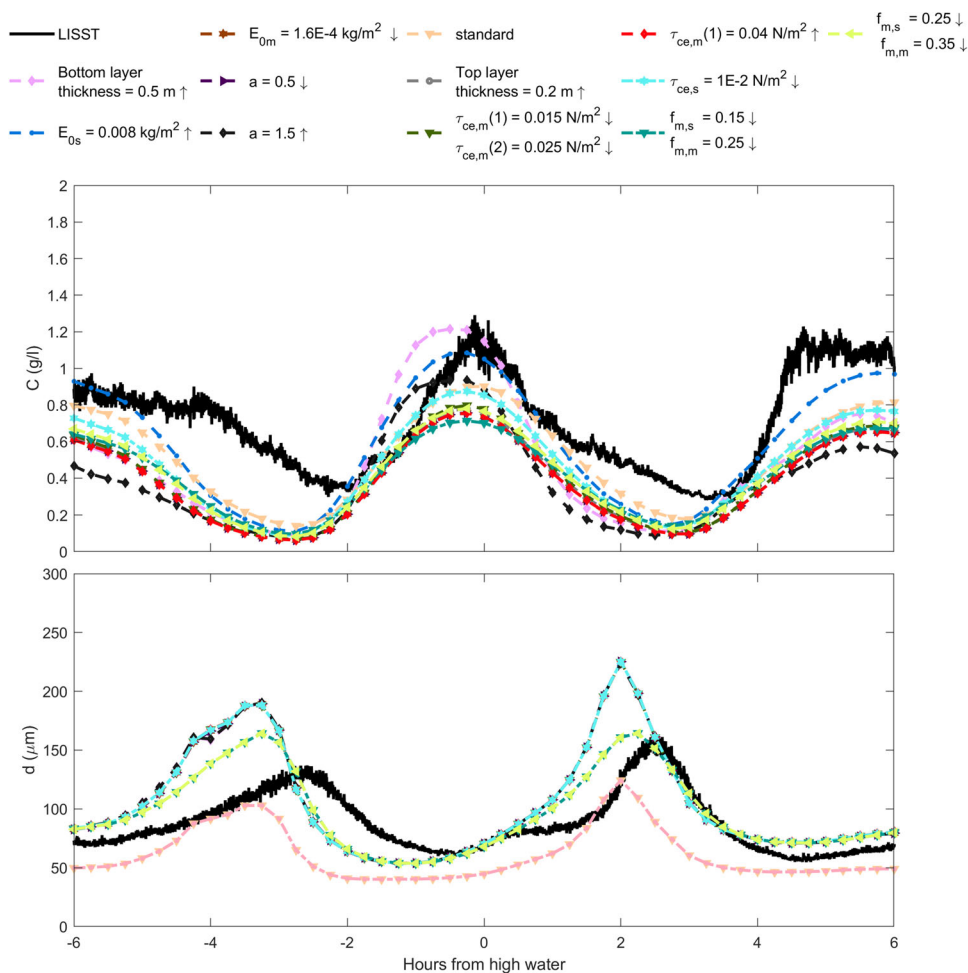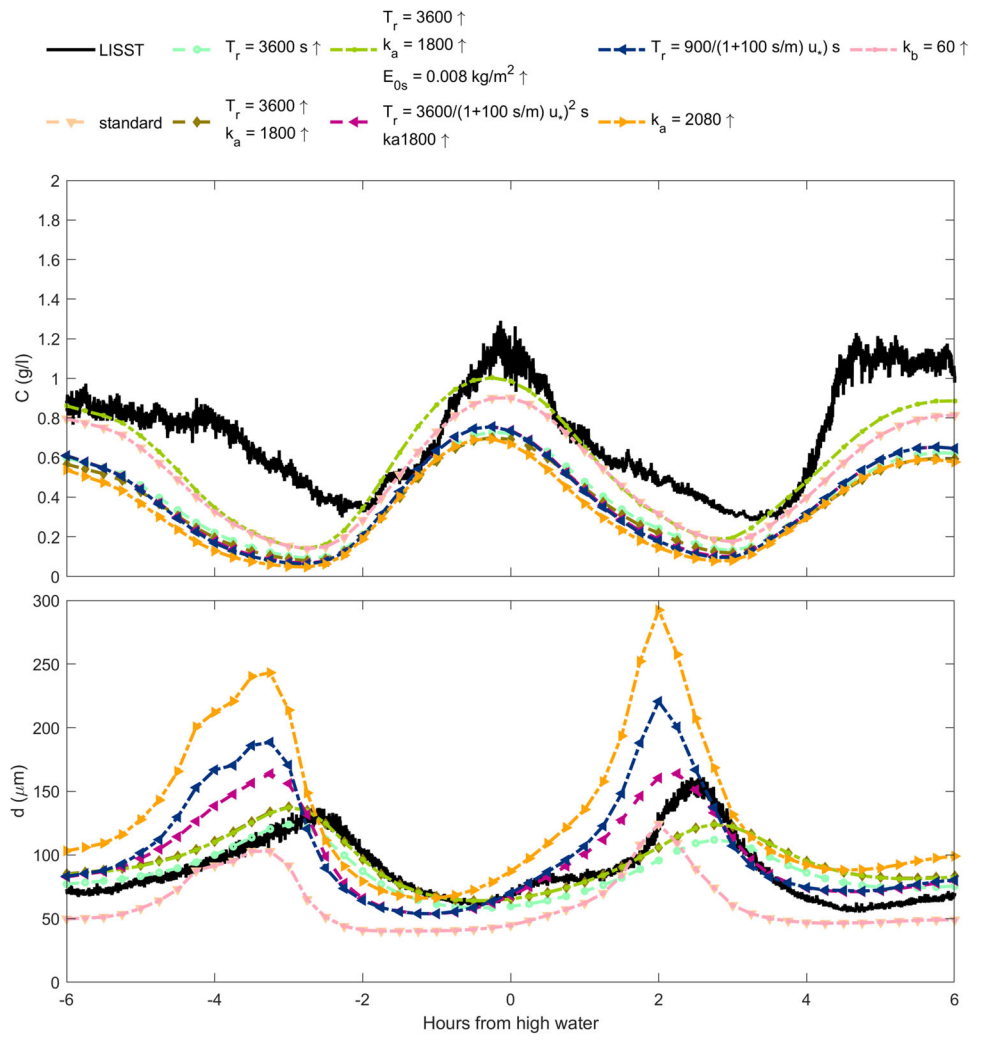
Fig. 15 Model calibration simulations in direct connection with the floc size. The arrows on the figure legend indicate an increase (↑) or decrease (↓) in the parameter values relative to the standard simulation. LISST-measurements (black solid line) are included for reference

Table 4 Calibration performance in relation to measurements at the MOW1 station. The bold text highlights the best performing simulation based on the RMSE obtained both for the suspended sediment concentration and the floc size

Name	RMSE		Ranking
	C (g/l)	d (m)	
STANDARD	0.33	29.85	2
E0S0008	0.30	46.08	5
E0V00016	0.45	45.97	12
Erosion law NS 05	0.45	45.97	11
Erosion law NS 1 5	0.46	46.14	16
tau ce m0015	0.44	46.35	13
tau ce m004	0.46	46.42	17
tau ce s001	0.38	46.43	10
tshld 15 25	0.43	32.12	6
tshld 25 35	0.42	32.11	4
Top thickness 0.2	0.45	46.43	15
Bottom thickness 0.5	0.40	46.12	8
Tr3600	0.44	19.86	3
Tr3600 ka1800	0.46	23.76	9
Tr3600 ka1800 E0S0008	**0.29**	**23.22**	**1**
Trvar3600 ka1800	0.45	32.08	7
Trvar 900	0.46	45.22	14
ka2080	0.50	72.34	18
kb60	0.33	29.85	2

Appendix B: Hydrodynamics-waves model assessment

The performance of the BCG model hydrodynamics are assessed for the month of March 2009. The comparison with measurements was done according to data availability, thus not all measuring stations have the same variables.

Simulated tides are in agreement with the measurements data (see Fig. 16). The maximum RMSE is 0.20 m, at the Scheur Wielingen station. Wandelaar and the A2 stations had have RMSE values of 0.17 m and 0.18 m respectively.

The flow velocities are overall on the same range of measurements, although there are noticeable phase mismatches during slack waters, both from ebb to flood and from flood to ebb tides (see Figs. 17 and 6). The RMSE at the Scheur Wielingen is 0.22 m/s, and at Bol van Heist it is 0.21 m/s (Fig. 6).

Modelled wave integrated variables are well in agreement with the measurements. The RMSE at Scheur Wielingen (Fig. 18), Wandelaar (Fig. 19) and A2 (Fig. 20) are 0.17 m, 0.15 m, and 0.16 m respectively. The mean wave period is slightly overestimated, with RMSE values of 0.64 s, 0.67 s, and 0.61 s.
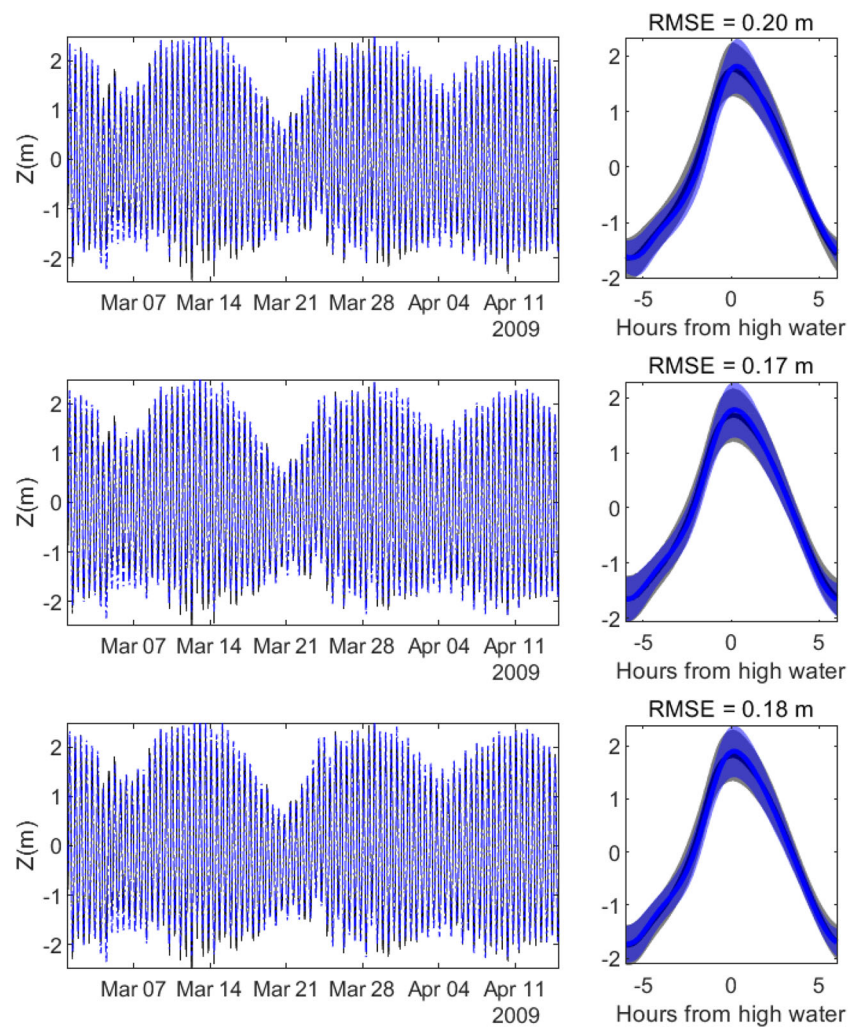

Fig. 16 Comparison of tide measurements and results of the BCG model at the Scheur Wielingen (top), Wandelaar (middle) and A2 (bottom) measuring stations. The right column shows the ensemble averages of the times series (left colum), the solid lines are temporal means and the shaded areas are the standard deviation

Fig. 17 Comparison of current velocity measurements and results of the BCG model at the Scheur Wielingen station
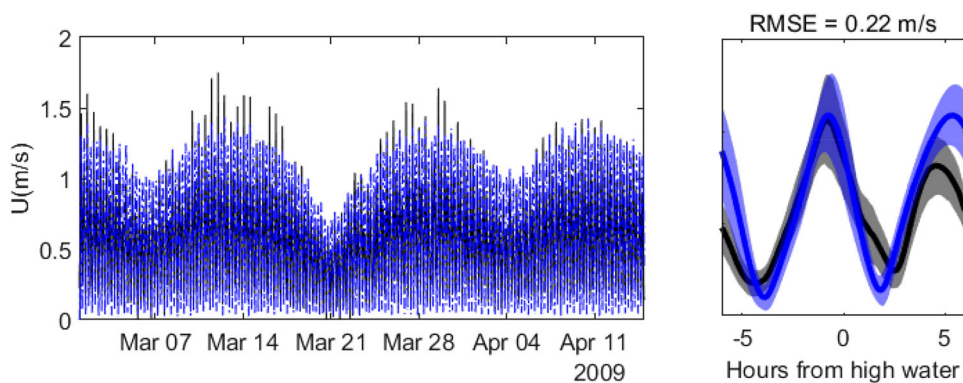

Fig. 18 Comparison of wave measurements and results of the BCG model at the Scheur Wielingen station. The black solid lines are measurements from the Flemish Banks Monitoring Network, and the blue lines are results from the BCG model
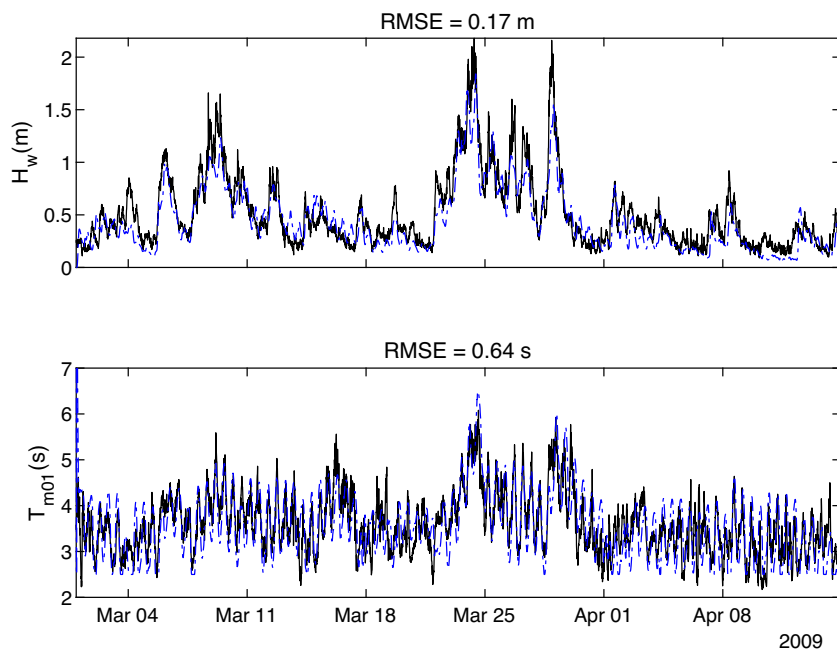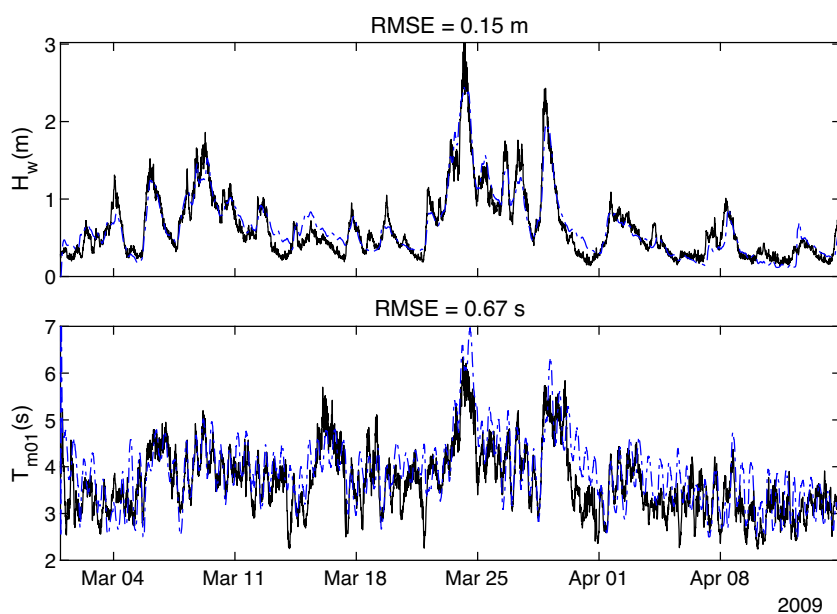

Fig. 19 Comparison of wave measurements and results of the BCG model at the Wandelaar station. The black solid lines are measurements from the Flemish Banks Monitoring Network, and the blue lines are results from the BCG model
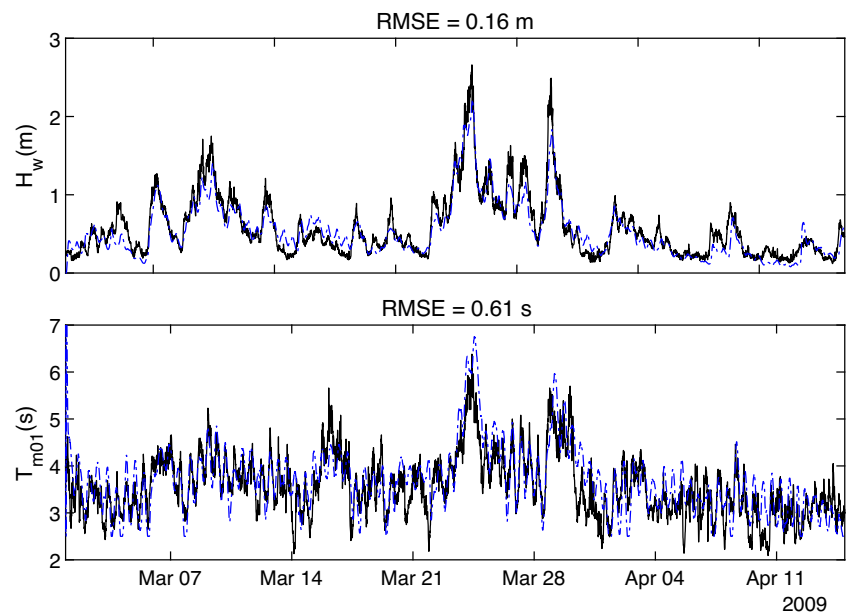
Fig. 20 Comparison of wave measurements and results of the BCG model at the A2 station. The black solid lines are measurements from the Flemish Banks Monitoring Network, and the blue lines are results from the BCG model

References

Alldredge AL, Silver MW (1988) Characteristics, dynamics and significance of marine snow. Prog Oceanogr 20(1):41–82. https://doi.org/10.1016/0079-6611(88)90053-5

AMDK (2017) Bathymetrie vooroever Vlaamse Kust. Agentschap Maritieme Dienstverlening en Kust

Andrews S, Nover D, Schladow SG (2010) Using laser diffraction data to obtain accurate particle size distributions: the role of particle composition. Limnology and Oceanography: Methods 8(10):507–526. https://doi.org/10.4319/lom.2010.8.507

Baeye M, Fettweis M, Voulgaris G, Van Lancker V (2011) Sediment mobility in response to tidal and wind-driven flows along the Belgian inner shelf, southern North Sea. Ocean Dyn 61(5):611–622. https://doi.org/10.1007/s10236-010-0370-7

Baeye M, Fettweis M, Legrand S, Dupont Y, Van Lancker V (2012) Mine burial in the seabed of high-turbidity area-Findings of a first experiment. Cont Shelf Res 43:107–119. https://doi.org/10.1016/j.csr.2012.05.009

Battjes JA, Janssen JPFM (1978) Energy Loss and Set-Up Due to Breaking of Random Waves. Coast Eng Proc 16:32. https://doi.org/10.1061/9780872621909.034

Benoit M, Marcos F, Becq F (1997) TOMAWAC. A prediction model for offshore and nearshore storm waves

Benson TD (2005) In: In situ particle size instrumentation for improved parameterisation and validation of estuarine sediment transport models. University of London, University College London (United Kingdom)

Berrisford P, Dee D, Fielding K, Fuentes M, Kallberg P, Kobayashi S et al (2009) The ERA-interim archive. ERA Rep Ser 1:1–16

Bi Q, Toorman EA (2015) Mixed-sediment transport modelling in Scheldt estuary with a physics-based bottom friction law. Ocean Dyn 65(4):555–587. https://doi.org/10.1007/s10236-015-0816-z

Bi Q, Shen X, Lee BJ, Toorman E (2020) Investigation on estuarine turbidity maximum response to the change of boundary forcing using 3CPBE flocculation model. In: Online proceedings of the papers submitted to the 2020 TELEMAC-MASCARET User Conference October 2020. p 26–34

Bolle A, Bing Wang Z, Amos C, De Ronde J (2010) The influence of changes in tidal asymmetry on residual sediment transport in the Western Scheldt. Cont Shelf Res 30(8):871–882. https://doi.org/10.1016/j.csr.2010.03.001

Brand E, De Sloover L, De Wulf A, Montreuil AL, Vos S, Chen M (2019) Cross-shore suspended sediment transport in relation to topographic changes in the intertidal zone of a macro-tidal beach (Mariakerke, Belgium). J Mar Sci Eng 7(6):172

Breugem W, Fonias E, Wang L, Bolle A, Kolokythas G, De Maerschalck B (2019) TEL2TOM: coupling TELEMAC2D and TOMAWAC on arbitrary meshes. In: XXVIth TELEMAC-MASCARET User Conference, 15th to 17th October 2019. Toulouse

Chakraborti RK, Gardner KH, Atkinson JF, Van Benschoten JE (2003) Changes in fractal dimension during aggregation. Water Res 37(4):873–883. https://doi.org/10.1016/S0043-1354(02)00379-2

Chang TS, Joerdel O, Flemming B, Bartholomä A (2006) The role of particle aggregation/disaggregation in muddy sediment dynamics and seasonal sediment turnover in a back-barrier tidal basin, East Frisian Wadden Sea, southern North Sea. Mar Geol 235:49–61. https://doi.org/10.1016/j.margeo.2006.10.004

Chapalain M, Verney R, Fettweis M, Jacquet M, Le Berre D, Le Hir P (2019) Investigating suspended particulate matter in coastal waters using the fractal theory. Ocean Dyn 69. https://doi.org/10.1007/s10236-018-1229-6

Cox TJS, Maris T, Van Engeland T, Soetaert K, Meire P (2019) Critical transitions in suspended sediment dynamics in a temperate meso-tidal estuary. Sci Rep 9(1):12745. https://doi.org/10.1038/s41598-019-48978-5

Dietrich WE (1982) Settling velocity of natural particles. Water Resour Res 18(6):1615–1626. https://doi.org/10.1029/WR018i006p01615

Dushaw BD, Egbert GD, Worcester PF, Cornuelle BD, Howe BM, Metzger K (1997) A TOPEX/POSEIDON global tidal model (TPXO. 2) and barotropic tidal currents determined from long-range acoustic transmissions. Progress Oceanogr 40(1-4):337–367

Duy Vinh V, Ouillon S, Van Uu D (2018) Estuarine Turbidity Maxima and Variations of Aggregate Parameters in the Cam-Nam Trieu Estuary, North Vietnam, in Early Wet Season. Water 10(1). https://doi.org/10.3390/w10010068

Dyer KR (1989) Sediment processes in estuaries: Future research requirements. J Geophys Res Oceans 94(C10):14327–14339.

https://doi.org/10.1029/JC094iC10p14327. https://agupubs.onlinelibrary.wiley.com/doi/pdf/10.1029/JC094iC10p14327

Fettweis M, Baeye M (2015) Seasonal variation in concentration, size, and settling velocity of muddy marine flocs in the benthic boundary layer. J Geophys Res Oceans 120(8):5648–5667

Fettweis M, Nechad B, Van den Eynde D (2007) An estimate of the suspended particulate matter (SPM) transport in the southern North Sea using SeaWiFS images, in situ measurements and numerical model results. Cont Shelf Res 27(10–11):1568–1583

Fettweis M, Baeye M, Lee B, Chen P, Yu J (2012) Hydro-meteorological influences and multimodal suspended particle size distributions in the Belgian nearshore area (southern North Sea). Geo-Mar Lett 32(2):123–137

Fettweis M, Baeye M, Cardoso C, Dujardin A, Lauwaert B, Van den Eynde D et al (2016) The impact of disposal of fine-grained sediments from maintenance dredging works on SPM concentration and fluid mud in and outside the harbor of Zeebrugge. Ocean Dyn 66(11):1497–1516

Fettweis M, Baeye M, Francken F, Van den Eynde D, Natuur-BMM KO (2019) MOnitoring en MOdellering van het cohesieve sediment-transport en evaluatie van de effecten op het mariene ecosysteem ten gevolge van bagger-en stortoperatie (MOMO). Geosciences 9:34

Fettweis M, Riethmüller R, Verney R, Becker M, Backers J, Baeye M et al (2019) Uncertainties associated with in situ high-frequency long-term observations of suspended particulate matter concentration using optical and acoustic sensors. Prog Oceanogr 178:102162. https://doi.org/10.1016/j.pocean.2019.102162

Fettweis M, Schartau M, Desmit X, Lee BJ, Terseleer N, Van der Zande D et al (2022) Organic Matter Composition of Biomineral Flocs and Its Influence on Suspended Particulate Matter Dynamics Along a Nearshore to Offshore Transect. J Geophys Res Biogeosci 127. https://doi.org/10.1029/2021JG006332

Fettweis M, Lee BJ (2017) Spatial and Seasonal Variation of Biomineral Suspended Particulate Matter Properties in High-Turbid Nearshore and Low-Turbid Offshore Zones. Water 9(9). https://doi.org/10.3390/w9090694

Flather RA (1979) Recent Results from a Storm Surge Prediction Scheme for the North Sea. In: Nihoul JCJ, editor. Marine Forecasting. vol. 25 of Elsevier Oceanography Series. Elsevier, p 385–409

Fouquet T (2020) Tomawac User Manual Version 8.1. http://www.opentelemac.org/index.php/manuals

Graham G, Davies E, Nimmo-Smith W, Bowers D, Braithwaite K (2012) Interpreting LISST-100X measurements of particles with complex shape using digital in-line holography. J Geophys Res Oceans 117(C5)

Hasselmann K, Barnett T, Bouws E, Carlson H, Cartwright D, Enke K et al (1973) Measurements of wind-wave growth and swell decay during the Joint North Sea Wave Project (JONSWAP). Ergänzungsheft 8-12

Hasselmann S, Hasselmann K, Allender J, Barnett T (1985) Computations and parameterizations of the nonlinear energy transfer in a gravity-wave spectrum. Part II: Parameterizations of the nonlinear energy transfer for application in wave models. J Phys Oceanogr 15(11):1378–1391

Hervouet JM (2000) TELEMAC modelling system: an overview. Hydrol Process 14(13):2209–2210

Ho QN, Fettweis M, Spencer KL, Lee BJ (2022) Flocculation with heterogeneous composition in water environments: A review. Water Res 213:118147. https://doi.org/10.1016/j.watres.2022.118147

Horemans DML, Dijkstra YM, Schuttelaars HM, Meire P (2020) Cox TJS. Unraveling the Essential Effects of Flocculation on Large-Scale Sediment Transport Patterns in a Tide-Dominated Estuary. J Phys Oceanogr 50(7):1957–1981. https://doi.org/10.1175/JPO-D-19-0232.1

Hulburt HM, Katz S (1964) Some problems in particle technology: A statistical mechanical formulation. Chem Eng Sci 19(8):555–574. https://doi.org/10.1016/0009-2509(64)85047-8

Khelifa A, Hill PS (2006) Models for effective density and settling velocity of flocs. J Hydraul Res 44(3):390–401. https://doi.org/10.1080/00221686.2006.9521690

Knaeps E, Sterckx S, Bhatia N, Bi Q, Monbaliu J, Toorman E et al (2017) Coastal turbidity monitoring using the PROBA-V satellite. Proc Coast Dyn 2017:1483–1494

Komen G, Hasselmann K, Hasselmann K (1984) On the existence of a fully developed wind-sea spectrum. J Phys Oceanogr 14(8):1271–1285

Komen GJ, Cavaleri L, Donelan M, Hasselmann K, Hasselmann S, Janssen P (1996) Dynamics and modelling of ocean waves. Cambridge University Press

Komijani H, Ortega H (2016) Opstellen van een hydrodynamische modellensuite TELEMAC-TOMAWAC voor de Broersbank. Vlaamse Baaien -Monitoring "Broersbank". KU Leuven

Kranenburg C (1994) The fractal structure of cohesive sediment aggregates. Estuar Coast Shelf Sci 39(6):451–460. https://doi.org/10.1016/S0272-7714(06)80002-8

Kuprenas R, Tran D, Strom K (2018) A Shear-Limited Flocculation Model for Dynamically Predicting Average Floc Size. J Geophys Res Oceans 123(9):6736–6752. https://doi.org/10.1029/2018JC014154

Le Hir P, Cayocca F, Waeles B (2011) Dynamics of sand and mud mixtures: A multiprocess-based modelling strategy. Proceedings of the 9th International Conference on Nearshore and Estuarine Cohesive Sediment Transport Processes 31(10):S135–S149. https://doi.org/10.1016/j.csr.2010.12.009

Lee BJ, Fettweis M, Toorman E, Molz FJ (2012) Multimodality of a particle size distribution of cohesive suspended particulate matters in a coastal zone. J Geophys Res Oceans 117(C3)

Lee BJ, Toorman E, Molz FJ, Wang J (2011) A two-class population balance equation yielding bimodal flocculation of marine or estuarine sediments. Water Res 45(5):2131–2145

Maerz J, Hofmeister R, van der Lee EM, Gräwe U, Riethmüller R, Wirtz KW (2016) Maximum sinking velocities of suspended particulate matter in a coastal transition zone. Biogeosciences 13(17):4863–4876. https://doi.org/10.5194/bg-13-4863-2016

Maerz J, Six KD, Stemmler I, Ahmerkamp S, Ilyina T (2020) Microstructure and composition of marine aggregates as co-determinants for vertical particulate organic carbon transfer in the global ocean. Biogeosciences 17(7):1765–1803. https://doi.org/10.5194/bg-17-1765-2020

Maggi F, Mietta F, Winterwerp JC (2007) Effect of variable fractal dimension on the floc size distribution of suspended cohesive sediment. J Hydrol 343(1):43 – 55. https://doi.org/j.jhydrol.2007.05.035

Manning AJ, Dyer KR (1999) A laboratory examination of floc characteristics with regard to turbulent shearing. Mar Geol 160(1):147–170. https://doi.org/10.1016/S0025-3227(99)00013-4

Margvelashvili N, Andrewartha J, Herzfeld M, Robson BJ, Brando VE (2013) Satellite data assimilation and estimation of a 3D coastal sediment transport model using error-subspace emulators. Environ Model Softw 40:191 – 201. https://doi.org/j.envsoft.2012.09.009

Maximova T, Ides S, De Mulder T, Mostaert F et al (2009) LTV O&M thema veiligheid: deelproject 1. Verbetering hydrodynamisch NEVLA model ten behoeve van scenario-analyse, WL Rapporten, p 756

McAnally WH, Mehta AJ (2000) Collisional aggregation of fine estuarial sediment. In: McAnally WH, Mehta AJ, editors. Coastal and Estuarine Fine Sediment Processes. vol. 3 of Proceedings in Marine Science. Elsevier, p 19–39

Nohe A, Goffin A, Tyberghein L, Lagring R, De Cauwer K, Vyverman W et al (2020) Marked changes in diatom and dinoflagellate

biomass, composition and seasonality in the Belgian Part of the North Sea between the 1970s and 2000s. Sci Total Environ 716:136316

Press WH, Teukolsky SA, Flannery BP, Vetterling WT (1992) In: Numerical recipes in Fortran 77: volume 1, volume 1 of Fortran numerical recipes: the art of scientific computing. Cambridge University Press

Randolph AD (1964) A population balance for countable entities. Can J Chem Eng 42(6):280–281. https://doi.org/10.1002/cjce.5450420612

Saffman PG, Turner JS (1956) On the collision of drops in turbulent clouds. J Fluid Mech 1(1):16–30. https://doi.org/10.1017/S0022112056000020

Shen X, Lee BJ, Fettweis M, Toorman EA (2018) A tri-modal flocculation model coupled with TELEMAC for estuarine muds both in the laboratory and in the field. Water Res (Oxf) 145:473–486

Shen X, Toorman EA, Fettweis M, Lee BJ, He Q (2019) Simulating multimodal floc size distributions of suspended cohesive sediments with lognormal subordinates: Comparison with mixing jar and settling column experiments. Coast Eng 148:36–48. https://doi.org/10.1016/j.coastaleng.2019.03.002

Shen X, Toorman EA, Lee BJ, Fettweis M (2018) Biophysical flocculation of suspended particulate matters in Belgian coastal zones. J Hydrol 567:238–252. https://doi.org/j.jhydrol.2018.10.028

SHOM (2015) MNT topo-bathymétrique côtier, descriptif de contenu du produit externe. Service hydrographique et océanographique de la marine, France

Smolders S, De Maerschalck B, Plancke Y, Vanlede J, Mostaert F (2019) Integraal Plan Boven-Zeeschelde: sub report 10. Scaldis Sand: a sand transport model for the Scheldt estuary. FHR Rep

Son M, Hsu TJ (2009) The effect of variable yield strength and variable fractal dimension on flocculation of cohesive sediment. Water Res 43(14):3582–3592. https://doi.org/10.1016/j.watres.2009.05.016

Soulsby RL, Clarke S (2005) Bed shear-stress under combined waves and currents on smooth and rough beds (TR 137). HR Wallingford. http://eprints.hrwallingford.com/id/eprint/558

Soulsby RL, Manning AJ, Spearman J, Whitehouse RJS (2013) Settling velocity and mass settling flux of flocculated estuarine sediments. Mar Geol 339:1–12. https://doi.org/10.1016/j.margeo.2013.04.006

Spencer KL, Wheatland JA, Bushby AJ, Carr SJ, Droppo IG, Manning AJ (2021) A structure-function based approach to floc hierarchy and evidence for the non-fractal nature of natural sediment flocs. Sci Rep 11(1):1–10

Stephens D, Diesing M (2015) Towards Quantitative Spatial Models of Seabed Sediment Composition. PLoS ONE 10(11):1–23. https://doi.org/10.1371/journal.pone.0142502

Tambo N, Watanabe Y (1984) Physical aspect of flocculation process: Flocculation process in a continuous flow flocculator with a back-mix flow. Water Res 18(6):695–707. https://doi.org/10.1016/0043-1354(84)90165-9

Tambo N, Watanabe Y (1979) Physical characteristics of flocs-I. The floc density function and aluminium floc. Water Res 13(5):409–419. https://doi.org/10.1016/0043-1354(79)90033-2

Tarpley DRN, Harris CK, Friedrichs CT, Sherwood CR (2019) Tidal Variation in Cohesive Sediment Distribution and Sensitivity to Flocculation and Bed Consolidation in An Idealized, Partially Mixed Estuary. J Mar Sci Eng 7(10). https://doi.org/10.3390/jmse7100334

Tassi P, Benson T, Delinares M, Fontaine J, Huybrechts N, Kopmann R et al (2023) GAIA - a unified framework for sediment transport and bed evolution in rivers, coastal seas and transitional waters in the TELEMAC-MASCARET modelling system. Environ Model Softw 159:105544. https://doi.org/10.1016/j.envsoft.2022.105544

Thierry S, Dick S, George S, Benoit L, Cyrille P (2019) EMODnet Bathymetry a compilation of bathymetric data in the European waters. In: OCEANS 2019-Marseille. IEEE, p 1–7

Toorman E (1997) Mechanics of cohesive sediment transport. Proceedings on 4th Nat Congr on Applied and Theoretical Mechanics

Toorman EA (2000) Suspension capacity of uniform shear flows. Report No. HYD/ET/00/COSINUS4. Hydraulics Laboratory, Katholieke Universiteit Leuven

Toorman EA (2003) Validation of macroscopic modelling of particle-laden turbulent flows. In: Proceedings 6th Belgian National Congress on Theoretical and Applied Mechanics, Gent. p 26–27

Toorman EA (2020) Background on the development and testing of a 2DH flocculation model. Hydraulics Section, Dept. of Civil Eng., KU Leuven

Toorman EA (2022) Modification of the Dietrich (1982) formula and a new closure for the terminal settling velocity of spherical particles. J Hydr Eng, ASCE (submitted)

Toorman EA, Bruens AW, Kranenburg C, Winterwerp JC (2002) Interaction of suspended cohesive sediment and turbulence. Fine Sediment Dyn Mar Environ 5:7–23. https://doi.org/10.1016/S1568-2692(02)80005-5

Tran D, Strom K (2017) Suspended clays and silts: Are they independent or dependent fractions when it comes to settling in a turbulent suspension? Cont Shelf Res 138:81–94. https://doi.org/10.1016/j.csr.2017.02.011

Turner JS (1973) Buoyancy effects in fluids. Cambridge University Press, Cambridge, Cambridge monographs on mechanics and applied mathematics

Turner JT (2015) Zooplankton fecal pellets, marine snow, phytodetritus and the ocean's biological pump. Prog Oceanogr 130:205–248. https://doi.org/10.1016/j.pocean.2014.08.005

Van den Eynde L (2018) Modelling of suspended matter for the Belgian coastal zone and the Scheldt estuary by means of PROBA-V remote sensing data. Dept. of Civil Engineering, KU Leuven

van Leussen W (2011) Macroflocs, fine-grained sediment transports and their longitudinal variations in the Ems Estuary. Ocean Dyn 61(2–3):387–401

Vanlede J, Dujardin A, Fettweis M, Hoestenberghe T, Martens C (2019) Mud dynamics in the Port of Zeebrugge. Ocean Dyn 69. https://doi.org/10.1007/s10236-019-01273-3

von Smoluchowski M (1917) Mathematical theory of the kinetics of the coagulation of colloidal solutions. Z Phys Chem 92:129–168

Waeles B, Le Hir P, Lesueur P, Delsinne N (2007) Modelling sand/mud transport and morphodynamics in the Seine river mouth (France): an attempt using a process-based approach. Hydrobiologia 588(1):69–82. https://doi.org/10.1007/s10750-007-0653-2

Wang D, Zhang J, He X, Chu D, Lv X, Wang YP et al (2018) Parameter estimation for a cohesive sediment transport model by assimilating satellite observations in the Hangzhou Bay: Temporal variations and spatial distributions. Ocean Model 121:34–48. https://doi.org/10.1016/j.ocemod.2017.11.007

Wang D, Zhang J, Mao X, Bian C, Zhou Z (2020) Simultaneously assimilating multi-source observations into a three-dimensional suspended cohesive sediment transport model by the adjoint method in the Bohai Sea. Estuar Coast Shelf Sci 241:106809. https://doi.org/10.1016/j.ecss.2020.106809

Weitz DA, Oliveria M (1984) Fractal Structures Formed by Kinetic Aggregation of Aqueous Gold Colloids. Phys Rev Lett 52:1433–1436. https://doi.org/10.1103/PhysRevLett.52.1433

Winterwerp JC (1998) A simple model for turbulence induced flocculation of cohesive sediment. J Hydraul Res 36(3):309–326. https://doi.org/10.1080/00221689809498621

Winterwerp JC (2002) On the flocculation and settling velocity of estuarine mud. Cont Shelf Res 22(9):1339–1360. https://doi.org/10.1016/S0278-4343(02)00010-9

Zhang Y, Ren J, Zhang W (2020) Flocculation under the control of shear, concentration and stratification during tidal cycles. J Hydrol 586:124908. https://doi.org/10.1016/j.jhydrol.2020.124908

Zhang Q, Escobar S, Toorman E, Monbaliu J (2020) Two-dimensional computations of Stokes drift and undertow at the near coast region. In: Online proceedings of the papers submitted to the 2020 TELEMAC-MASCARET User Conference October 2020. p 159–164

Authors and Affiliations

Sebastian Escobar[1,2] · **Qilong Bi[1,3]** · **Michael Fettweis[4]** · **Samor Wongsoredjo[1]** · **Jaak Monbaliu[1]** · **Erik Toorman[1]**

Qilong Bi
qilong.bi@deltares.nl

Michael Fettweis
mfettweis@naturalsciences.be

Samor Wongsoredjo
samor.wongsoredjo@kuleuven.be

Jaak Monbaliu
jaak.monbaliu@kuleuven.be

Erik Toorman
erik.toorman@kuleuven.be

[1] Hydraulics Laboratory, Department of Civil Engineering, KU Leuven, Kasteelpark Arenberg 40, Box 2448, Leuven 3001, Belgium

[2] HR Wallingford, Howbery Park, Wallingford OX10 8BA, United Kingdom

[3] Department of Ecosystems & Sediment Dynamics, Deltares, P.O. Box 177, Delft 2600, MH, The Netherlands

[4] Royal Belgian Institute of Natural Sciences, Vautier Street 29, Brussels 1000, Belgium